AD-A107 643 NAVAL SURFACE WEAPONS CENTER DAHLGREN VA F/G 17/7
TIME CORRECTION OF DATA FROM THE NAVSTAR GEODETIC RECEIVER SYST--ETC(U)
AUG 81 B R HERMANN
UNCLASSIFIED NSWC/TR-81-174 NL

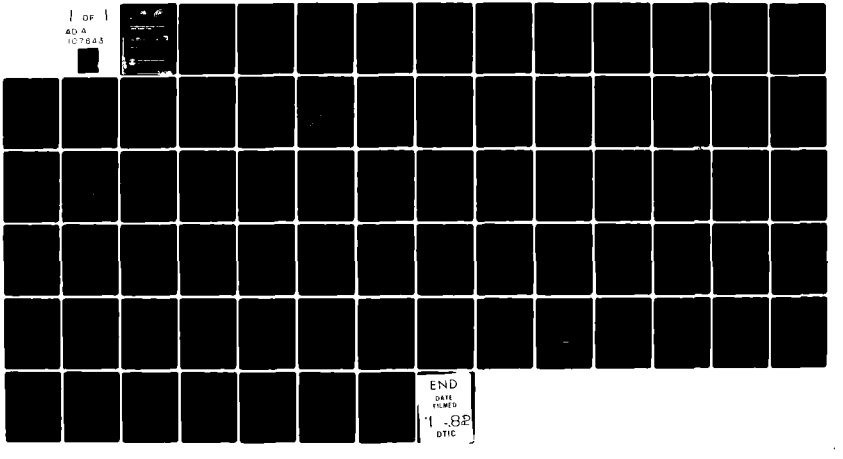

UNCLASSIFIED

SECURITY CLASSIFICATION OF THIS PAGE (When Data Entered)

REPORT DOCUMENTATION PAGE	READ INSTRUCTIONS BEFORE COMPLETING FORM
1. REPORT NUMBER: NSWC TR 81-174	2. GOVT ACCESSION NO.	3. RECIPIENT'S CATALOG NUMBER
4. TITLE (and Subtitle): TIME CORRECTION OF DATA FROM THE NAVSTAR GEODETIC RECEIVER SYSTEM .	5. TYPE OF REPORT & PERIOD COVERED: Final
	6. PERFORMING ORG. REPORT NUMBER
7. AUTHOR(s): Bruce R. Hermann	8. CONTRACT OR GRANT NUMBER(s)
9. PERFORMING ORGANIZATION NAME AND ADDRESS: Naval Surface Weapons Center (K13) Dahlgren, VA 22448	10. PROGRAM ELEMENT, PROJECT, TASK AREA & WORK UNIT NUMBERS: 63701B
11. CONTROLLING OFFICE NAME AND ADDRESS: Defense Mapping Agency Washington, DC 20362	12. REPORT DATE: August 1981
	13. NUMBER OF PAGES: 78
14. MONITORING AGENCY NAME & ADDRESS(if different from Controlling Office)	15. SECURITY CLASS. (of this report): UNCLASSIFIED
	15a. DECLASSIFICATION DOWNGRADING SCHEDULE

16. DISTRIBUTION STATEMENT (of this Report)

Approved for public release; distribution unlimited.

17. DISTRIBUTION STATEMENT (of the abstract entered in Block 20, if different from Report)

18. SUPPLEMENTARY NOTES

19. KEY WORDS (Continue on reverse side if necessary and identify by block number)

Global Positioning System
Geodetic applications
Geodetic Receiver System
Pseudorange
Doppler observations

20. ABSTRACT (Continue on reverse side if necessary and identify by block number)

The NAVSTAR Global Positioning System (NGPS) can be used for geodetic applications. The NAVSTAR Geodetic Receiver System (NGRS) has been developed to demonstrate this capability. In order to use the pseudorange and Doppler observations to do precise point positioning, the time of each observation must be known in the GPS time system. The method used to convert local (NGRS) time to GPS time is described.

DD FORM 1 JAN 73 1473 EDITION OF 1 NOV 65 IS OBSOLETE
S/N 0102-LF-014-6601

UNCLASSIFIED

SECURITY CLASSIFICATION OF THIS PAGE (When Data Entered)

FOREWORD

The development of the NAVSTAR Geodetic Receiver System (NGRS) was funded by the Defense Mapping Agency (DMA) as a means to demonstrate the capability of using the Global Positioning System (GPS) transmissions to achieve high accuracy geodetic point positioning. The receiver was designed by Stanford Telecommunications Incorporated. The supporting hardware and the system microprocessor controller software were proposed and implemented at the Naval Surface Weapons Center (NSWC) by the Electronics Systems Department, Advanced Projects Division. Data reduction was performed by the Space Flight Sciences Branch and the Physical Sciences Software Branch of the Space and Surface Systems Division of the Strategic Systems Department at NSWC. Technical and administrative assistance was received from the sponsor through the Defense Mapping Agency Hydrographic/Topographic Center in Washington, D. C.

Released by:

R. T. RYLAND, Head
Strategic Systems Department

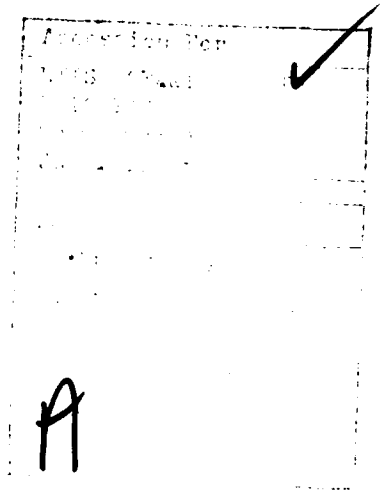

CONTENTS

LIST OF ILLUSTRATIONS

LIST OF TABLES

INTRODUCTION

The NAVSTAR Geodetic Receiver System (NGRS) records both pseudorange and Doppler observations from the Global Positioning System (GPS) satellites. Observations of pseudorange are available each 6 sec and a Doppler count each minute. In order to use these observations to do precise point positioning with the receiver or to do satellite orbit calculations, the time of each observation must be known with high accuracy in the GPS time system. At sites remote from the GPS Master Control Station (MCS), GPS time must be obtained indirectly, since the satellites do not transmit time signals that are synchronized with those kept at the MCS. The satellites do, however, broadcast correction coefficients in the navigation message. The NGRS method of converting local time to GPS time is described in the following sections.

USE OF TIME-TAGS

The Doppler count start and stop times are controlled by the local clock minute epochs and are therefore time-tagged with these epochs. These epochs are not, however, synchronized with the GPS time system and must be corrected in some manner so that they also reflect true GPS time. The accuracy to which this correction must be made can be estimated in the following way.

A worst-case relative velocity between a satellite at GPS altitude and a station on the earth is about 1400 m/sec.[1] If 1 cm is taken as an allowable range error, then the time required for the satellite-ground station range to change by 1 cm is

$$\Delta t = 0.01 \text{ m} \left(\frac{1}{1400} \frac{\text{sec}}{\text{m}} \right) = 7.1 \ \mu\text{sec}$$

Therefore, if time tags on the NGRS observations are corrected to GPS time with an accuracy of about ± 7 μsec, the error in the calculated satellite range will be less than 1 cm.

The satellite position is obtained from a post-fit ephemeris that lists positions at specific GPS times. Positions intermediate to those given are obtained by interpolation. Thus, it is clear that the correct GPS time is essential, if the satellite position is to be calculated accurately at the time of each observation. Once calculated, it is used in one of two ways depending upon the problem being studied.

If improvement in the satellite orbit is the object, then the calculated satellite position is used as the nominal to form differences with the observations. It is important that this nominal be time-tagged correctly from observation to observation so that a minimum amount of "noise" from the calculated satellite position is introduced into the computation. If absolute positioning

of the receiver is the goal, then the calculated satellite positions are treated as the truth, and the site position is computed from them by using the observations. Clearly an error in satellite position will translate into an error in the computed receiver position.

METHOD OF TIME-TAG CORRECTION

The satellites transmit time tags as part of the GPS navigation message.[2] These time tags are keyed to agree with the pseudorandom code sequence that is continuously transmitted. However, these time tags are not aligned with GPS time, and, in fact, each satellite clock drifts by different and time variable amounts. This is a consequence of the fact that each satellite's frequency reference is necessarily allowed to run free. This situation is tolerable because the time offset between each satellite and GPS time is predicted in advance, and corrections to the transmitted time can be computed by the individual user, if he is able to decode the satellite navigation message. The corrections to the apparent satellite time are designated τ_s in Figure 1. The other offsets that are relevant to this problem are also defined in that figure.

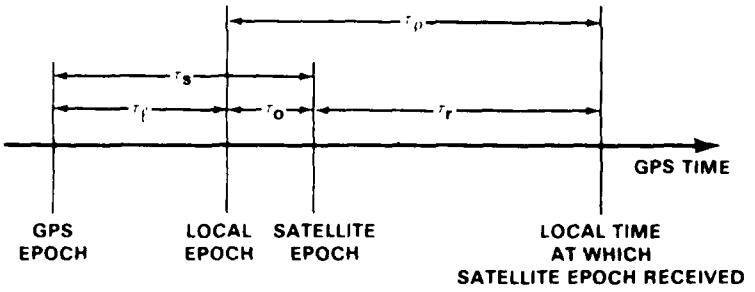

τ_r = PROPAGATION DELAY
τ_o = EPOCH OFFSET (LOCAL-SATELLITE)
τ_ρ = OBSERVATION OF PSEUDO RANGE = $\tau_o + \tau_r$
τ_f = EPOCH OFFSET (GPS-LOCAL)
τ_s = EPOCH OFFSET (GPS-SATELLITE) = $\tau_o + \tau_f$
A VALUE FOR τ_s IS FOUND IN THE SATELLITE DATA MESSAGE

Figure 1. Diagram Illustrating the Relation Between Epochs

The significance of the events illustrated in Figure 1 is the following. At a particular satellite epoch, the signal indicating that particular epoch is transmitted. This signal is received τ_r sec later by the NGRS. In order to calculate the geometric range corresponding to τ_r, the satellite position at transmission and the receiver position at reception are both needed in a common time system. The satellite position at transmission can be obtained, if the satellite epoch can be converted to the corresponding GPS time. The NGRS position at reception can be obtained, if the local epochs can be converted to the corresponding GPS time. As stated previously, the correction, τ_s, to the satellite epoch is available from the individual satellites' navigation message. The correction to the local clock, τ_ℓ, involves some additional computations using the observed pseudorange τ_ρ.

Using the notation from Figure 1, the GPS time of transmission is $t_{GPS} + \tau_s$, and the locally generated epoch that corresponds to the satellite epoch is $t_{GPS} + \tau_\ell$. The GPS time of reception of the transmitted epoch is $t_{GPS} + \tau_\ell + \tau_\rho$. In order to evaluate τ_ℓ, we can write an equation that states that the time of transmission plus the geometric progagation delay, τ_r, equals the time of reception.

$$t_{GPS} + \tau_s + \tau_r = t_{GPS} + \tau_\ell + \tau_\rho \qquad (1)$$

The local offset must then be $\tau_\ell = \tau_s + \tau_r - \tau_\rho$, where τ_s comes from the navigation message, τ_r is calculated from the ephemeris, and τ_ρ is the pseudorange observation expressed in seconds.

Calculation of τ_r requires the satellite position at the time of transmission $t_{GPS} + \tau_s$ and the receiver position at the time of reception $t_{GPS} + \tau_s + \tau_r$. However, since τ_r is not yet known, we can take the time of reception equal to the time transmission and calculate an approximate value for τ_r. Then we can use this τ_r to refine the approximation indefinitely or until the change in τ_r after each iteration becomes insignificant.

All Doppler count intervals recorded by the NGRS are adjusted to begin and end at local 1-min epochs. Since the local clock, like the individual satellite clocks, is free running, these epochs need to be converted to GPS time. Since we have calculated the local offset τ_ℓ from the pseudorange data, it is a straightforward process to make this correction. Adopting the convention in Figure 1, the local epoch occurs after the GPS epoch. Therefore, the GPS time of the local epochs is the indicated local time plus τ_ℓ.

$$t_{GPS} = t_{Local} + \tau_\ell \qquad (2)$$

We assume in doing this that the indicated local epoch and the GPS epoch are identical. All Doppler time tags should be corrected by the value of τ_ℓ current at the epoch of interest because τ_ℓ itself is a slowly varying function of time.

AN EXAMPLE OF LOCAL OFFSET

Some pseudorange observations from the NGRS were made available for a 15-day span, in order to test the formulation described in the previous section. The reference ephemeris for this span was obtained from the least-square batch fit to monitor station data that is performed routinely at the Naval Surface Weapons Center (NSWC) for the GPS Master Control Station.[3] The satellite clock corrections were obtained directly from the satellite navigation message. Figure 2 is a plot of the computed offset $-\tau_\ell$. Data from four satellites are plotted together in this figure and illustrate that the computed local offset is independent of satellite to within a tolerance of about ±100 nsec. Since the pseudorange observations used in this computation were single frequency (L_1), the systematic spread seen in the figure is probably primarily due to the variation of ionospheric delay with elevation angle. If the observations with elevation angles less than 45° are deleted from the plot, as in Figure 3, the spread is considerably reduced.

At NSWC, SV-8 passes within 10° of the zenith once a day. Data from this satellite are plotted in Figure 4 when the elevation angle is 75° or greater. At this high elevation, the ionospheric contribution to the L_1 range would be a minimum, and the observations would be collected at nearly the same time each day. At this time of the year, this high elevation pass occurred at about 4.4 hr GPS or 23.4 hr EST. Table 1 lists the coefficients of a linear fit to this data and also to all the data plotted in Figure 2. The root mean square (RMS) residual of a linear fit to the high elevation data over the observation span was 11.5 nsec, which is approximately one quarter the RMS of all the data over the entire span.

In effect, a time transfer has been accomplished with quite high accuracy over more than 10 days. The time drift between GPS and the local reference can also be determined from Table 1. The fit parameter, a_1, indicates the drift to be about 66 nsec per day or 0.000764 nsec per second. The quadratic term seems to be quite small and consequently has not been evaluated.

The deviations of the observations from the linear fit are plotted in Figure 5 versus the elevation angle of the observation. The fit parameters used to form these residuals were taken from the fit to the high-elevation SV-8 data only. The propagation path length would be expected to increase at lower elevations due to the effects of the ionosphere; consequently, the differences of all data with the SV-8 fit should show positive residuals. The zero residual line in Figure 5 should, therefore, be an approximate lower bound to the offset residuals. Figure 5 shows that this is not the case. Figure 5 shows that there are offset residuals both above and below the zero residual line. The observed scatter must be due to variations in the reference ephemeris. An error source such as this would produce residuals that were independent of elevation angle. There does exist a preference for positive residuals at low elevations. This is probably due to the expected propagation effects and also to the inclusion of data from satellites not observed at high elevations.

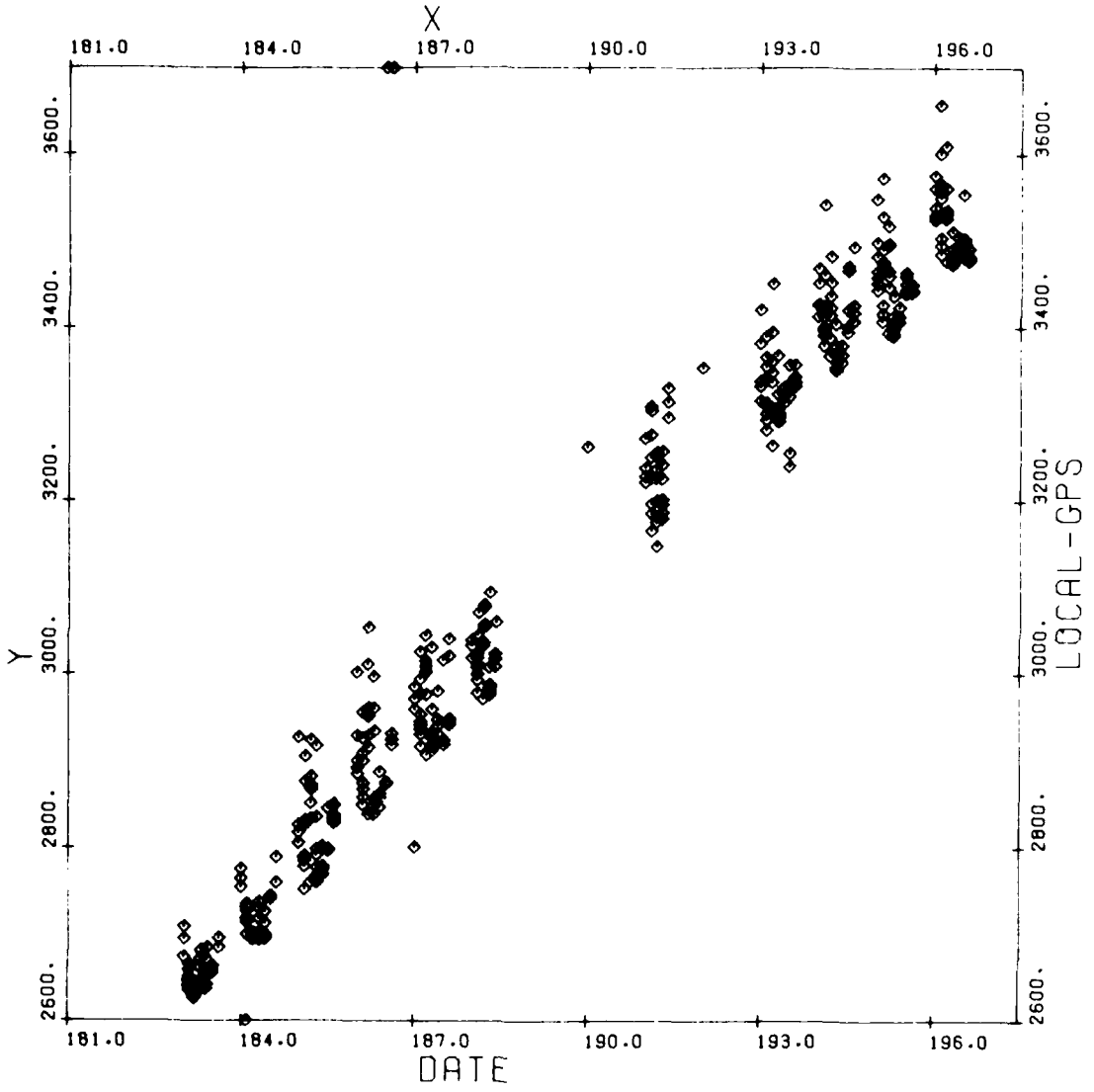

Figure 2. Clock Offset, NGRS-GPS (nsec) vs Date, SV-5, 6, 8, 9; NSWC Post-fit Ephemeris, NSWC Dahlgren, Days 182-197 1980

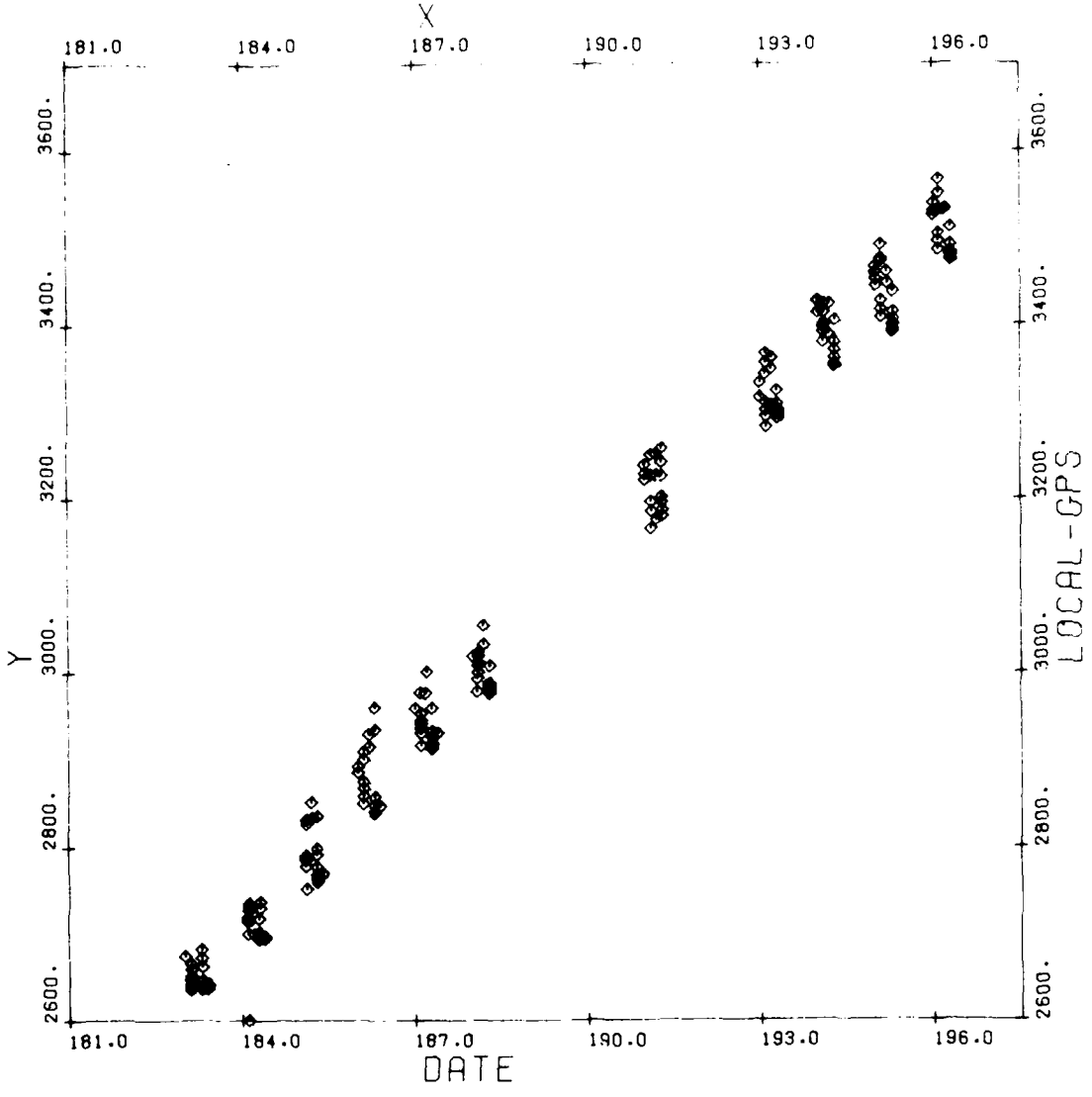

Figure 3. Clock Offset, NGRS-GPS (nsec) vs Date, SV-5, 6, 8, 9; NSWC Post-fit Ephemeris, Elevation >45°, NSWC Dahlgren, Days 182-197 1980

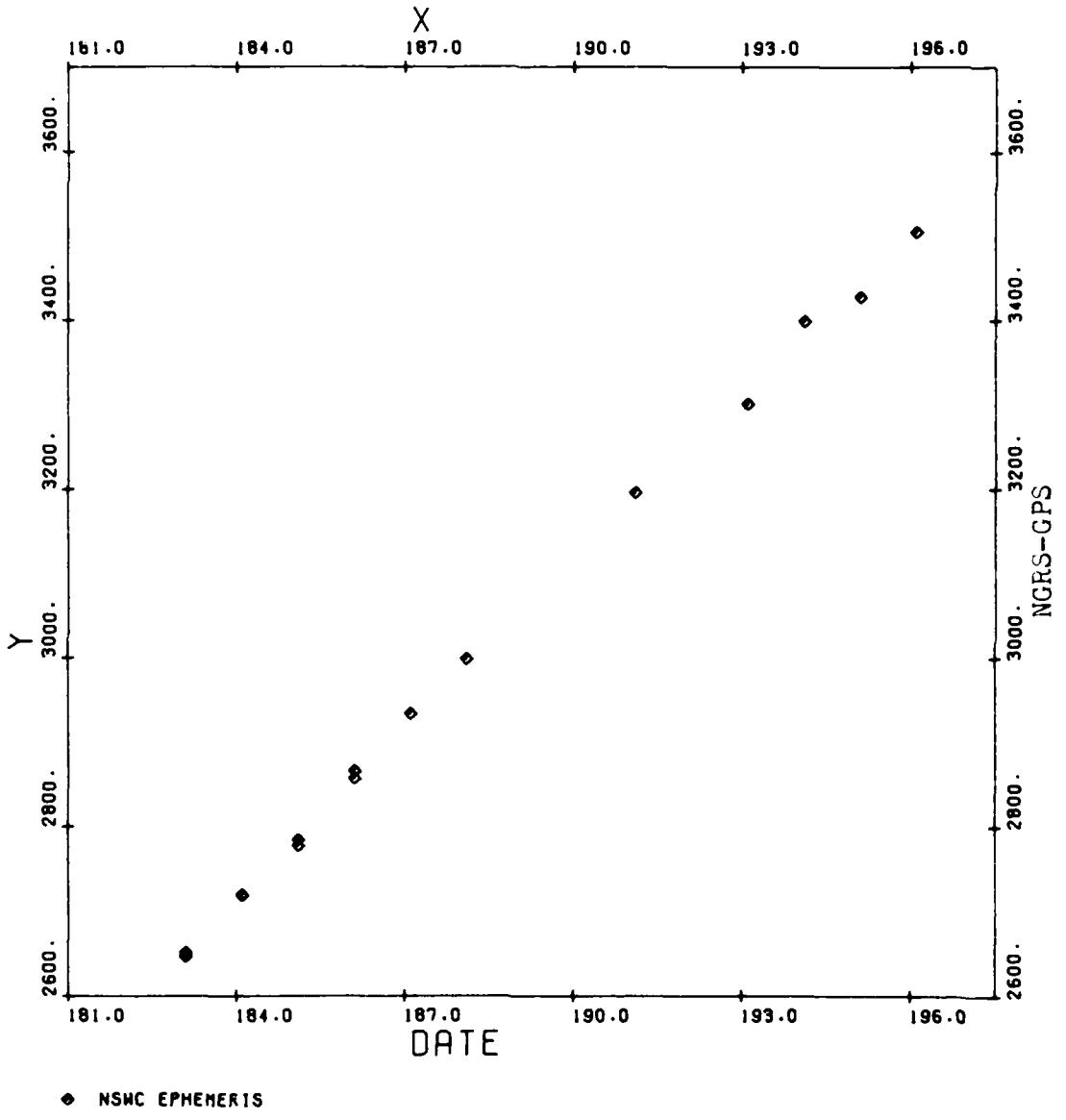

Figure 4. Clock Offset, NGRS-GPS (nsec) vs Date, NSWC Post-fit Ephemeris, Elevation >75°, GPS SV-8; NSWC Dahlgren, Days 182-197 1980

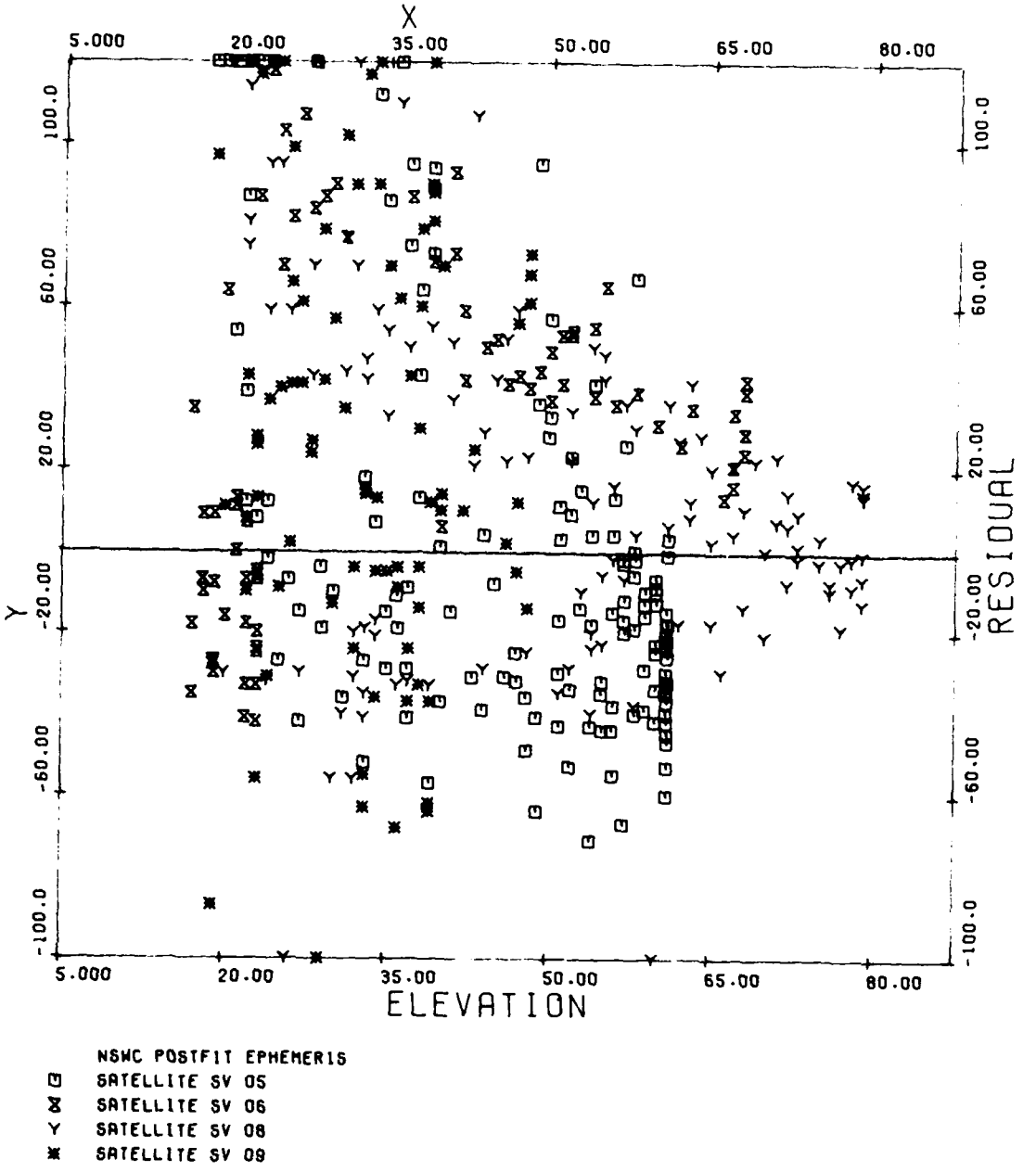

Figure 5. Clock Offset Residual (nsec) vs Elevation (°), NSWC Dahlgren, Days 182-197 1980

Table 1. Linear Fit to Local-GPS Clock Offset

Ephemeris	a_o (nsec)	a_1 (nsec/day)	RMS (nsec)	PTS
NSWC				
$\varepsilon > 75°$	-9438.1	66.0486	11.47	16
all data	-9237.3	65.0626	47.82	414
Broadcast				
$\varepsilon > 75°$	-9543.4	66.5893	10.32	16
all data	-9221.0	65.0882	37.12	376

Figure 5 illustrates that the reference trajectories of the four satellites observed are consistent to within about ±60 nsec (±18 m), if the low elevation bias toward positive residuals is neglected. The consistency is likely to be better than ±60 nsec because these residuals include the predicted satellite clock correction. This clock correction is derived independently of the NSWC satellite ephemeris. The two, therefore, cannot be expected to be as consistent as they might be, if both clock correction and ephemeris were obtained simultaneously from the same data.

The time drift described above can also be interpreted as a fractional frequency deviation $\frac{\Delta f}{f}$. In order to show this, the frequency standard can be represented by two equivalent expressions:

$$\Phi_1 (t) = \phi_o + 2\pi f \tau(t) \tag{3}$$

$$\Phi_2 (t) = \phi_o + 2\pi \xi(f) t \tag{4}$$

In Equation (3), the time argument, τ, is a function of the parameter, t, which is the time argument of Equation (4). For our purposes $\tau(t)$ will be defined as

$$\tau(t) = a_o + (1+a_1)\ t$$

where a_o is the time offset at t = o and a_1 is the time drift (sec per sec). This form has the following properties:

$$\tau(0) = a_o \quad \text{and} \quad \tau(t) = a_o + t \quad \text{if } a_1 = o$$

Under the latter condition, ξ tracks t exactly and differs only by a_0.

In $\Phi_2(t)$, the frequency ξ is a function of the frequency used in $\Phi_1(t)$. Let ξ be offset slightly from t.

$$\xi(t) = t + \Delta t$$

Since these two Φ expressions are equivalent, they can be equated and solved for $\frac{\Delta t}{t}$.

$$\Phi_1(t) = \Phi_2(t)$$

$$2\pi f[a_0 + (1+a_1)t] = 2\pi f(t+\Delta t)$$

$$\frac{\Delta t}{t} = \frac{a_0}{t} + a_1$$

The term $\frac{a_0}{t}$ becomes small after a long time, so it is permissible to take the offset to be zero, or t large. Under these conditions, the fractional frequency deviation $\frac{\Delta t}{t}$ is equivalent to time drift.

$$a_1 = \frac{\Delta t}{t} = 3.64 \times 10^{-13}$$

This number represents the fractional frequency deviation between the local cesium reference and the ensemble that defines the GPS time system. The specification for the long-term fractional frequency deviation of the local cesium is $\pm 7 \times 10^{-12}$. This observed value is well within the specification.

A SECOND EXAMPLE

The same data span was reevaluated for the local offset using the same formulation as previously described. In this case, however, the satellite trajectory was computed using the broadcast ephemeris instead of a post-fit ephemeris. This technique allows more timely results to be obtained because all the information needed is contained in the data as recorded by NGRS from the satellite NAVDATA message.

Figure 6 is the plot of the computed offset, $-\tau_\ell$, from all data. It shows a few more wild points than the corresponding figure from the NSWC post-fit ephemeris, but this may be due to our implementation of the algorithm and not intrinsic to the broadcast ephemeris itself. Otherwise, the agreement between the two ephemerides is excellent. Figure 7 is a plot using the data from SV-8, which was from the portion of the pass whose elevation angle was greater than 75°. Table 1 indicates that the solution to the two sets of data differed by only 5.3 nsec in a_0 and by 0.5 nsec per day in a_1. The RMS computed from all data was 10 nsec less for the broadcast ephemeris when compared to the NSWC

ephemeris, but this was after all observations greater than three times the RMS were eliminated from both sets of data. No observations were eliminated from the SV-8 fits where the elevation angle was greater than 75°.

When the fit to the high-elevation data is used to form residuals with the rest of the observations evaluated using the broadcast ephemeris, the result is quite different from that obtained using the NSWC ephemeris. In this case, illustrated in Figure 8, bias toward positive residuals at lower elevation angles is quite apparent. This would seem to imply that the random component due to ephemeris error is somewhat less for the broadcast ephemeris. If the plot is used as a guide, an estimate of the scatter is about ±40 nsec (±12 m). Since the same satellite clock corrections are used in both cases discussed, a comparison of Figures 5 and 8 is an indication of the relative consistency of those clock corrections with each of the ephemerides. As expected, the broadcast ephemeris fits the broadcast clock corrections better than the NSWC ephemeris does. This result would follow from the methods of computation employed in each case.[3]

CONCLUSIONS

The comparison of the broadcast ephemeris with the NSWC post-fit ephemeris indicates that the algorithm to implement the broadcast ephemeris is being applied correctly. The use of the broadcast ephemeris is an advantage because it can be recorded on-line at the same time the observations are made. As a by-product of this checkout procedure, an indication of the relative scatter of local clock residuals computed by using the two satellite ephemerides, but the same observations and satellite clock corrections, have been made. These residuals indicate that the broadcast ephemeris performance is slightly better than the post-fit ephemeris when used in conjunction with the broadcast clock corrections.

Of primary significance is the behavior of the receiver, peripherals, and local frequency standard. No significant problems were experienced throughout this 14-day period, and the data received were of high quality. An indication of the data quality is illustrated by the plots in Appendix A.

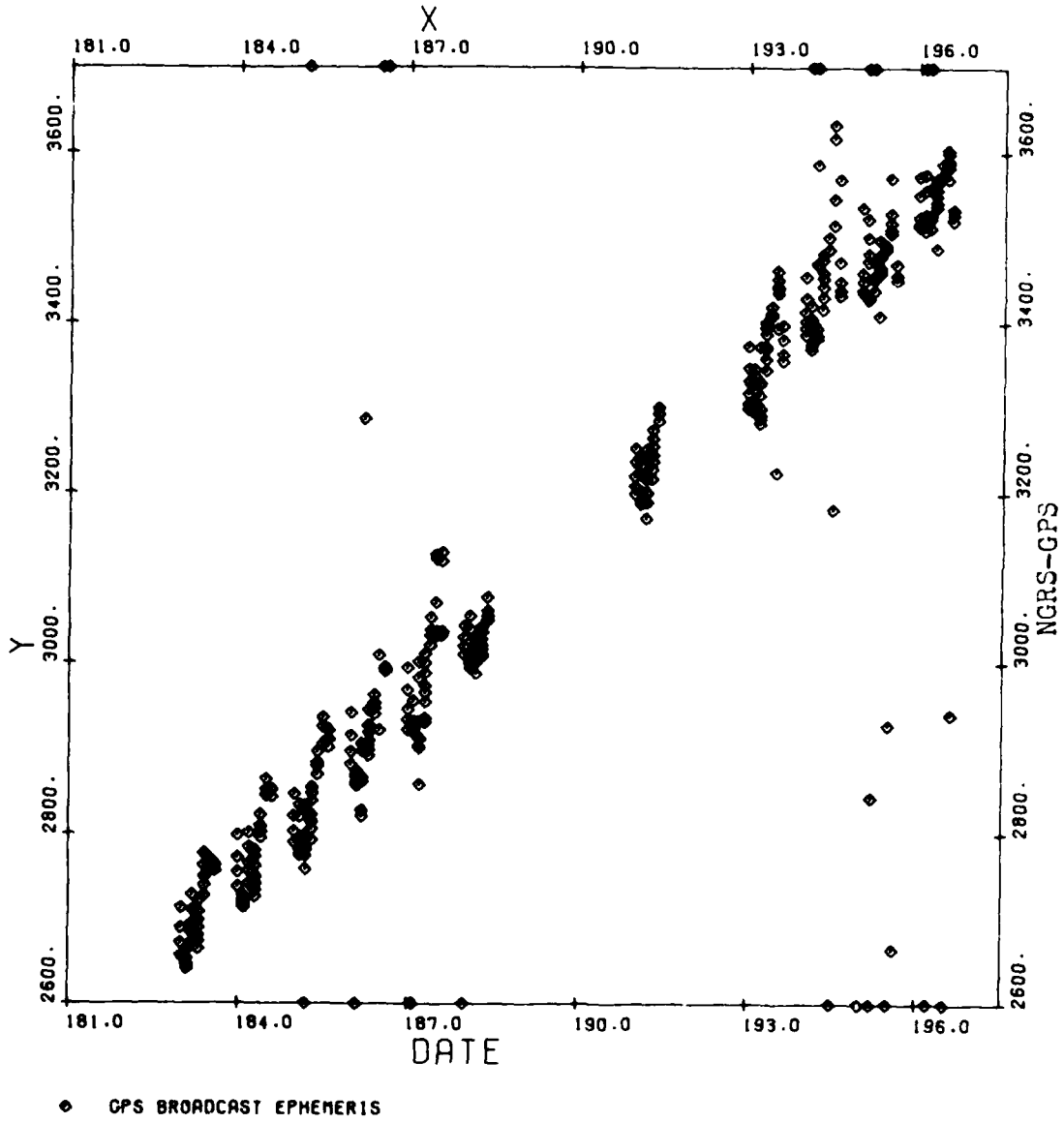

Figure 6. Clock Offset, NGRS-GPS (nsec) vs Date, SV-5, 6, 8, 9, GPS Broadcast Ephemeris, NSWC Dahlgren, Days 182-197 1980

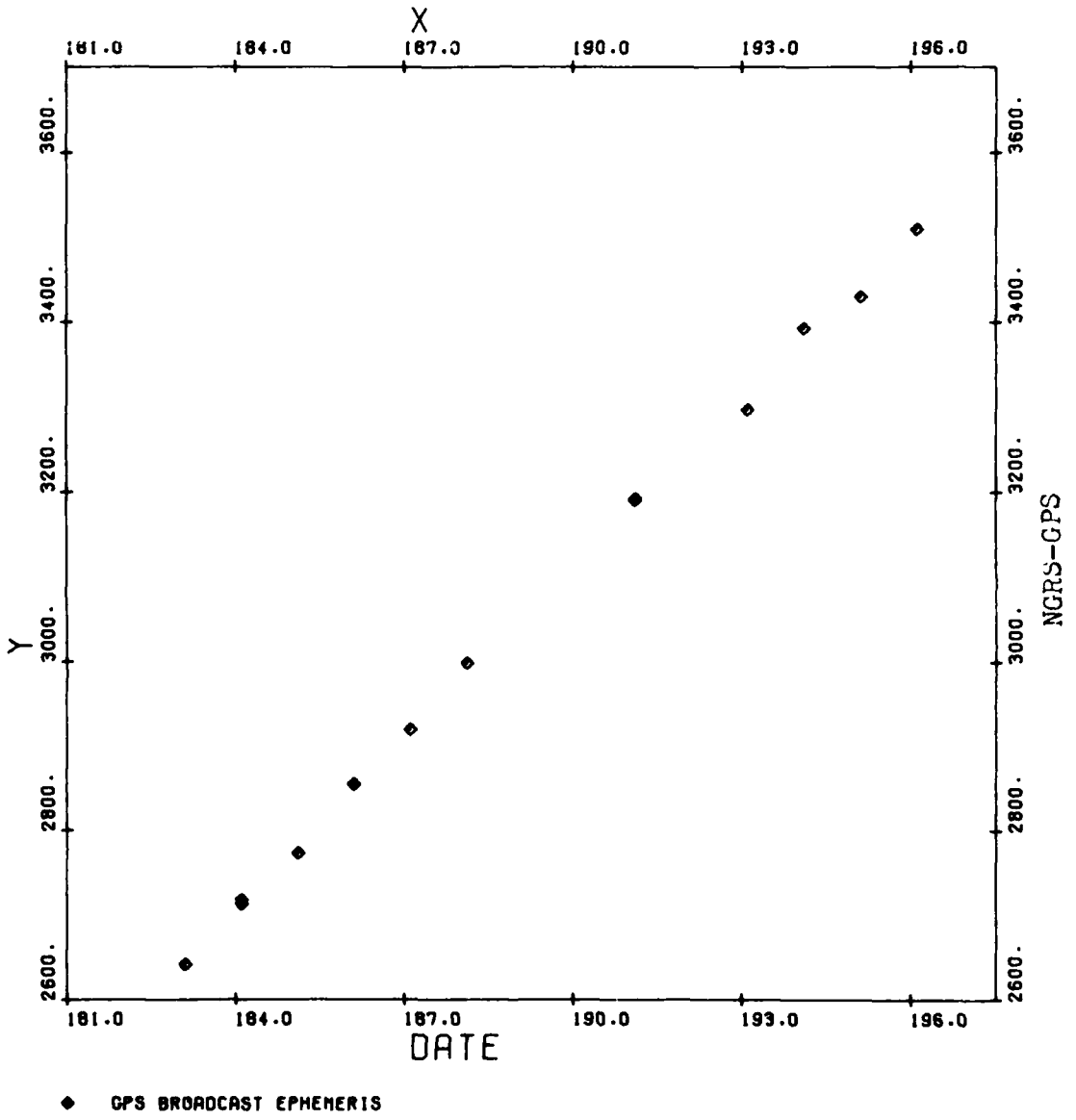

Figure 7. Clock Offset, NGRS-GPS (nsec) vs Date, GPS Broadcast Ephemeris, Elevation >75°, GPS SV-8, NSWC Dahlgren, Days 182-197 1980

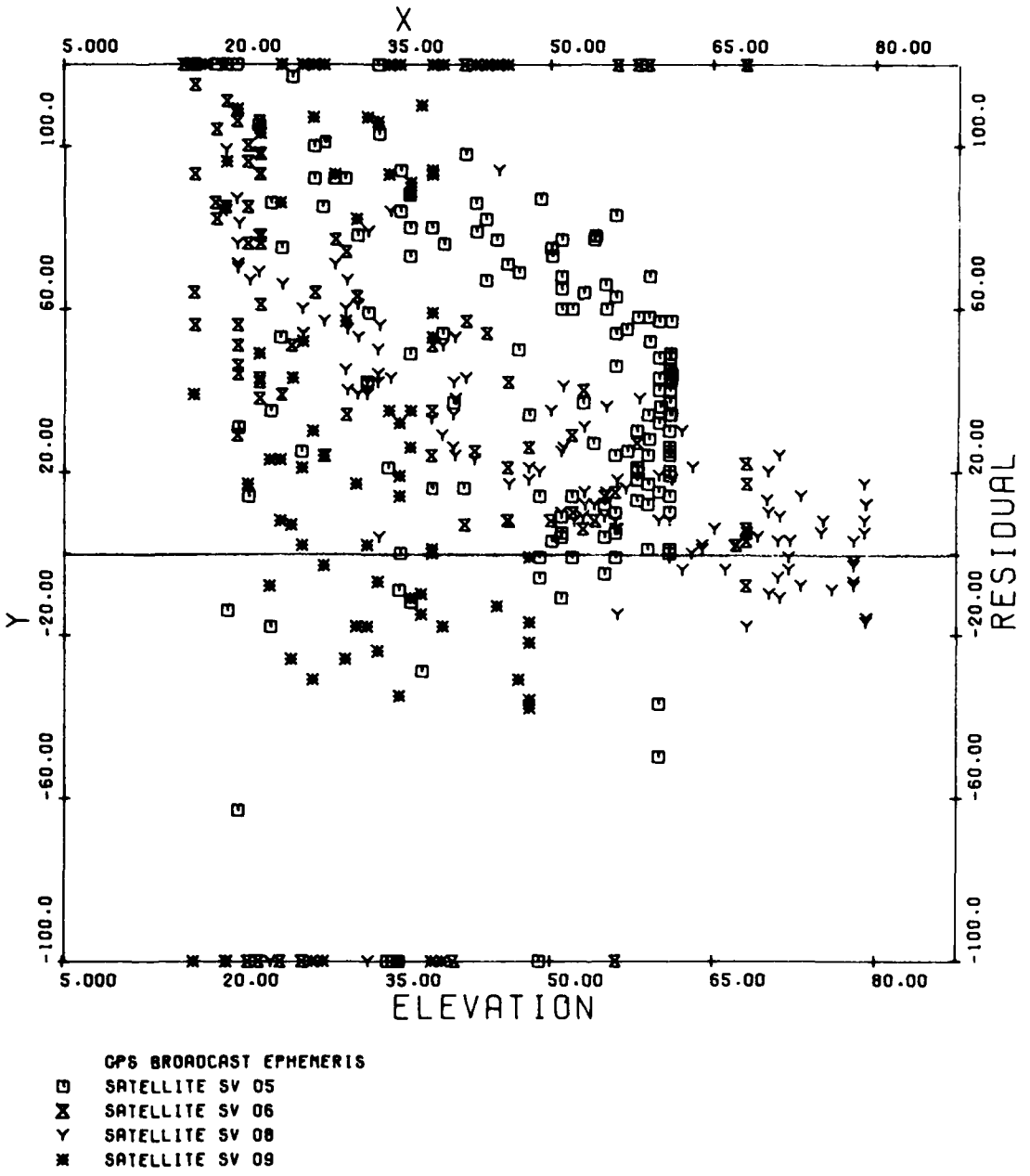

Figure 8. Clock Offset Residual (nsec) vs Elevation (°), NSWC Dahlgren, Days 182-197 1980

REFERENCES

1. B. R. Hermann, *Formulation for the NAVSTAR Geodetic Receiver System*, NSWC TR 80-348, (Dahlgren, Va., March 1981).

2. A. J. Van Dierendonck, S. S. Russell, E. R. Kopitske, and M. Birnbaum, "The GPS Navigation Message," *Navigation, 25*, No. 2, (Summer 1978).

3. A. J. Van Dierendonck, W. C. Melton, M. Birnbaum, M. D. Harkins, "The Approach to Satellite Ephemeris Determination for the NAVSTAR Global Positioning System," *Navigation, 23*, No. 1 (Spring 1976).

APPENDIX A

APPENDIX A

The data contained in this appendix was compiled to perform diagnostic checks on the operation of the NGRS hardware. During the 182-197-day span considered in this report, performance of the system was quite satisfactory as the plots that follow illustrate.

In the NGRS, range and Doppler observations are obtained independently, pseudorange data from L_1 only, and Doppler from L_1 and L_2 simultaneously. The pseudorange data rate was one observation each 6 sec; the Doppler rate was one observation each 60 sec. In order to produce the plots, data from 10 to 20 min of continuous observations were smoothed by fitting the pseudorange with a fourth-degree polynomial, and the range differences with a third-degree polynomial. The RMS of the residuals between the fit and the observations is used as the primary indicator of performance.

Fourth degree fits to pseudorange and third-degree fits to range difference over 20 min produce residuals that have few systematic trends remaining. The residuals are indicative of the observational noise from the various contributing sources such as preamplifier noise, receiver phase jitter, frequency standard fluctuations, and measurement error sources. Results obtained from examination of the plots are summarized in Table A-1.

Table A-1. Average RMS of Residuals (cm)

SV:	5	6	8	9
Pseudorange RMS (L_1)	76.9	66.1	68.8	76.6
Range Difference RMS (L_1)	3.5	3.2	4.1	6.3
Range Difference RMS (L_2)	3.5	3.2	4.1	6.3
Range Difference RMS (corrected)	3.7	3.4	4.2	6.4
Range Difference RMS (ionosphere)	0.8	0.9	0.7	0.9

It is interesting to note that SV-9, whose reference frequency standard is a cesium, indicates a higher RMS residual than the other three satellites whose frequency standards are rubidiums. The NGRS reference is an HP-5061-004 high-performance cesium. The 3-cm residual RMS is probably due to this local reference. Experiments with other cesiums, rubidiums, and quartz oscillators have caused this floor RMS to change as would be expected for the other types of standards. Note that the ionospheric correction RMS is below 1 cm. In calculating this number, much of the correlated noise contribution contained in L_1 and L_2 is removed. For this reason 1 cm is more representative of the system noise from uncorrelated sources.

A set of 12 plots is used to judge the performance of the system over the time span of interest. A set is generated for each satellite observed so that satellite-related anomalies are readily apparent.

1. 20-MIN PSEUDORANGE RMS (cm) VS DATE

The RMS of the residuals of a fourth-degree polynomial fit to 20-min segments of 6-sec L_1 pseudoranges are displayed in the first plot. As was noted in Table A-1, the RMS from all four satellites give about the same results, and there is little variation with date. The 70- to 80-cm RMS represents a 2.7-nsec jitter in the measurement. The vertical spread in the RMS is due to some extent to variations in the elevation angle as is illustrated in the next plot.

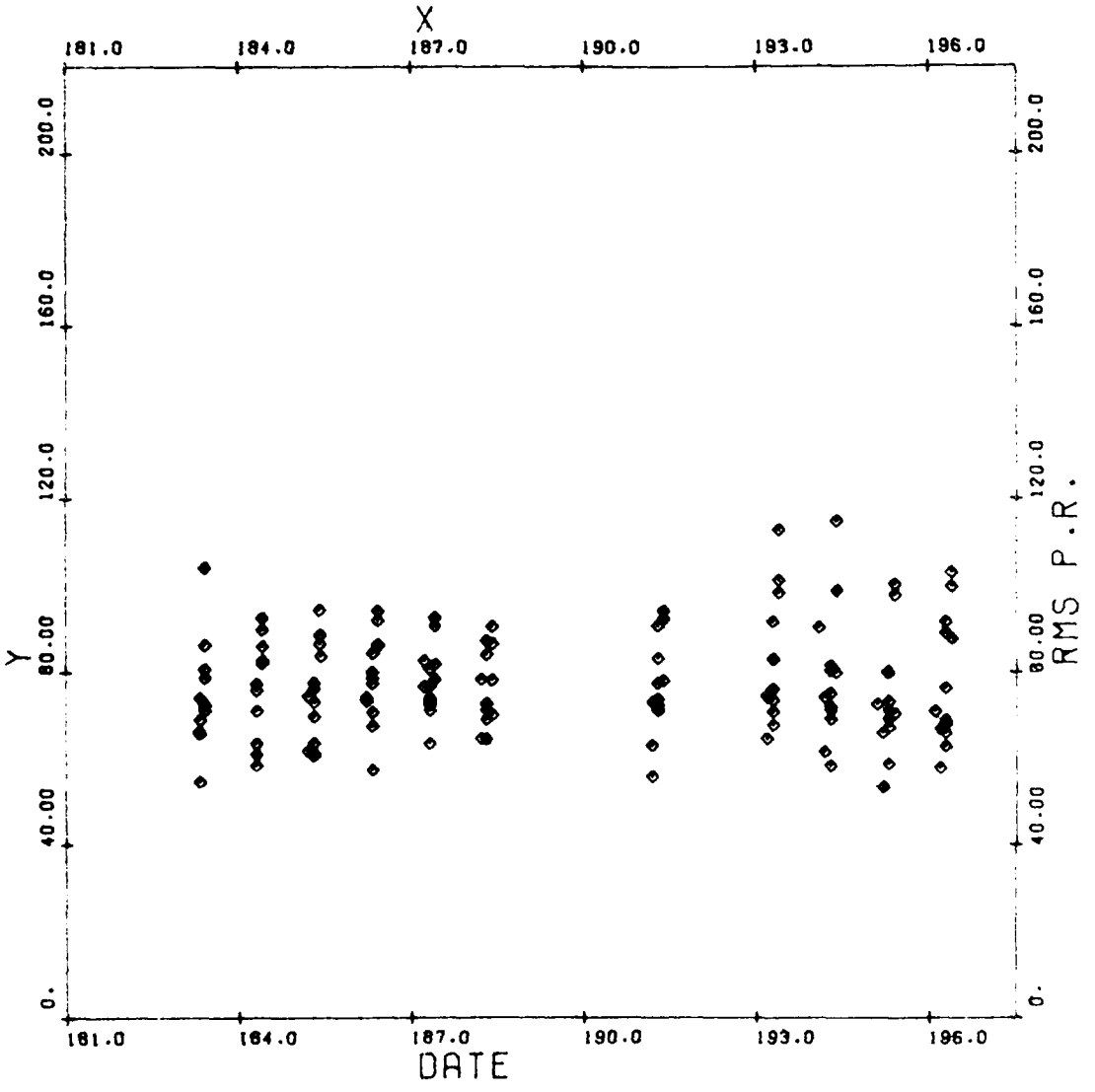

Figure A-1. 20-Min Pseudorange RMS (cm) vs Date, GPS SV-5, NSWC Dahlgren, Days 182-197 1980

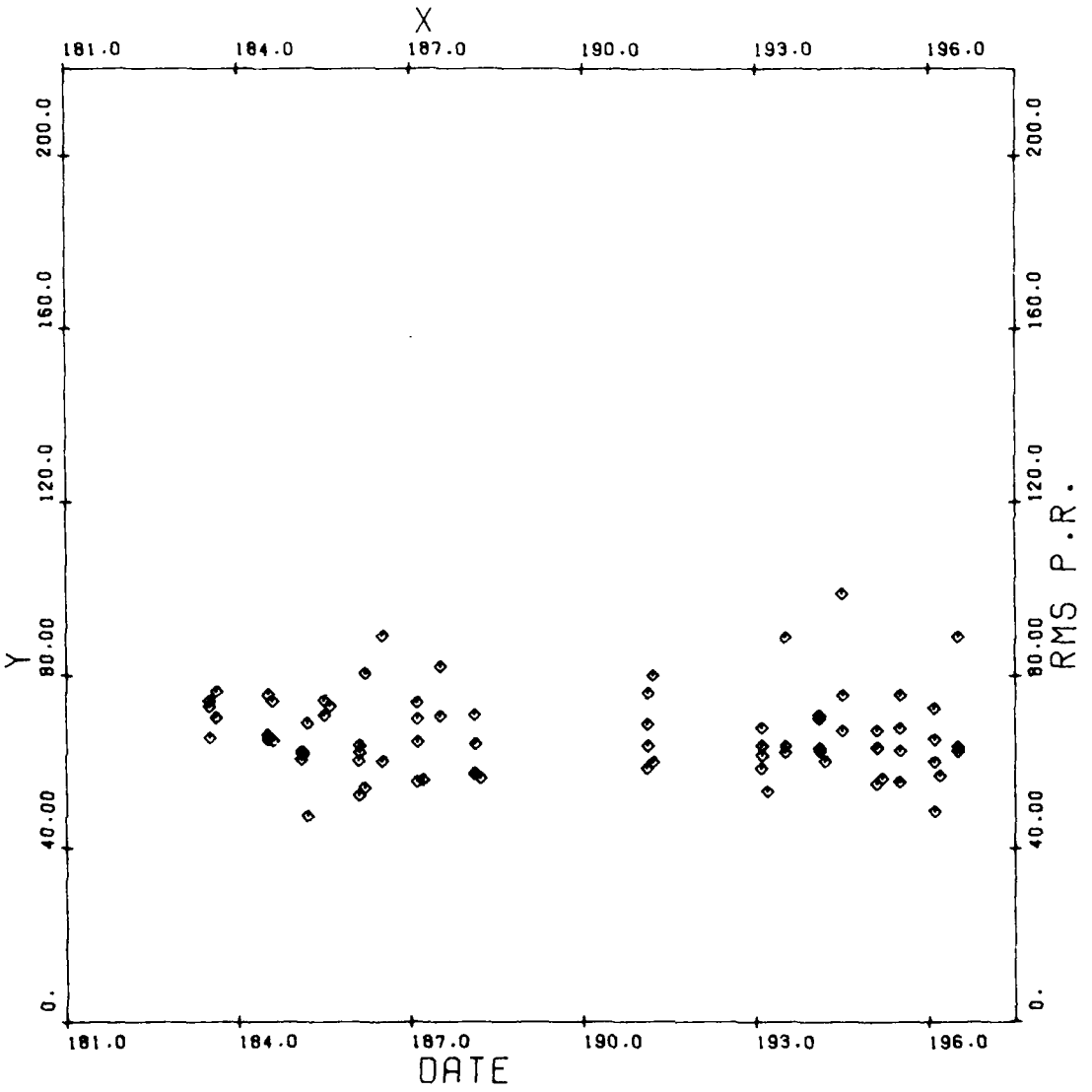

Figure A-2. 20-Min Pseudorange RMS (cm) vs Date, GPS SV-6, NSWC Dahlgren, Days 182-197 1980

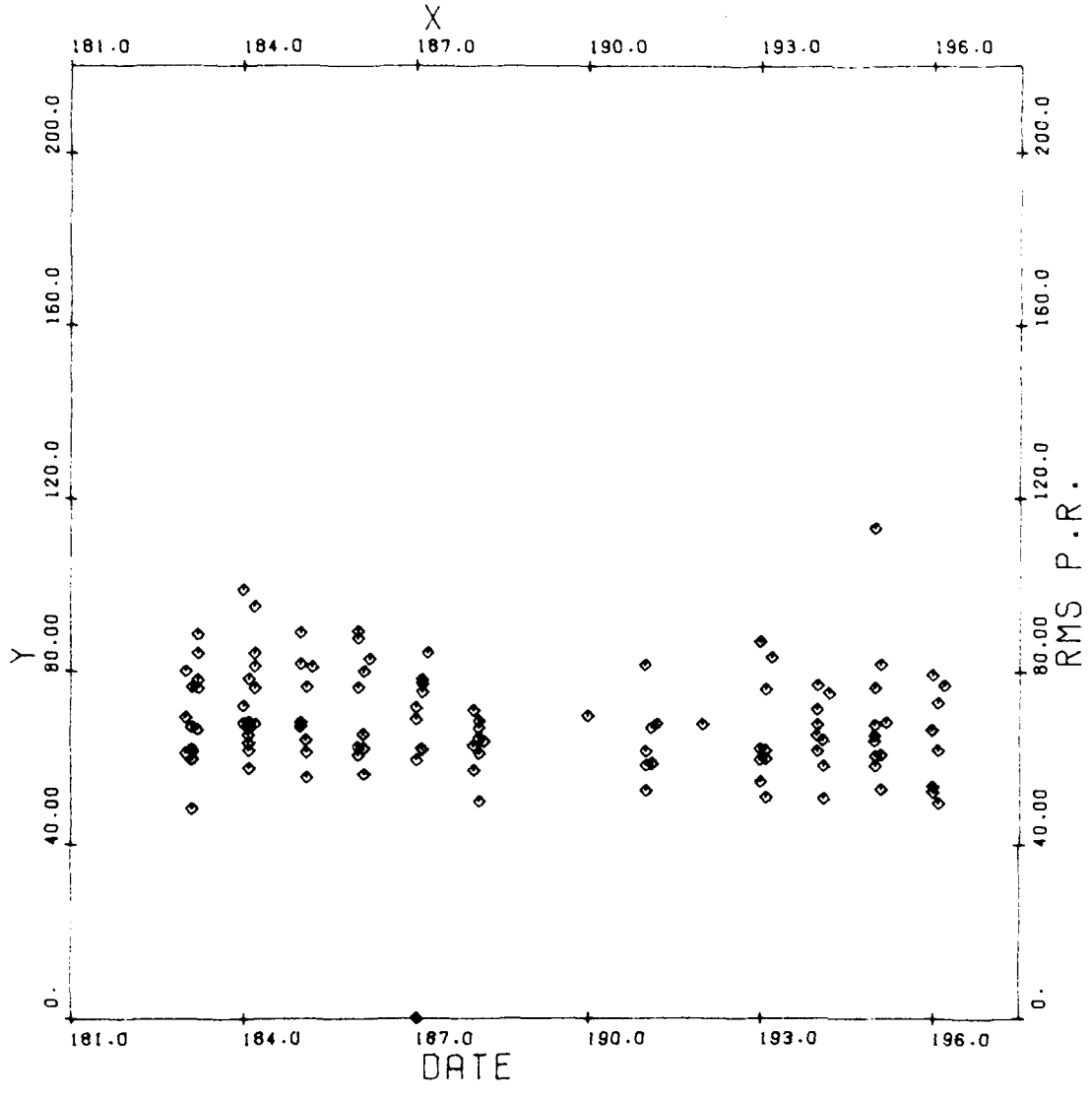

Figure A-3. 20-Min Pseudorange RMS (cm) vs Date, GPS SV-8, NSWC Dahlgren, Days 182-197 1980

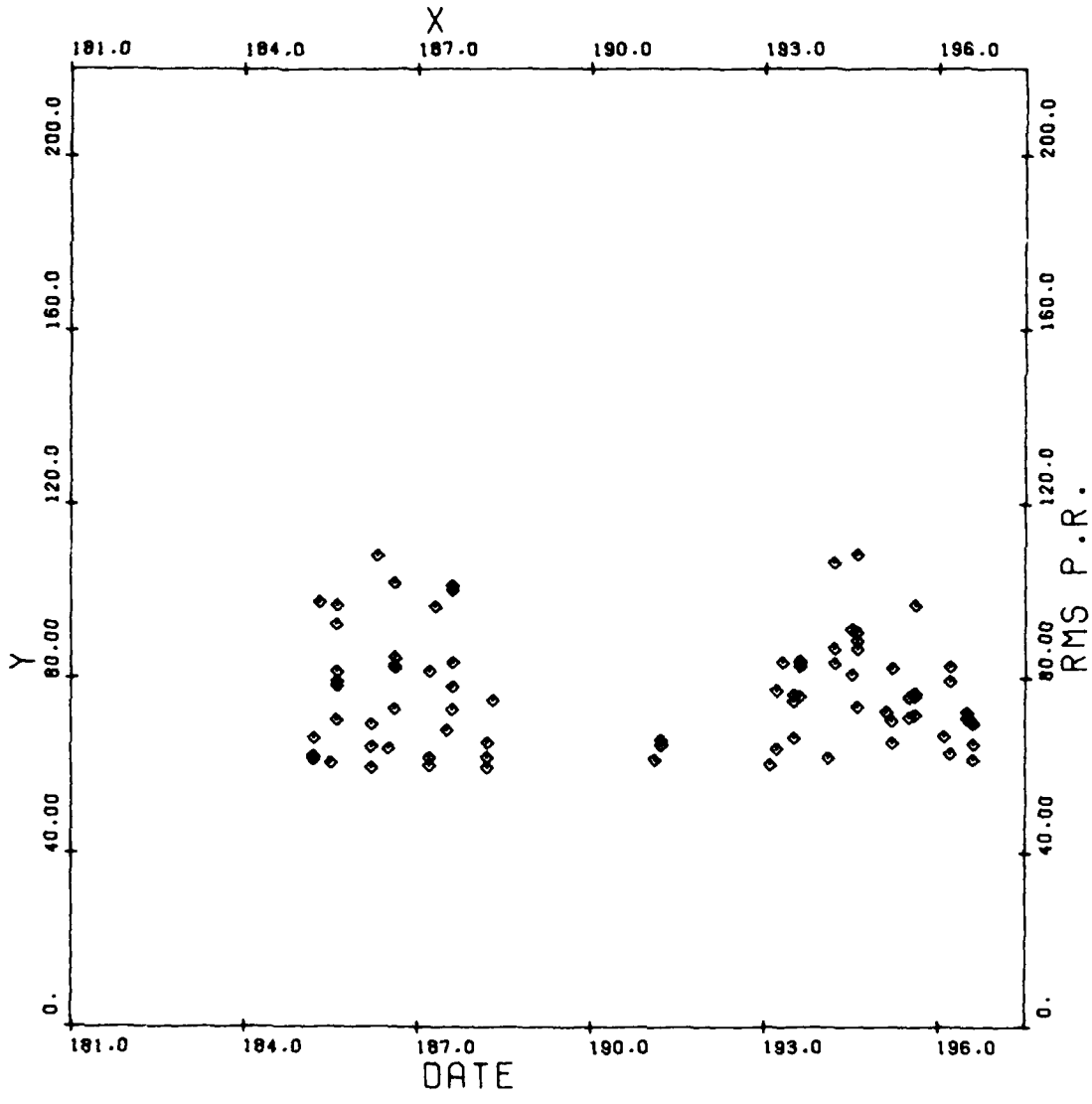

Figure A-4. 20-Min Pseudorange RMS (cm) vs Date, GPS SV-9, NSWC Dahlgren, Days 182-197 1980

2. 20-MIN PSEUDORANGE RMS (cm) VS ELEVATION (°)

In this plot, the pseudorange residuals are plotted versus elevation angle. They show a slight tendency to increase at lower elevations. This is best illustrated by SV-8 because data are available from 20 to 80° elevations. This effect could have two causes. Variations in the propagation path due to ionospheric or tropospheric irregularities would be more apparent at lower elevation angles; also the signal strength will decrease slightly due to increased range and reduced antenna gain.

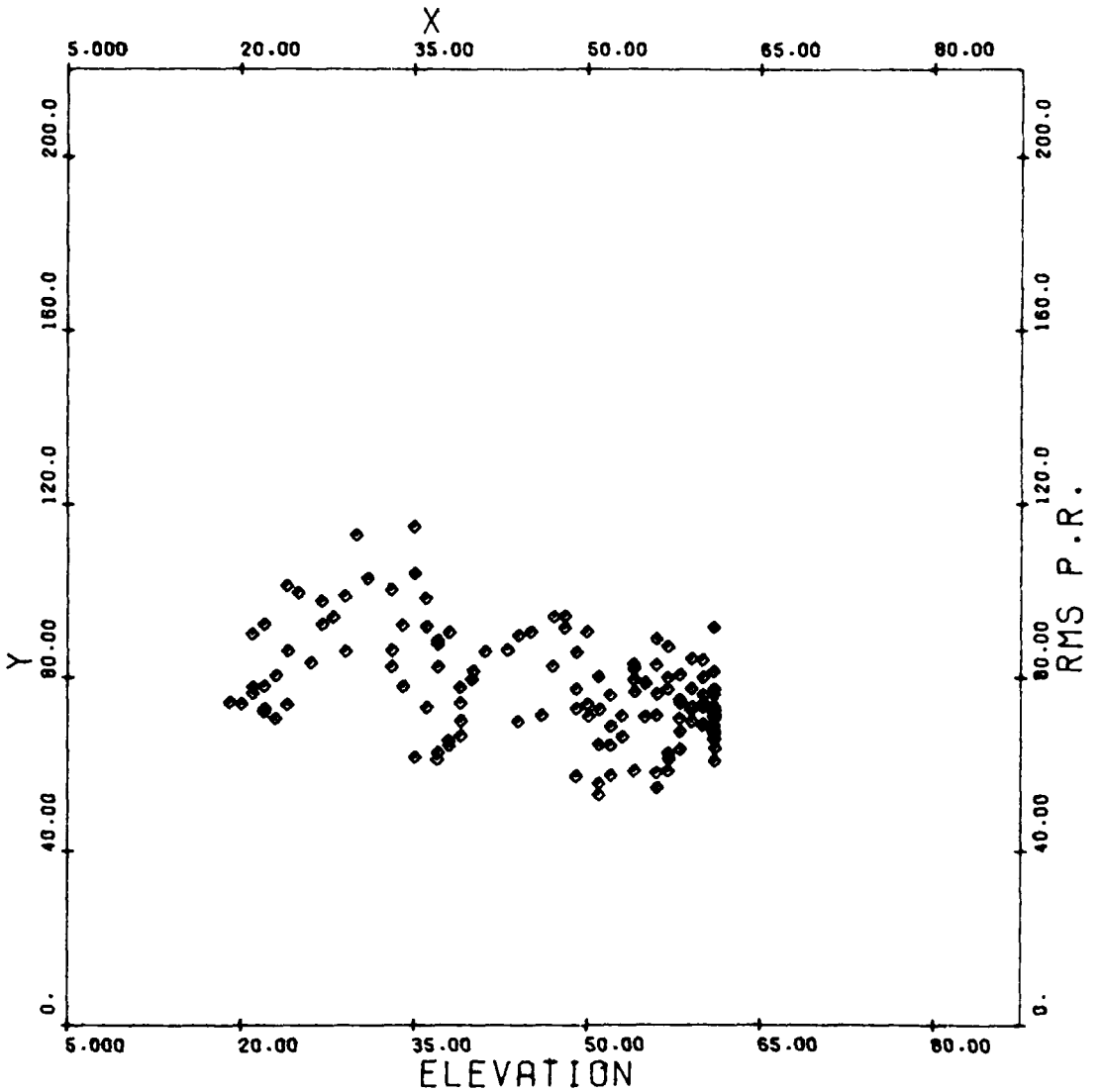

Figure A-5. 20-Min Pseudorange RMS (cm) vs Elevation (°), GPS SV-5, NSWC Dahlgren, Days 182-197 1980

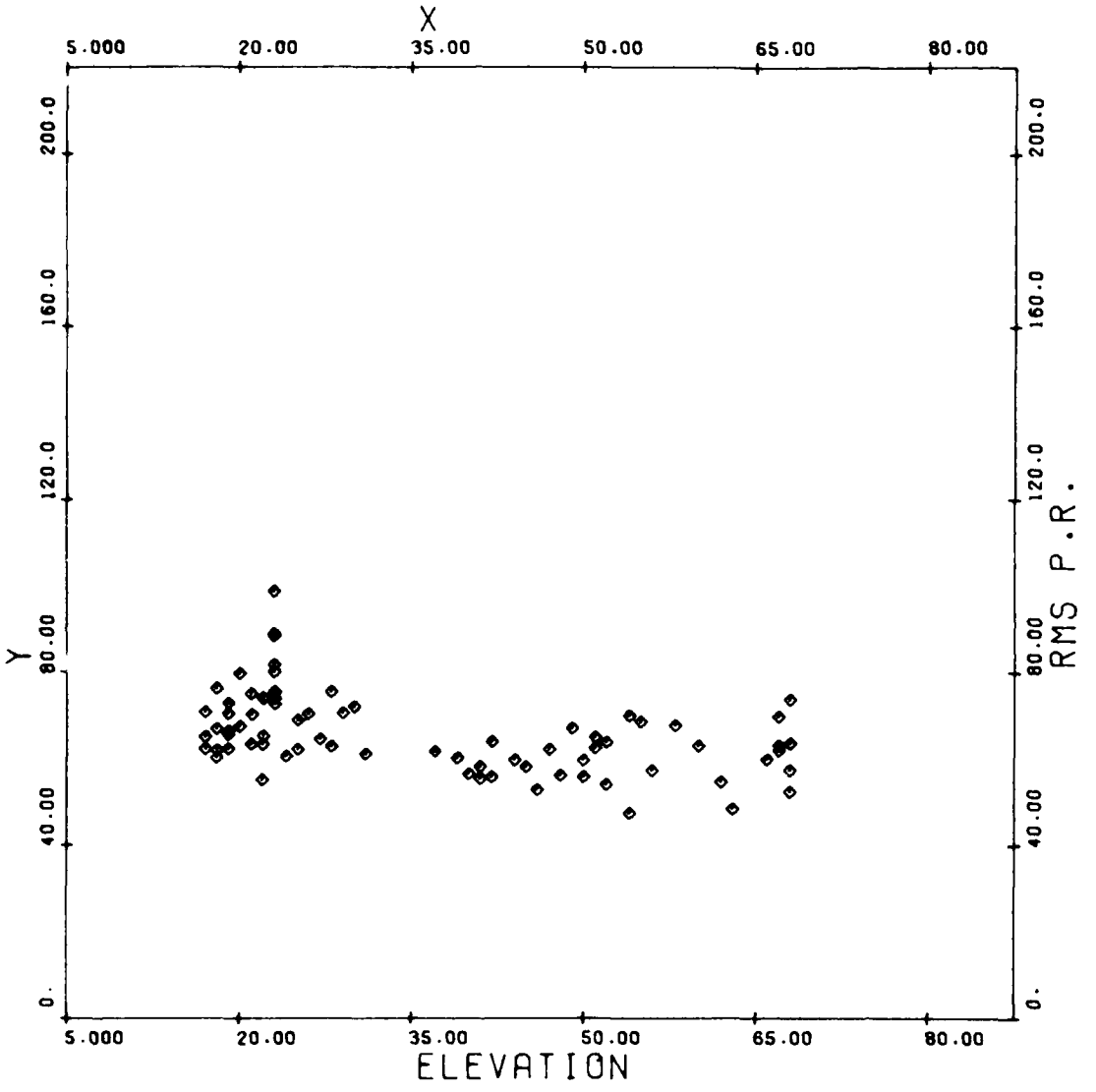

Figure A-6. 20-Min Pseudorange RMS (cm) vs Elevation (°), GPS SV-6, NSWC Dahlgren, Days 182-197 1980

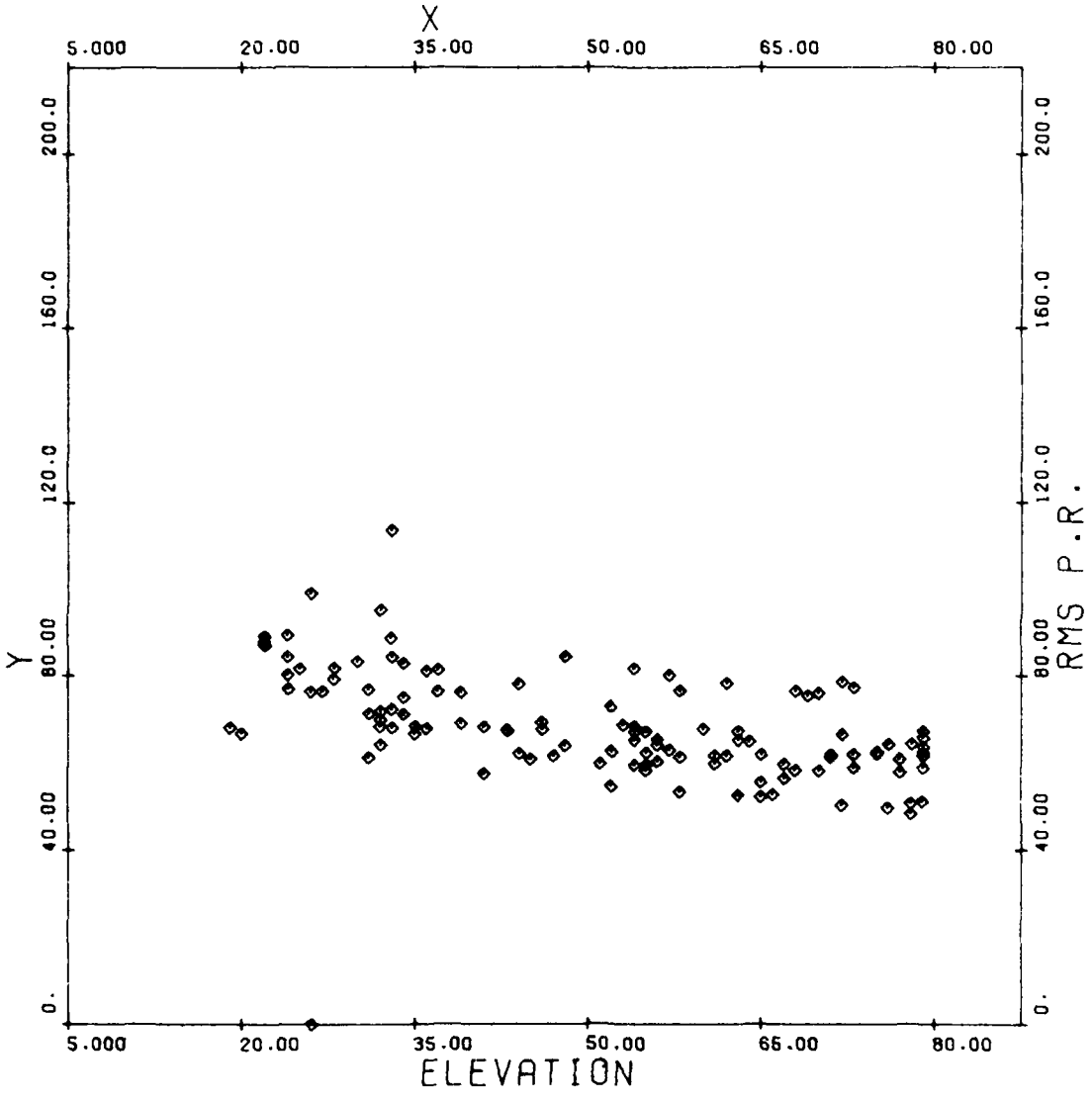

Figure A-7. 20-Min Pseudorange RMS (cm) vs Elevation (°), GPS SV-8, NSWC Dahlgren, Days 182-197 1980

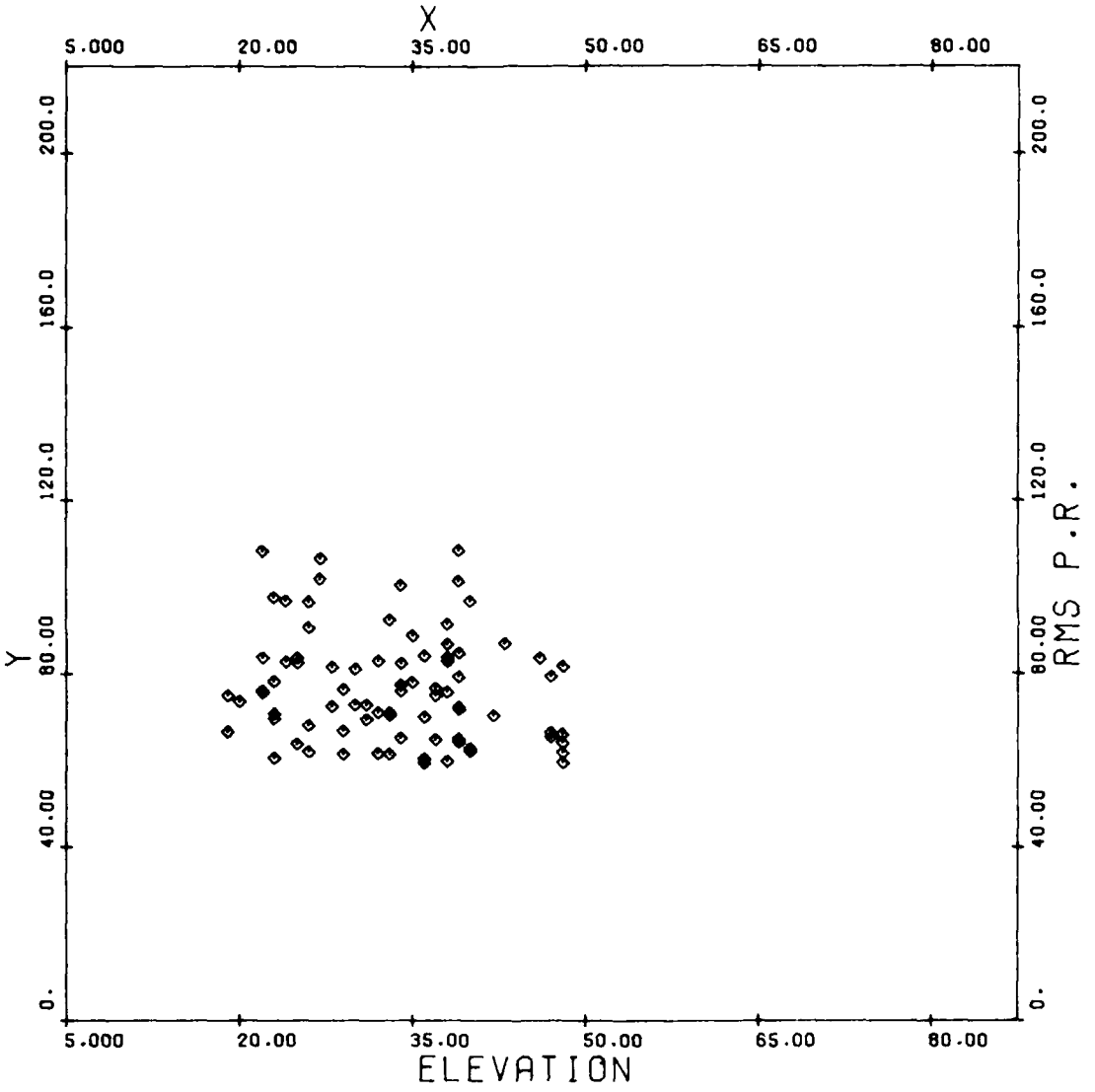

Figure A-8. 20-Min Pseudorange RMS (cm) vs Elevation (°), GPS SV-9, NSWC Dahlgren, Days 182-197 1980

3. 20-MIN L_1 RANGE DIFFERENCE RMS (cm) VS DOPPLER (Hz)

The RMS of the residuals of a third-degree polynomial fit to 20-min segments of 60-sec L_1 range differences (derived from Doppler) is displayed versus the Doppler frequency. A positive Doppler frequency indicates approach. There is little variation with Doppler frequency, and all residuals are clustered around 3.5 cm except for SV-9. This can be explained by the knowledge that the frequency standard being used in SV-9 was a cesium not a rubidium as in the other satellites. Since the other three satellites show little difference, the apparent 3.5-cm floor is probably due to the local frequency standard.

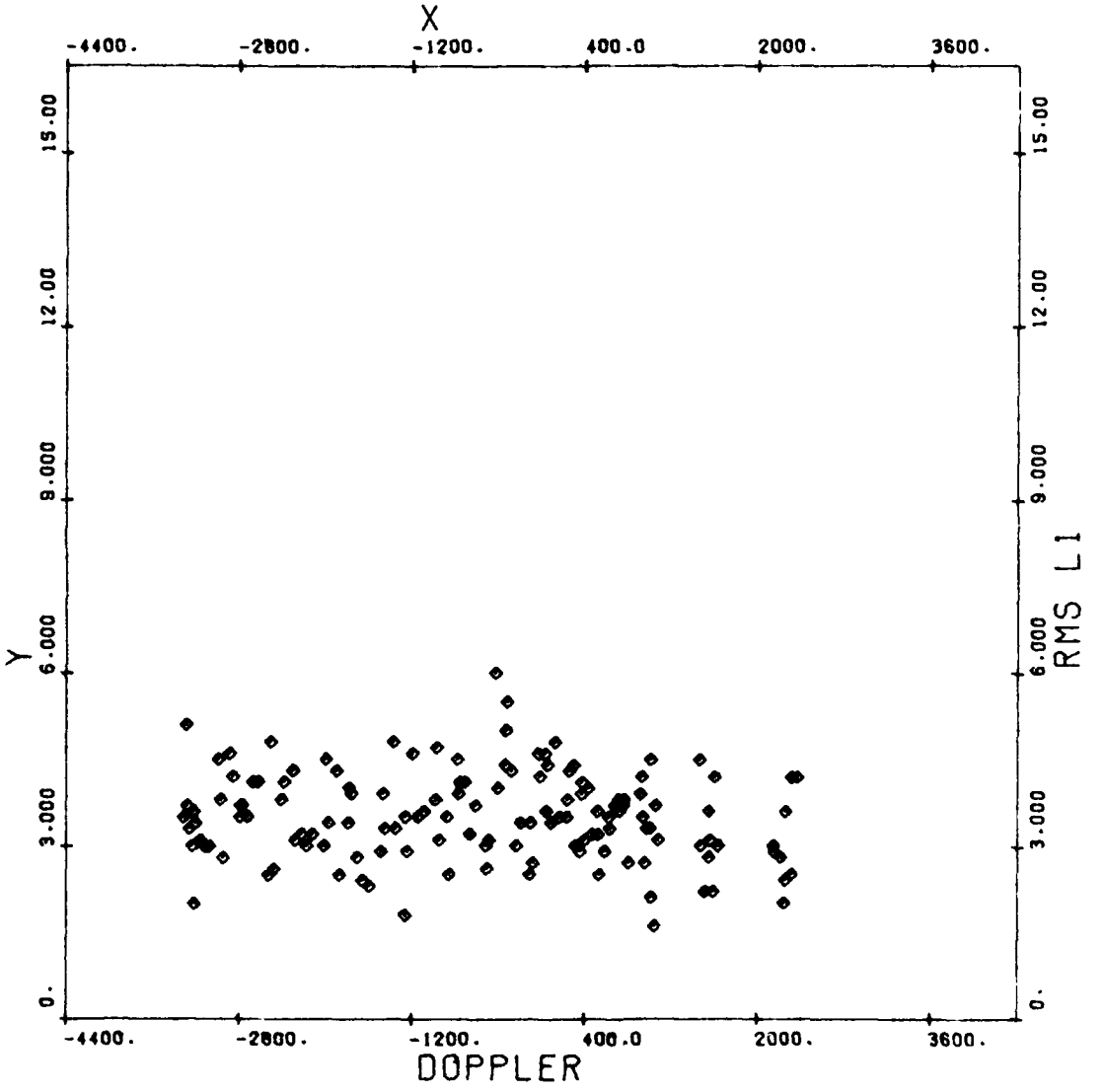

Figure A-9. 20-Min L_1 Range Difference RMS (cm) vs Doppler (Hz), GPS SV-5, NSWC Dahlgren, Days 182-197 1980

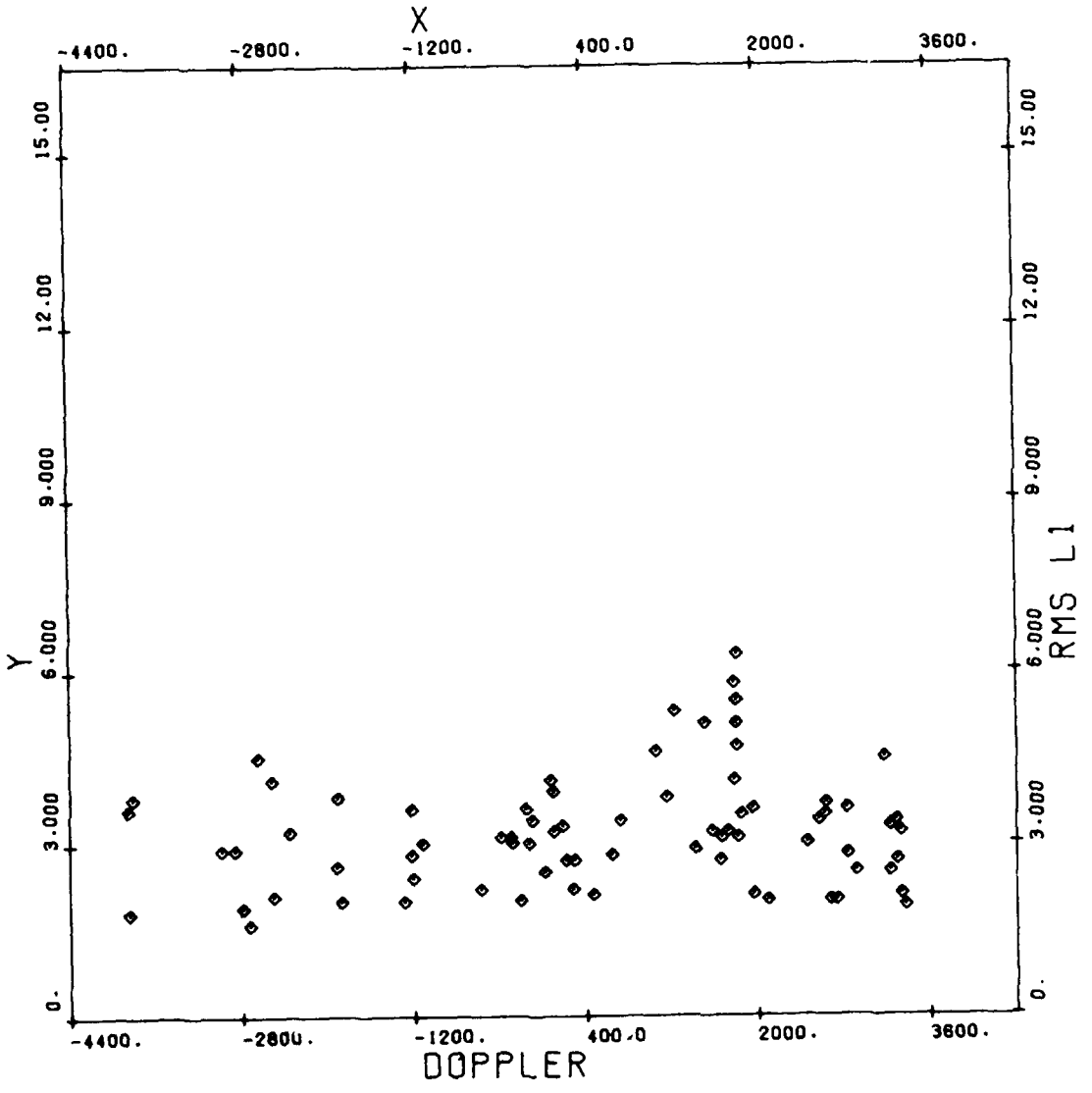

Figure A-10. 20-Min L_1 Range Difference RMS (cm) vs Doppler (Hz), GPS SV-6, NSWC Dahlgren, Days 182-197 1980

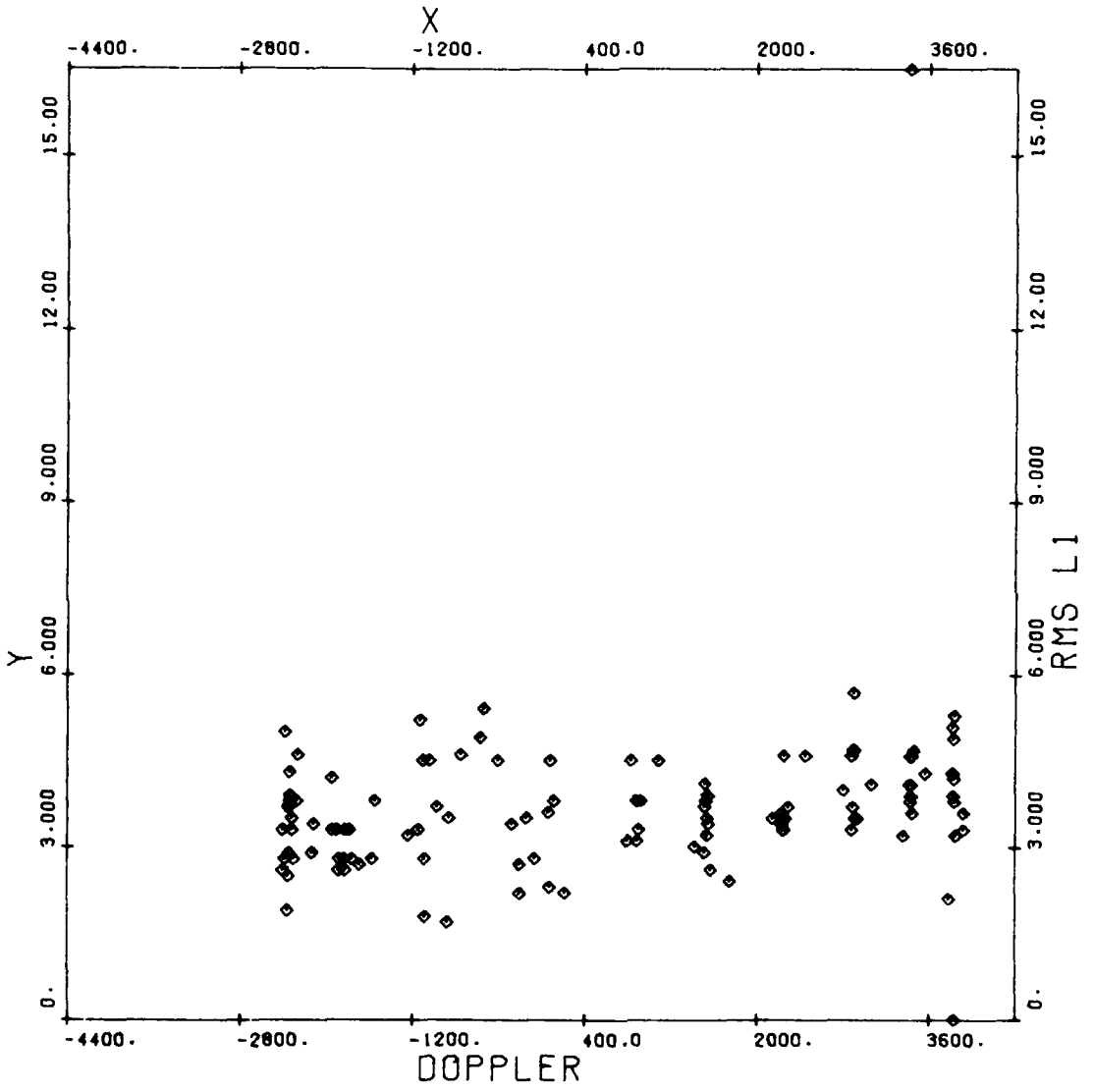

Figure A-11. 20-Min L_1 Range Difference RMS (cm) vs Doppler (Hz), GPS SV-8, NSWC Dahlgren, Days 182-197 1980

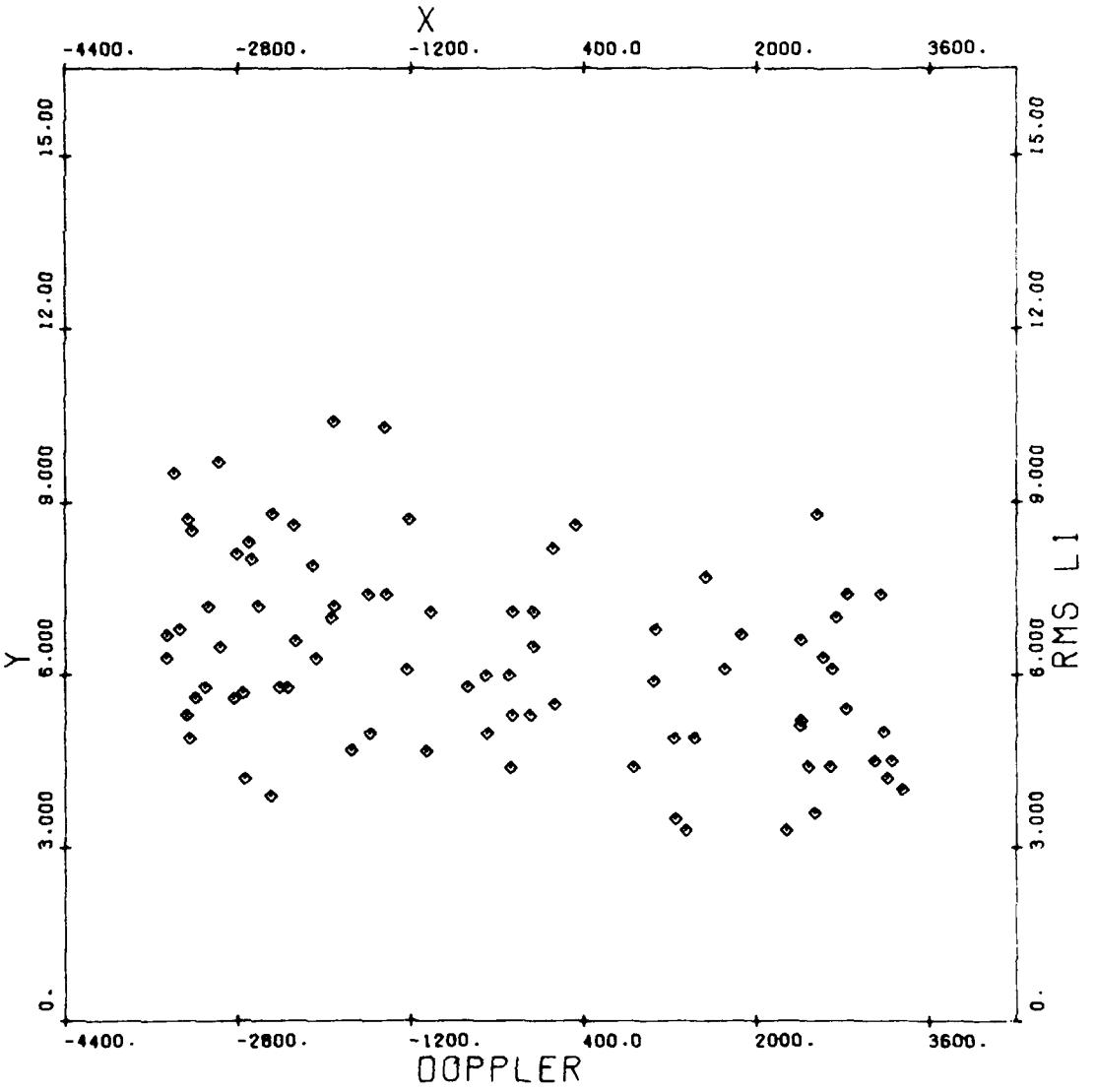

Figure A-12. 20-Min L_1 Range Difference RMS (cm) vs Doppler (Hz), GPS SV-9, NSWC Dahlgren, Days 182-197 1980

4. 20-MIN L_1 RANGE DIFFERENCE RMS (cm) VS ELEVATION (°)

The same range difference residuals appearing in plot 3 are presented versus elevation angle in plot 4. The data from SV-8 indicates that there is little or no variation from 20 to 80°. Only SV-6 suggests that low-elevation angles and larger RMS residuals correlate.

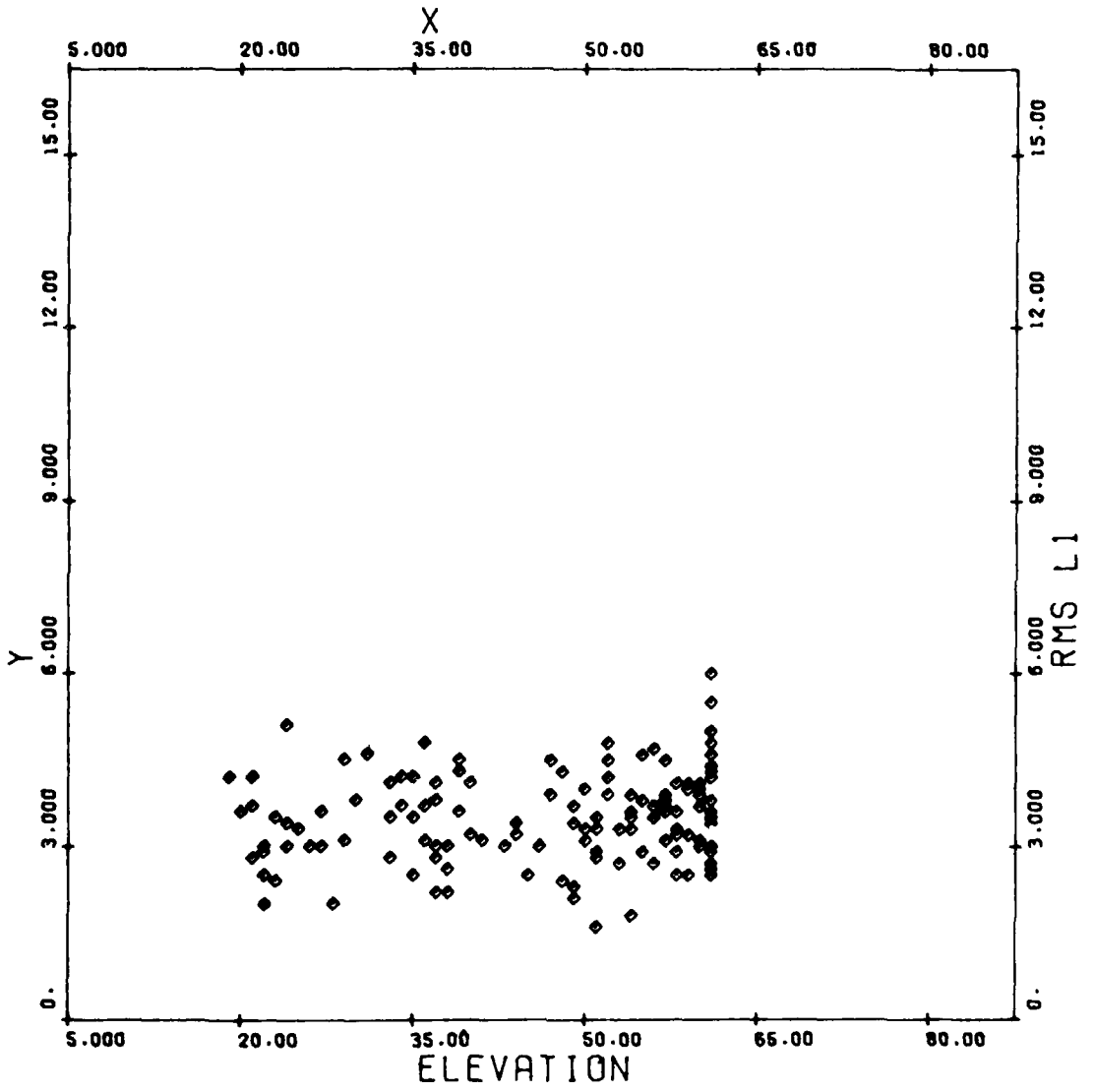

Figure A-13. 20-Min L_1 Range Difference RMS (cm) vs Elevation (°), GPS SV-5, NSWC Dahlgren, Days 182-197 1980

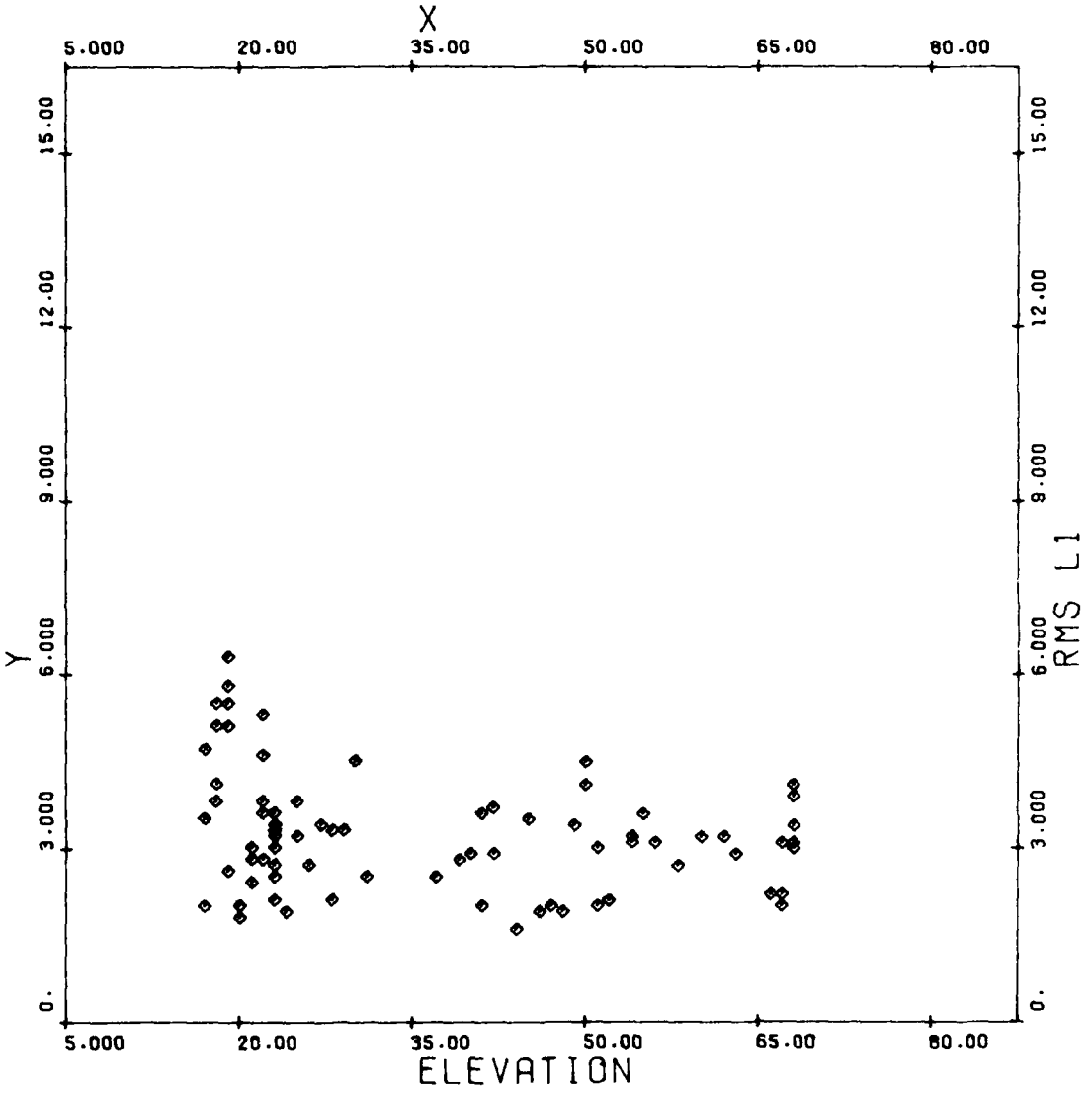

Figure A-14. 20-Min L_1 Range Difference RMS (cm) vs Elevation (°), GPS SV-6, NSWC Danlgren, Days 182-197 1980

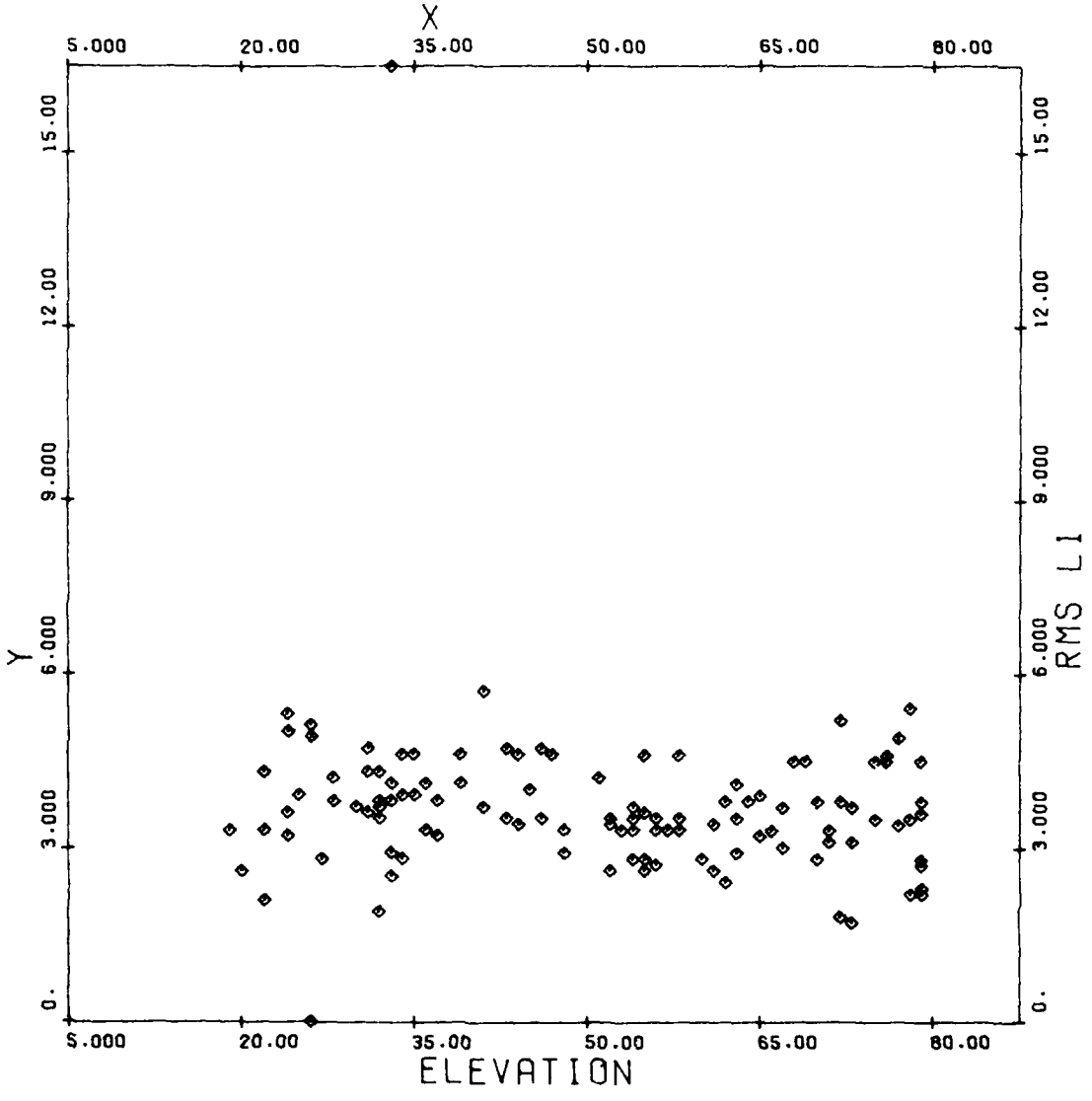

Figure A-15. 20-Min L_1 Range Difference RMS (cm) vs Elevation (°), GPS SV-8, NSWC Dahlgren, Days 182-197 1980

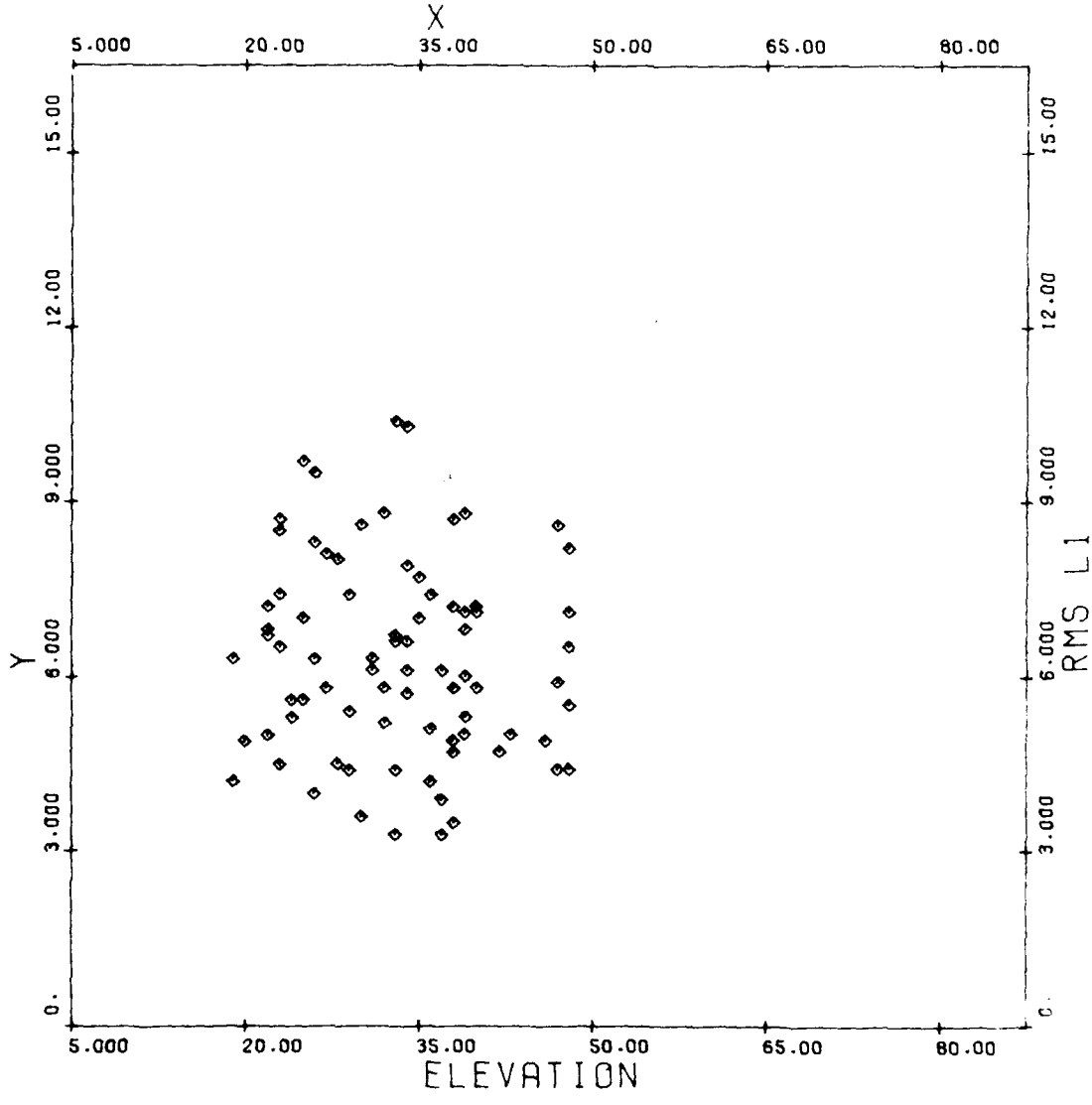

Figure A-16. 20-Min L_1 Range Difference RMS (cm) vs Elevation (°), GPS SV-9, NSWC Dahlgren, Days 182-197 1980

5. 20-MIN L_2 RANGE DIFFERENCE RMS (cm) VS DOPPLER (Hz)

The RMS of the range difference residuals from L_2 are displayed in plot 5. The comments attached to plot 3 also apply here. These L_1 and L_2 results are highly correlated by the common frequency standard.

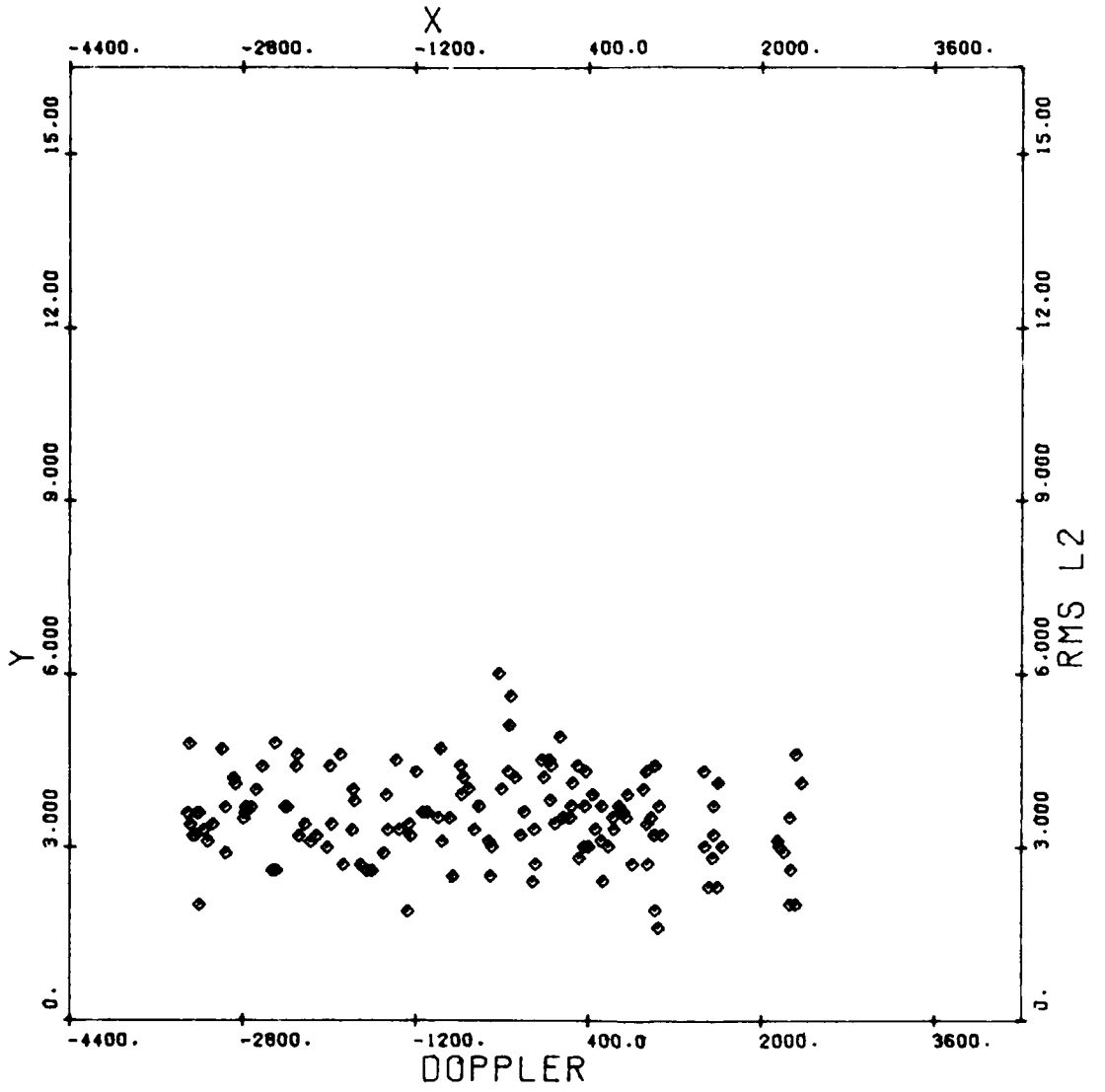

Figure A-17. 20-Min L_2 Range Difference RMS (cm) vs Doppler (Hz), GPS SV-5, NSWC Dahlgren, Days 182-197 1980

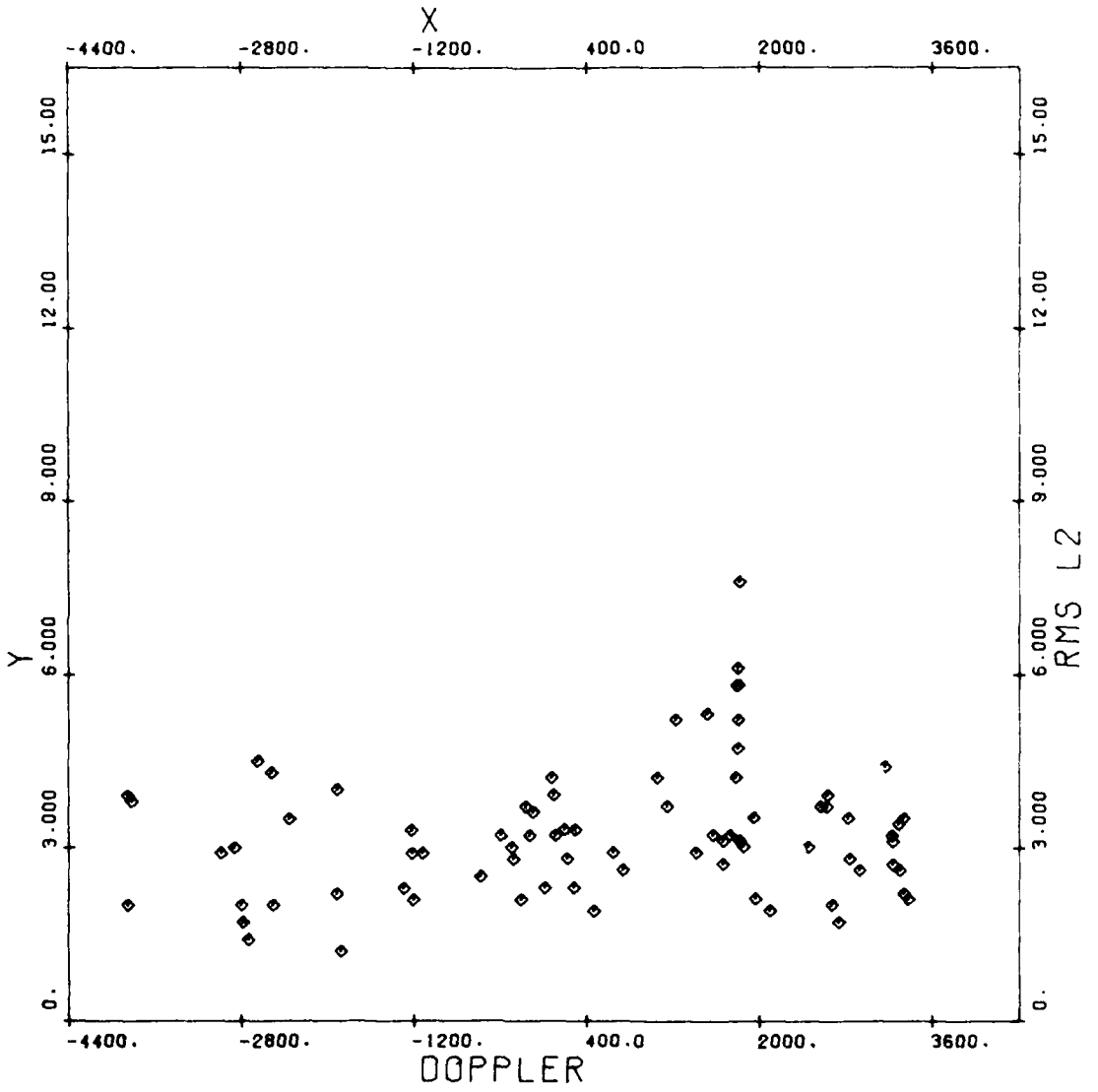

Figure A-18. 20-Min L_2 Range Difference RMS (cm) vs Doppler (Hz), GPS SV-6, NSWC Dahlgren, Days 182-197 1980

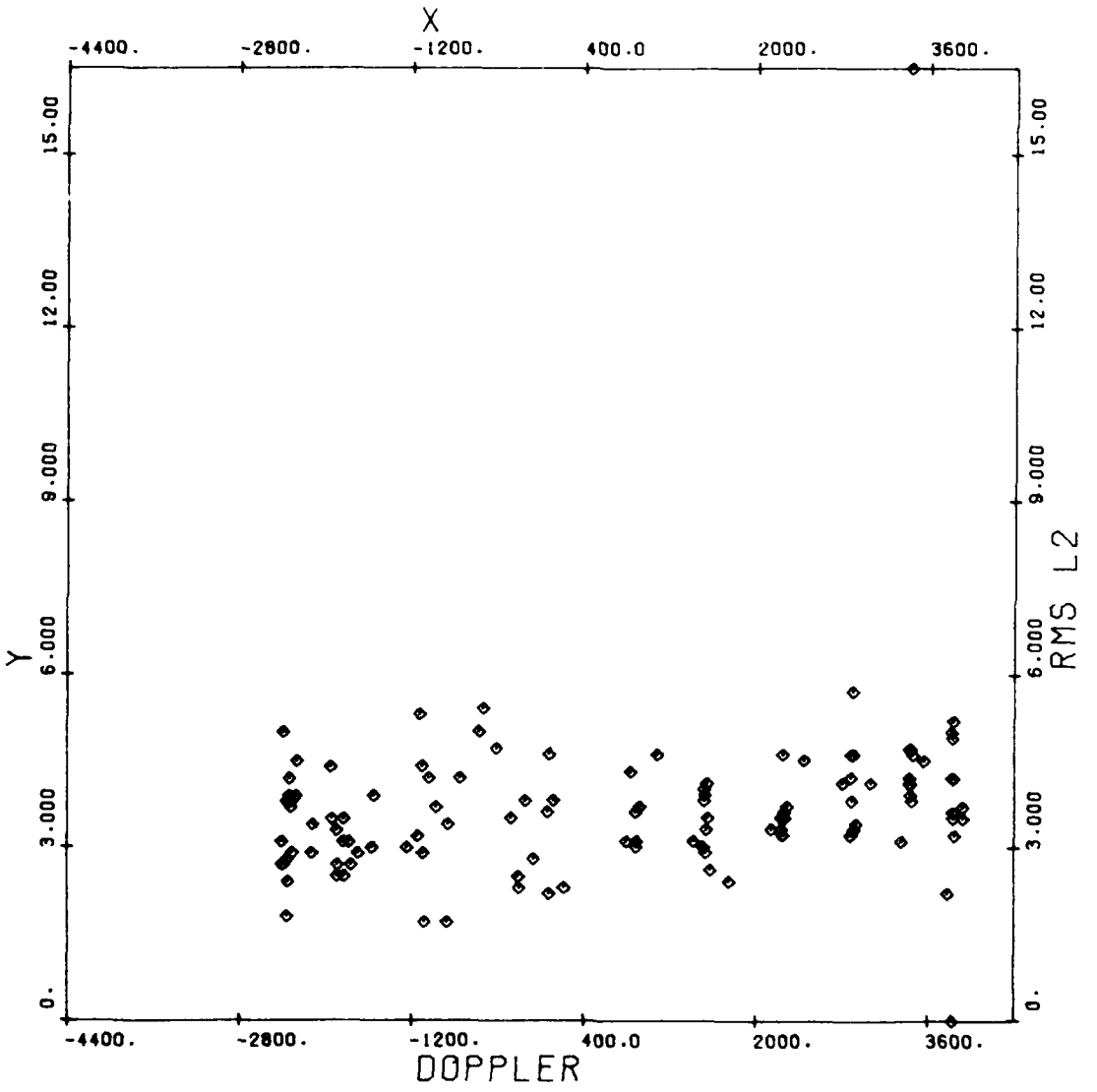

Figure 19. 20-Min L_2 Range Difference RMS (cm) vs Doppler (Hz), GPS SV-8, NSWC Dahlgren, Days 182-197 1980

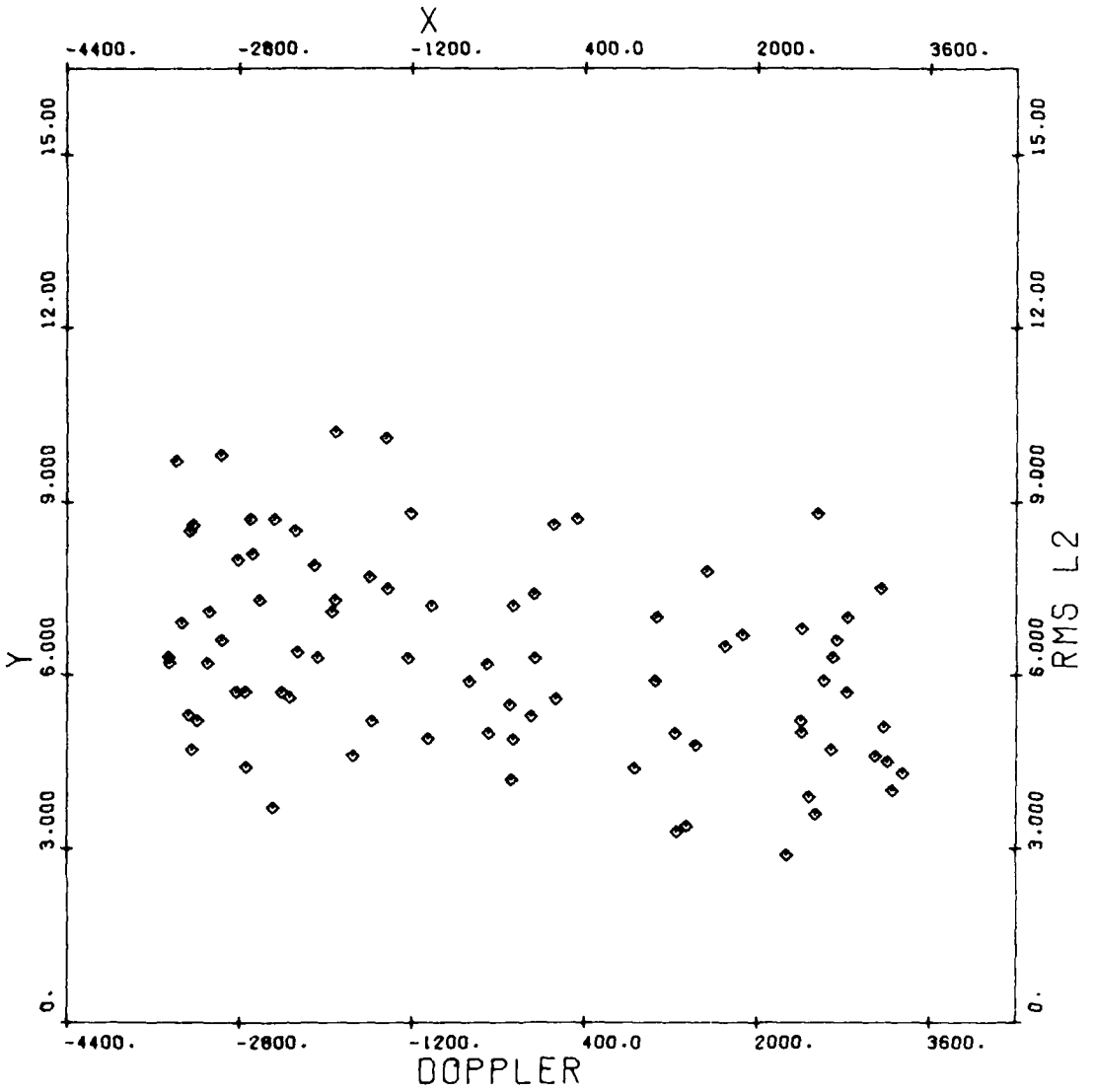

Figure A-20. 20-Min L_2 Range Difference RMS (cm) vs Doppler (Hz), GPS SV-9, NSWC Dahlgren, Days 182-197 1980

6. 20-MIN CORRECTED RANGE DIFFERENCE RMS (cm) VS DOPPLER (Hz)

The RMS of the ionospheric corrected range difference residuals shows that combining the L_1 and L_2 observations to obtain the correction does not degrade the observational accuracy to any great extent. This result is in contrast to the corrected pseudorange observation error.

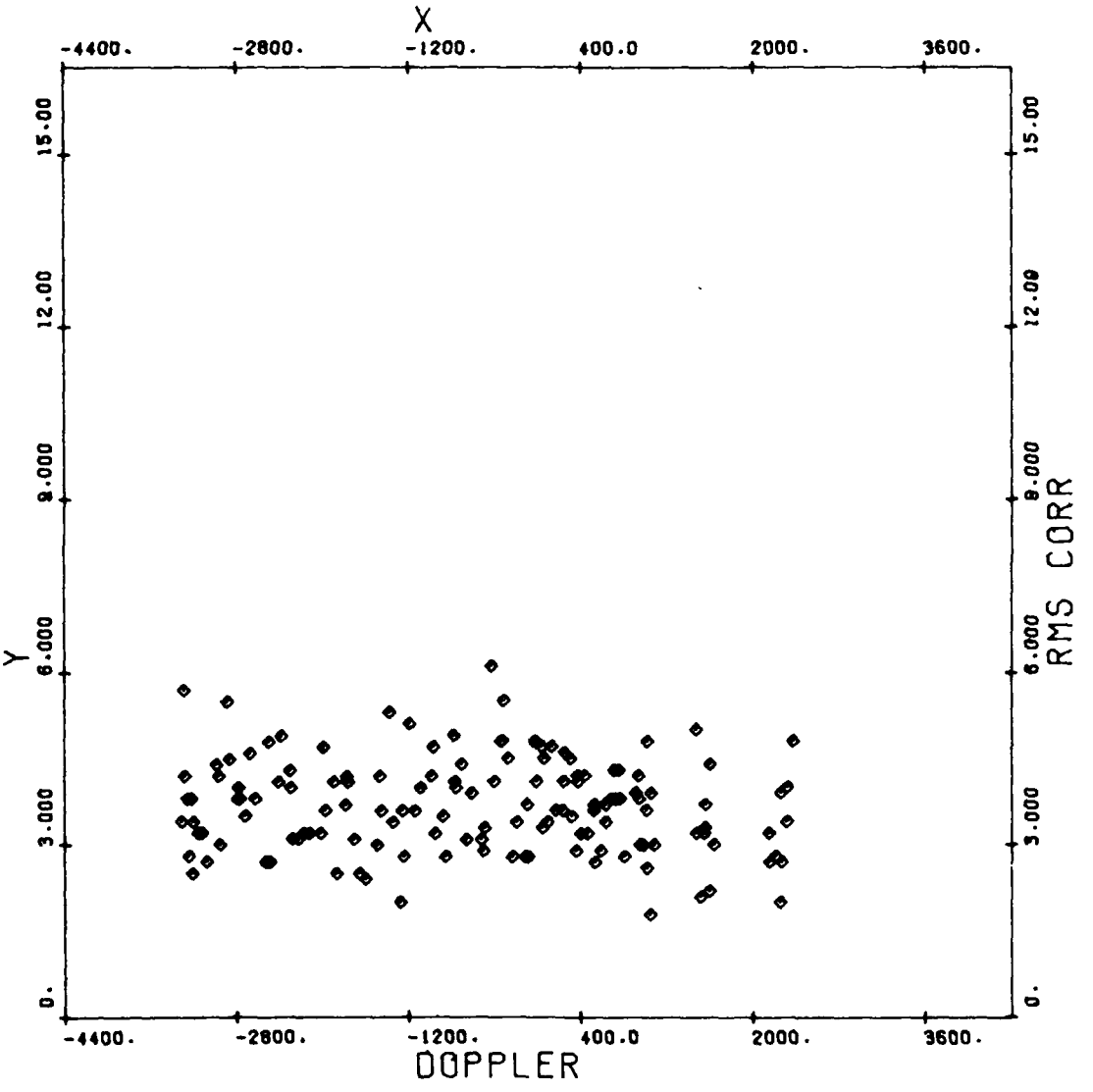

Figure A-21. 20-Min Corrected Range Difference RMS (cm) vs Doppler (Hz), GPS SV-5, NSWC Dahlgren, Days 182-197 1980

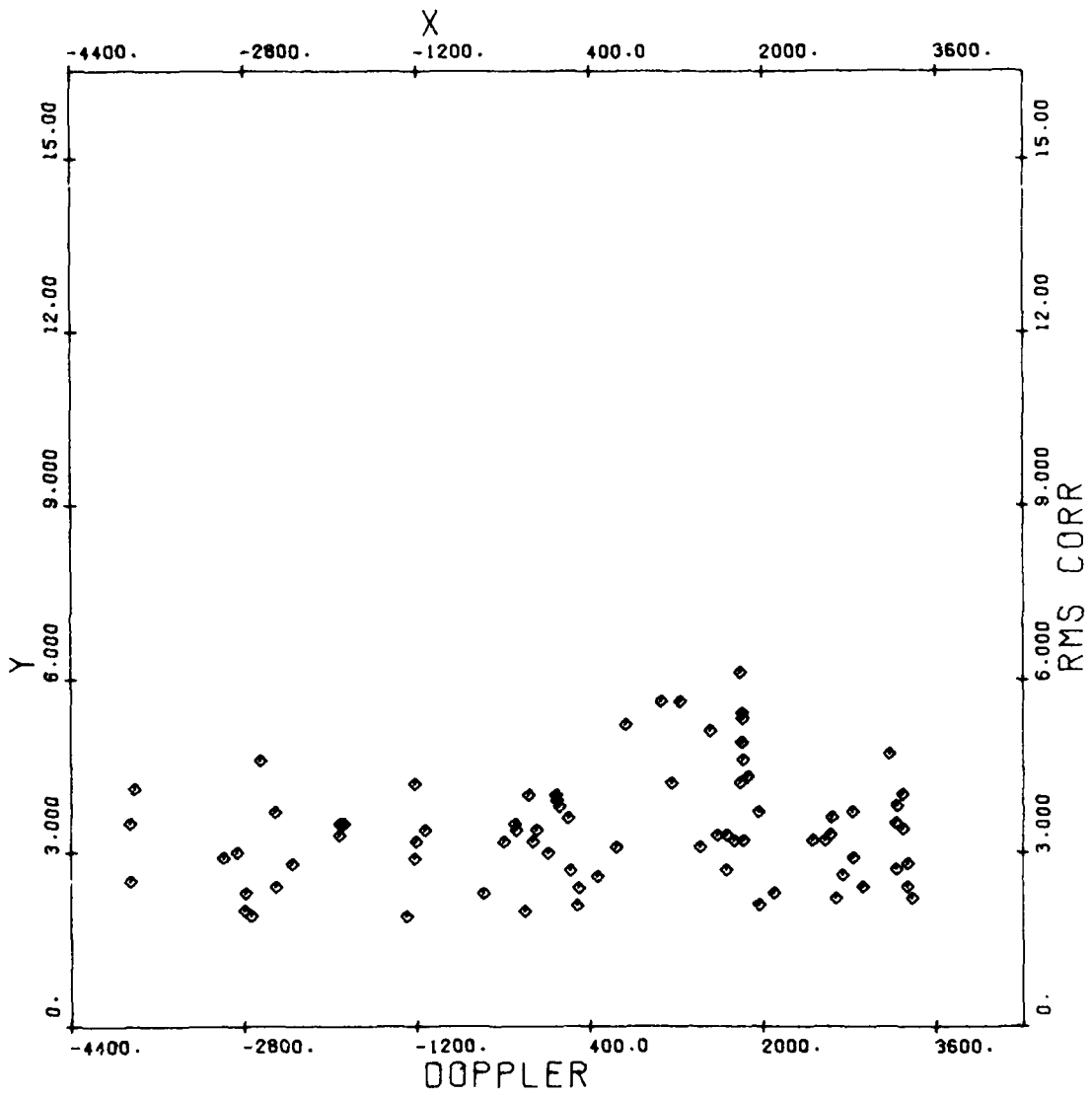

Figure A-22. 20-Min Corrected Range Difference RMS (cm) vs Doppler (Hz), GPS SV-6, NSWC Dahlgren, Days 182-197 1980

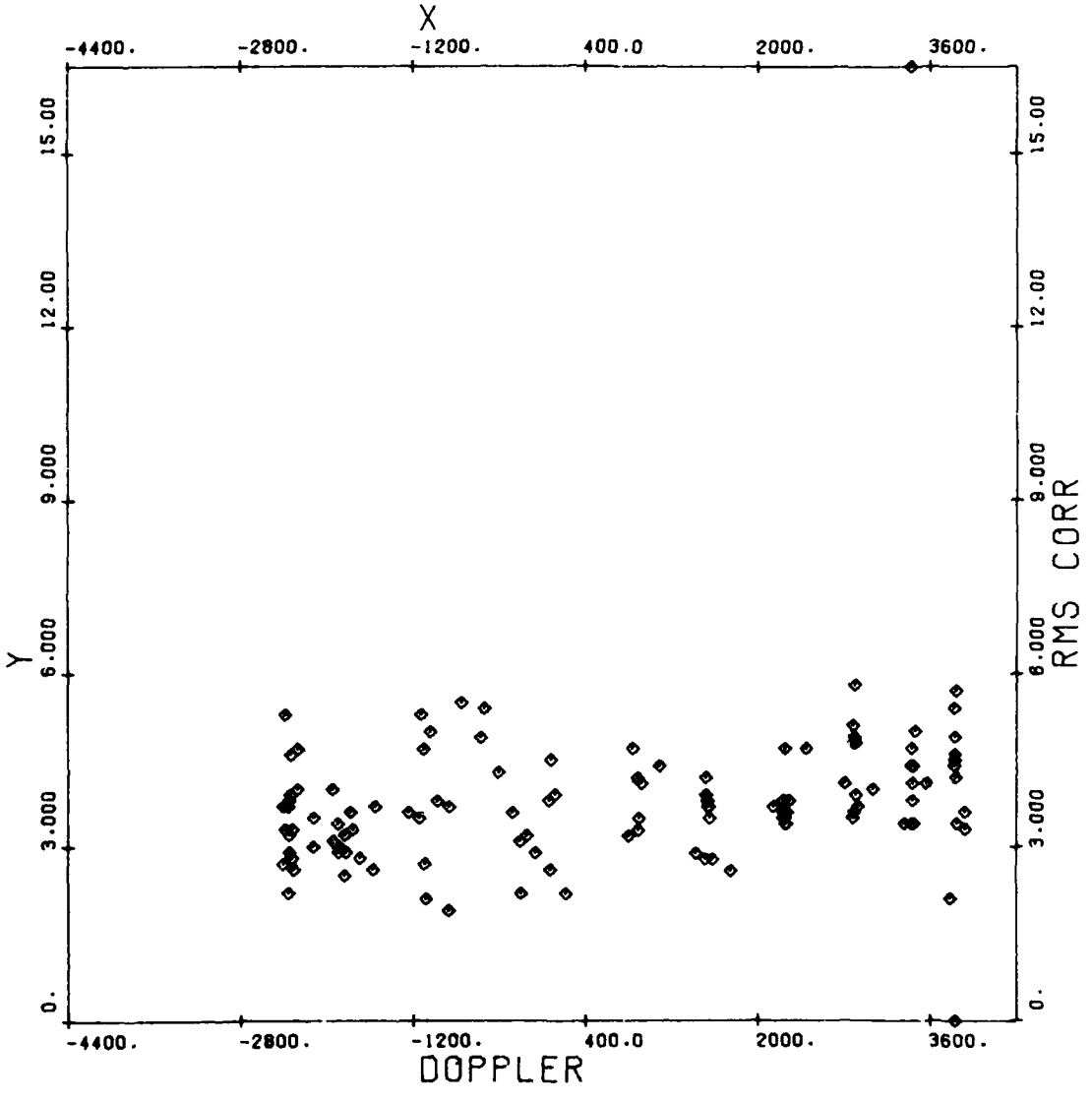

Figure A-23. 20-Min Corrected Range Difference RMS (cm) vs Doppler (Hz), GPS SV-8, NSWC Dahlgren, Days 182-197 1980

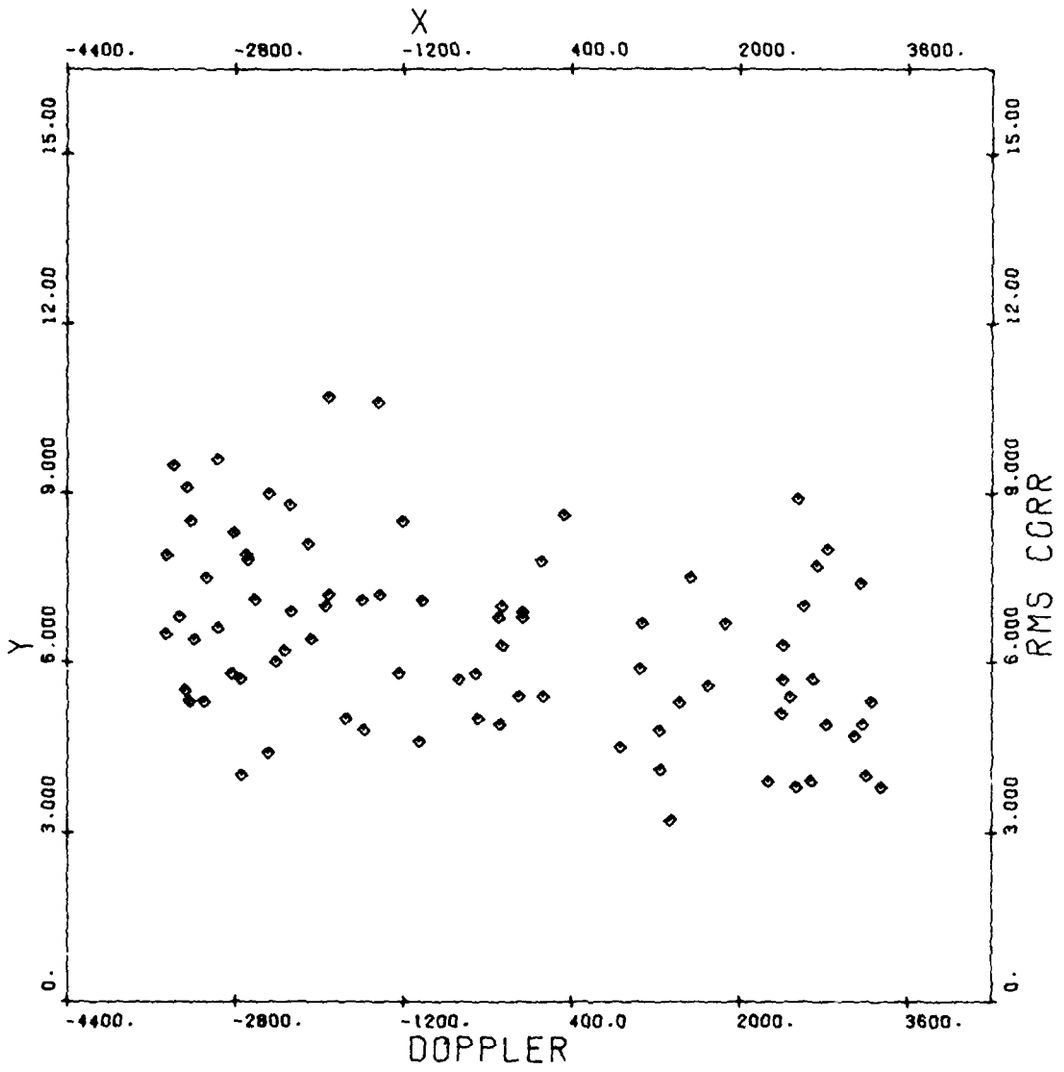

Figure A-24. 20-Min Corrected Range Difference RMS (cm) vs Doppler (Hz), GPS SV-9, NSWC Dahlgren, Days 182-197 1980

7. 20-MIN CORRECTED RANGE DIFFERENCE RMS (cm) VS DATE

The RMS of the ionospheric corrected range difference residuals is also plotted versus date, in order to identify any time variations that may have occurred. Satellites 5, 6, and 8 show little change; however, SV-9 may have improved slightly after day 190.

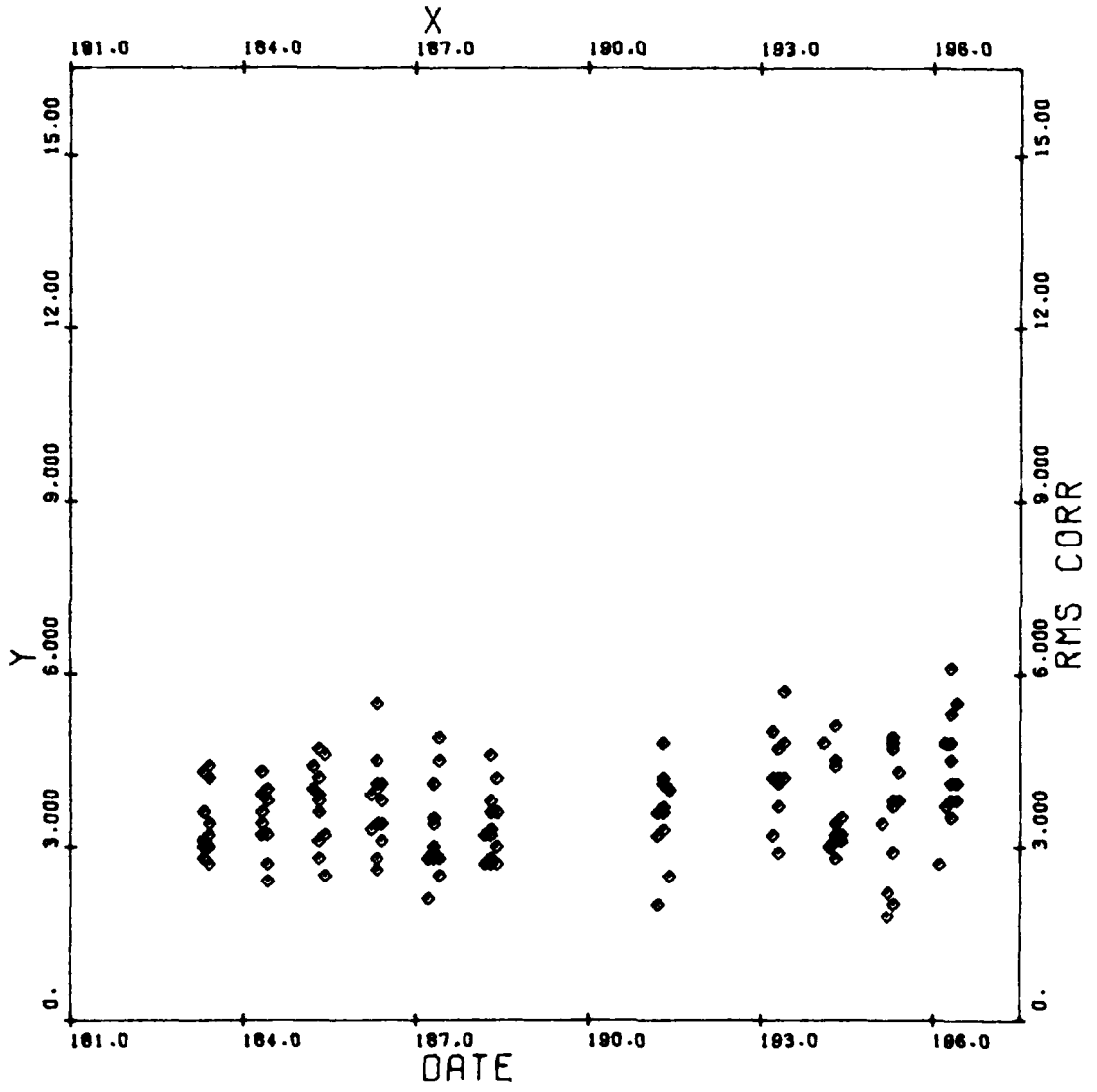

Figure A-25. 20-Min Corrected Range Difference RMS (cm) vs Date, GPS SV-5, NSWC Dahlgren, Days 182-197 1980

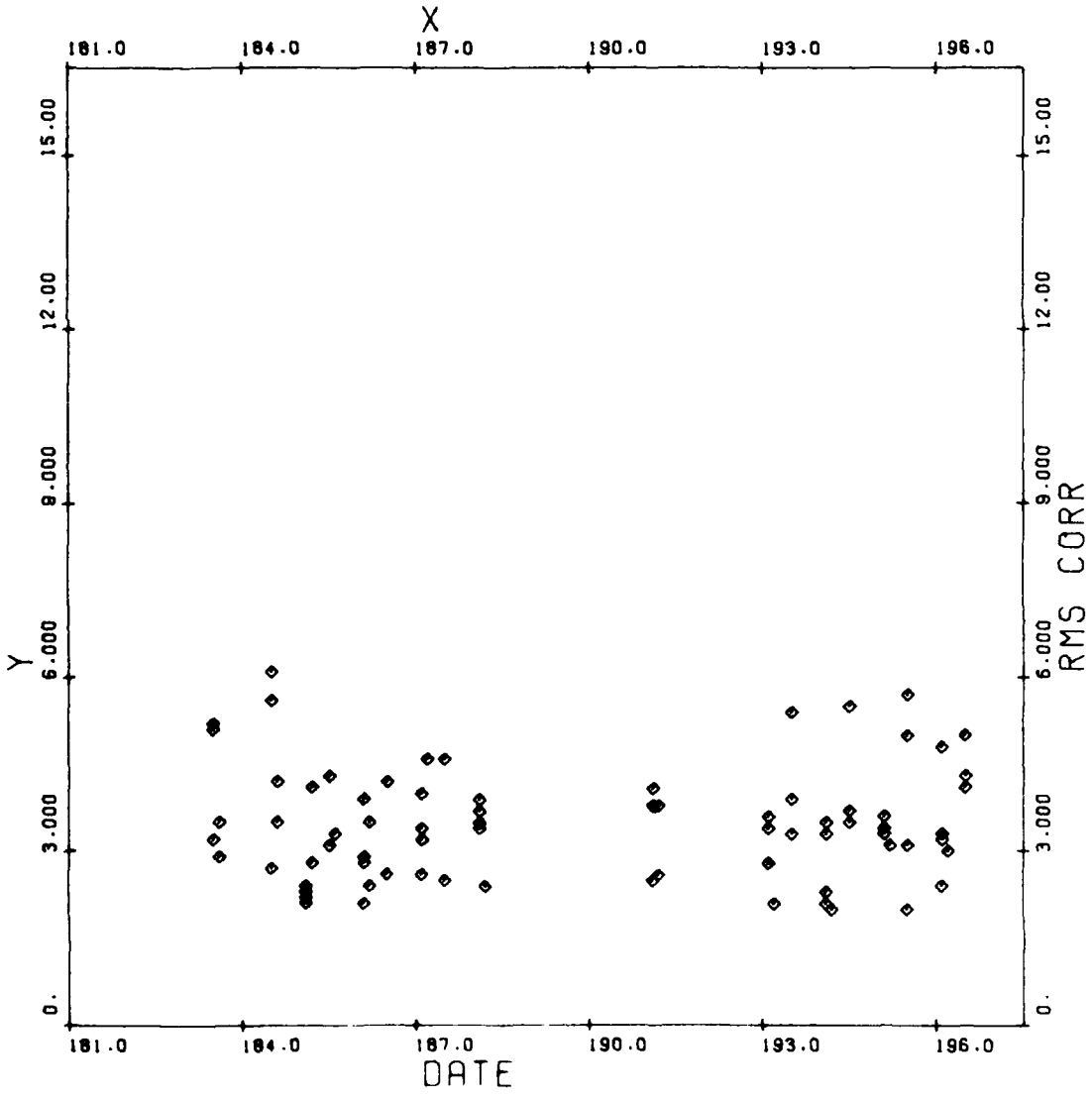

Figure A-26. 20-Min Corrected Range Difference RMS (cm) vs Date, GPS SV-6, NSWC Dahlgren, Days 182-197 1980

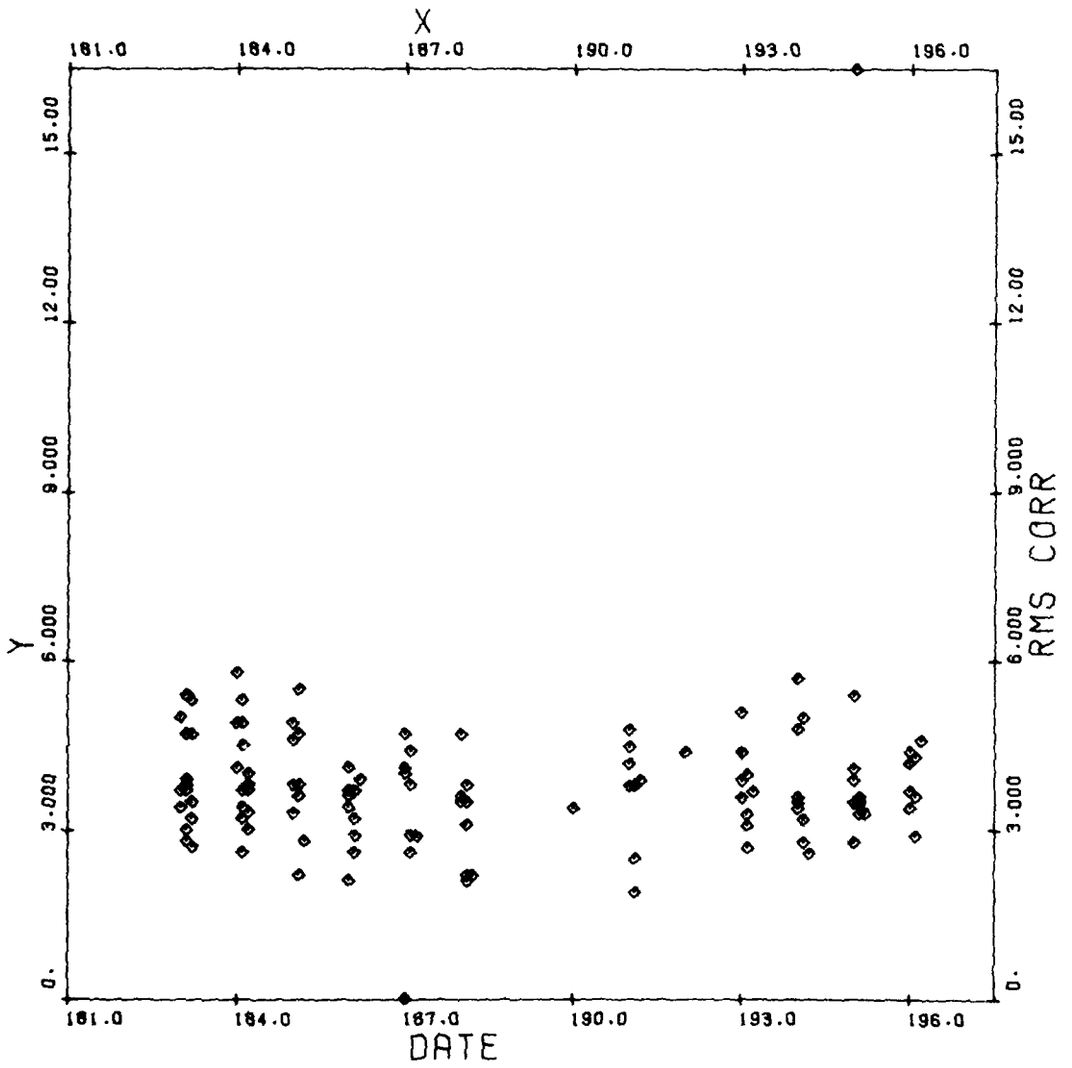

Figure A-27. 20-Min Corrected Range Difference RMS (cm) vs Date, GPS SV-8, NSWC Dahlgren, Days 182-197 1980

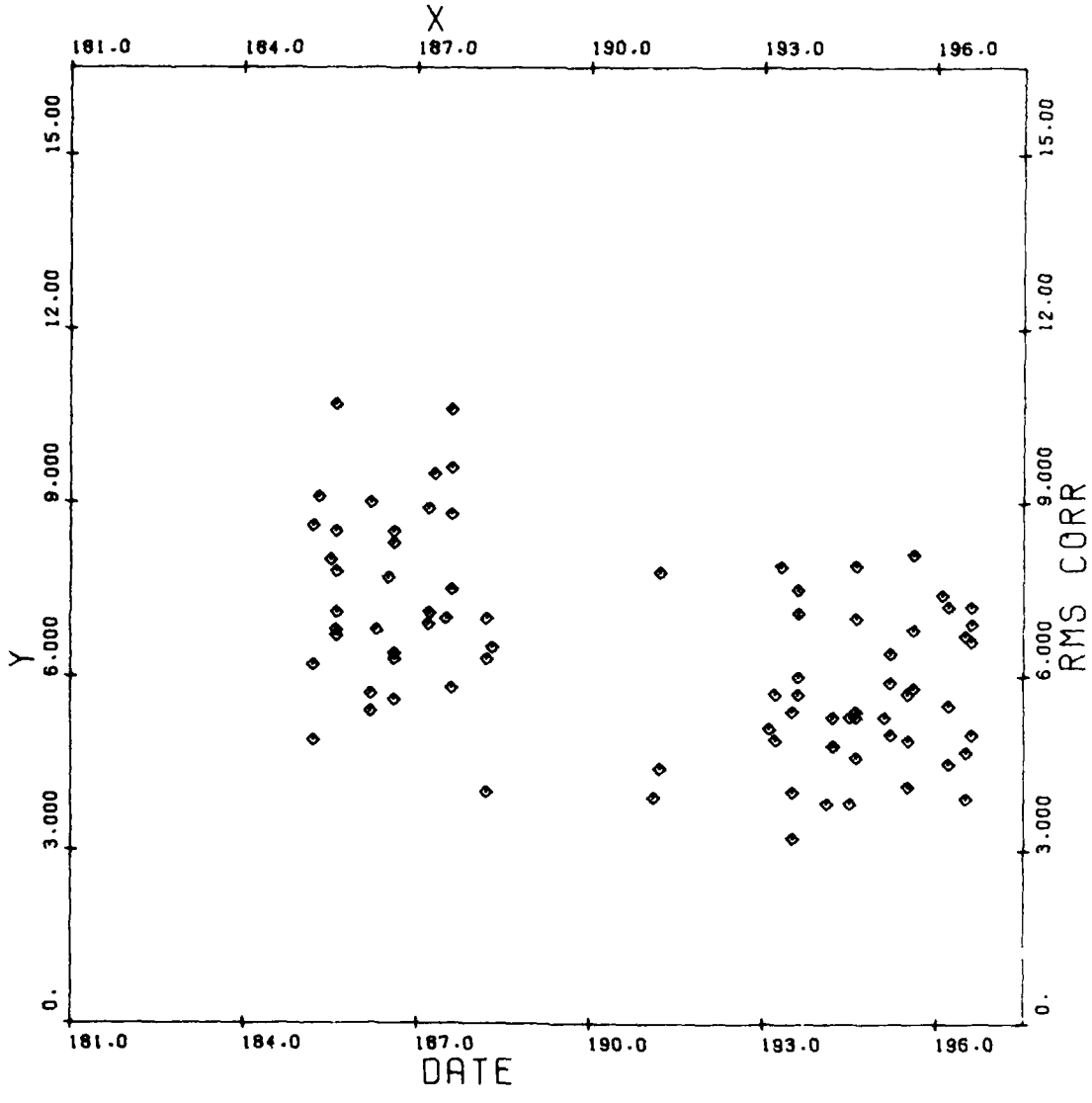

Figure A-28. 20-Min Corrected Range Difference RMS (cm) vs Date, GPS SV-9, NSWC Dahlgren, Days 182-197 1980

8. 20-MIN IONOSPERIC CORRECTION TO L_1 RMS (cm) VS DOPPLER (Hz)

The RMS of the ionospheric corrections is plotted versus the Doppler frequency in plot 8. Satellites 5, 8, and 9 are well-behaved with RMS values near 1 cm. The SV-5 and SV-8 are particularly impressive with most values less than 1 cm. The SV-9 and SV-6 demonstrate a wider scatter whose origin must be due to a pecularity of these satellites or propagation paths. Since the satellite observations were sequential and interleaved, the receiver cannot be the cause of the observed differences.

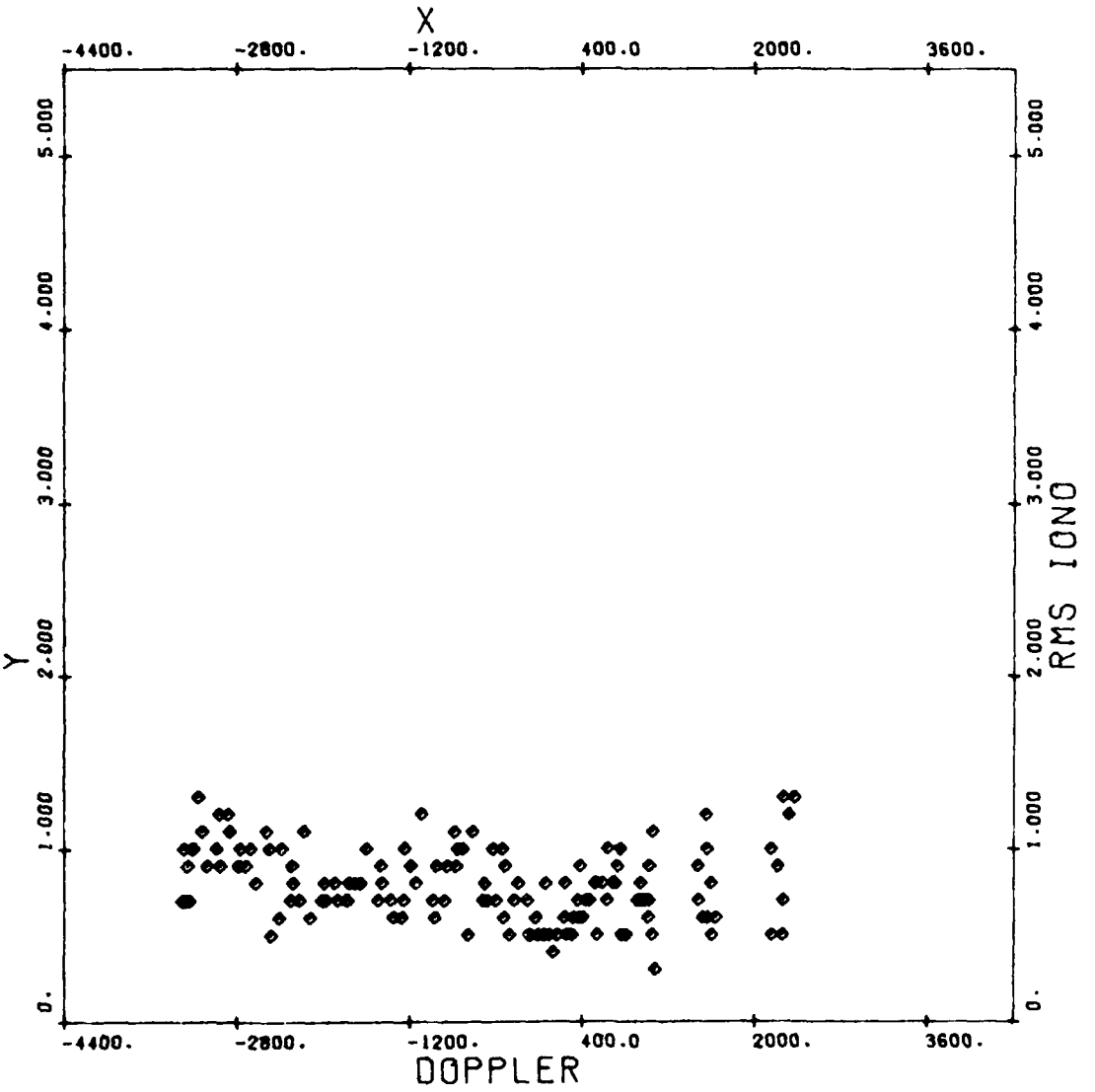

Figure A-29. 20-Min Corrected Range Difference RMS (cm) vs Date, GPS SV-5, NSWC Dahlgren, Days 182-197 1980

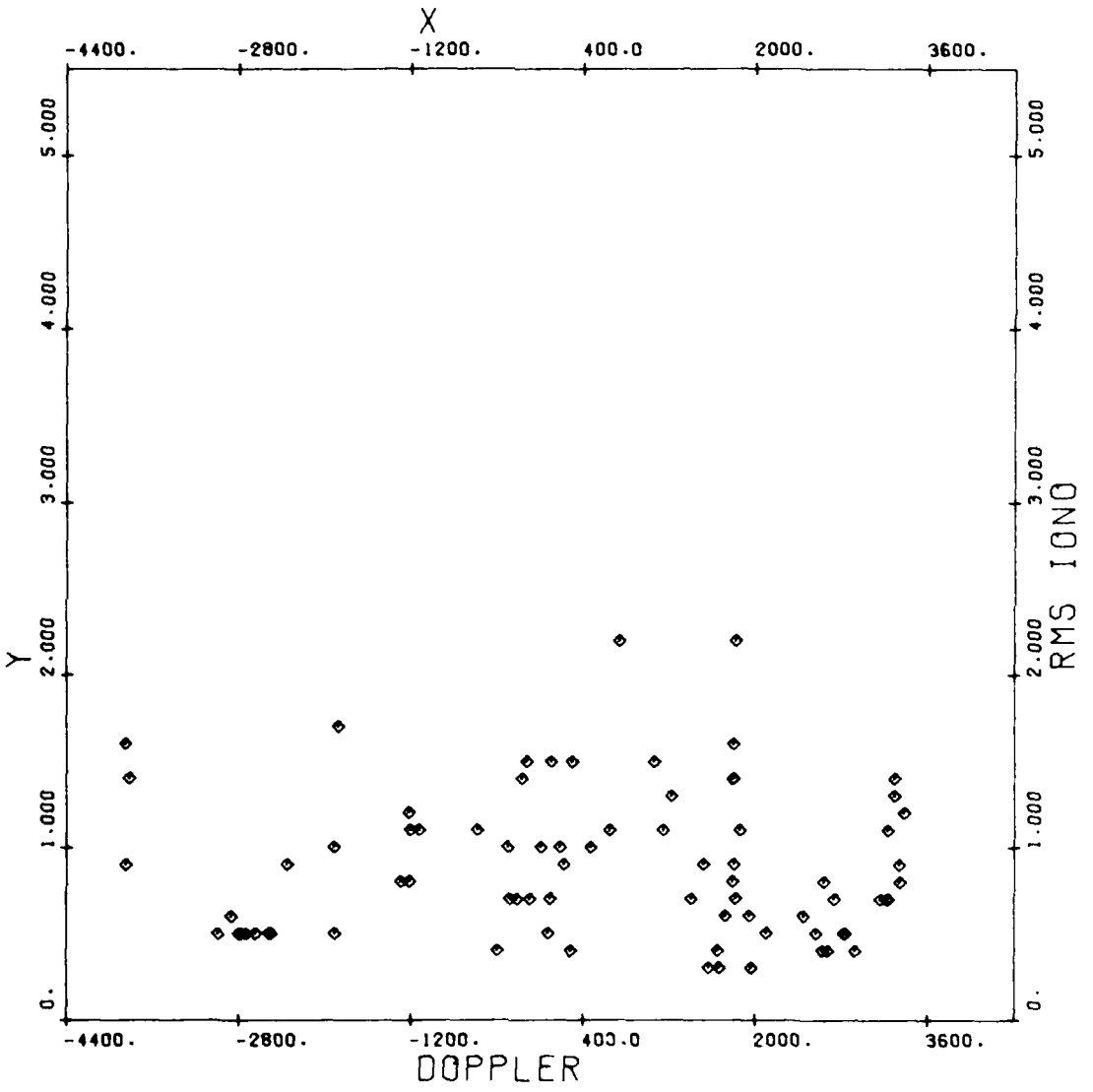

Figure A-30. 20-Min Ionospheric Correction to L_1 RMS (cm) vs Doppler (Hz), GPS SV-6, NSWC Dahlgren, Days 182-197 1980

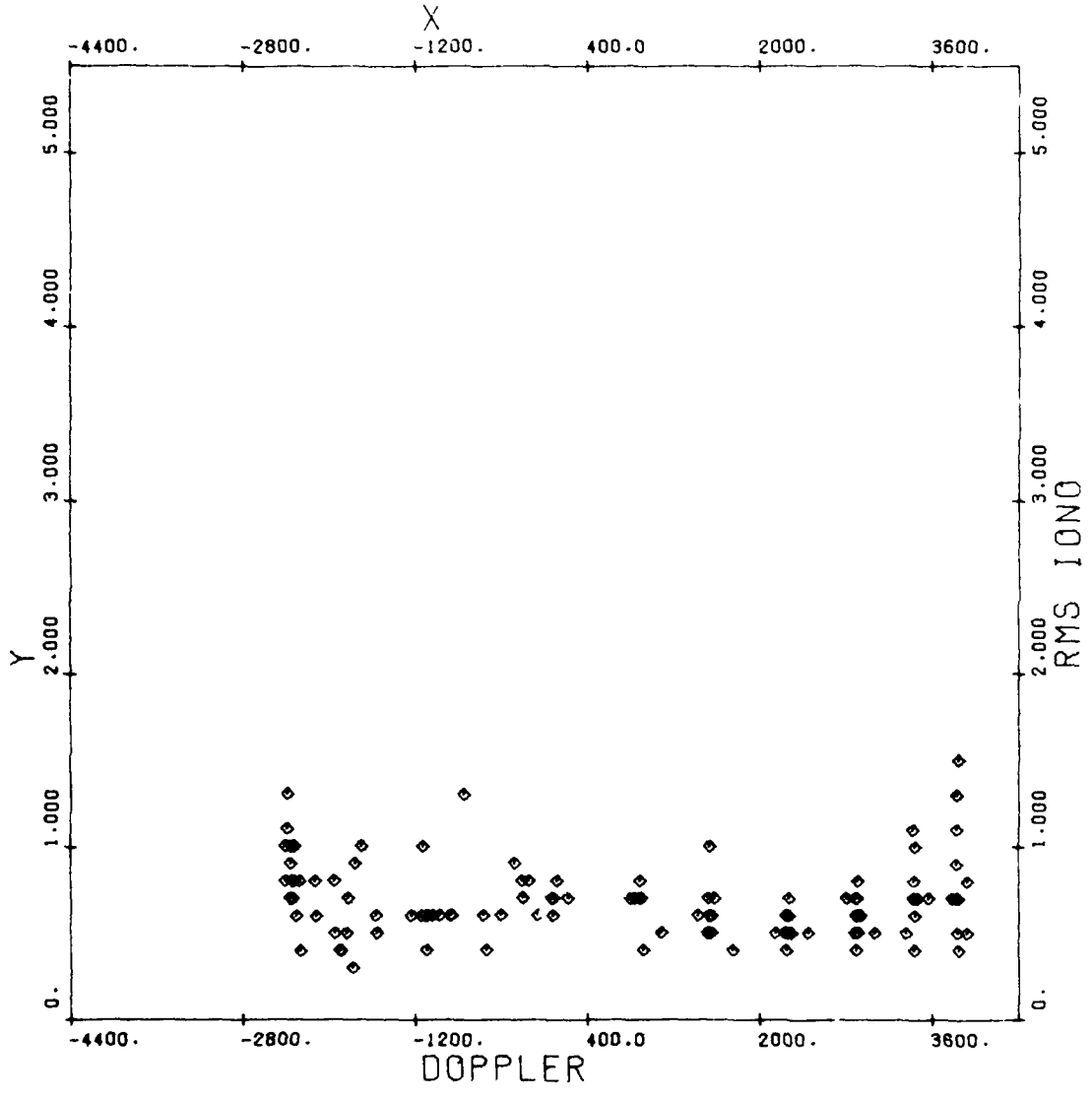

Figure A-31. 20-Min Ionospheric Correction to L_1 RMs (cm) vs Doppler (Hz), GPS SV-8, NSWC Dahlgren, Days 182-197 1980

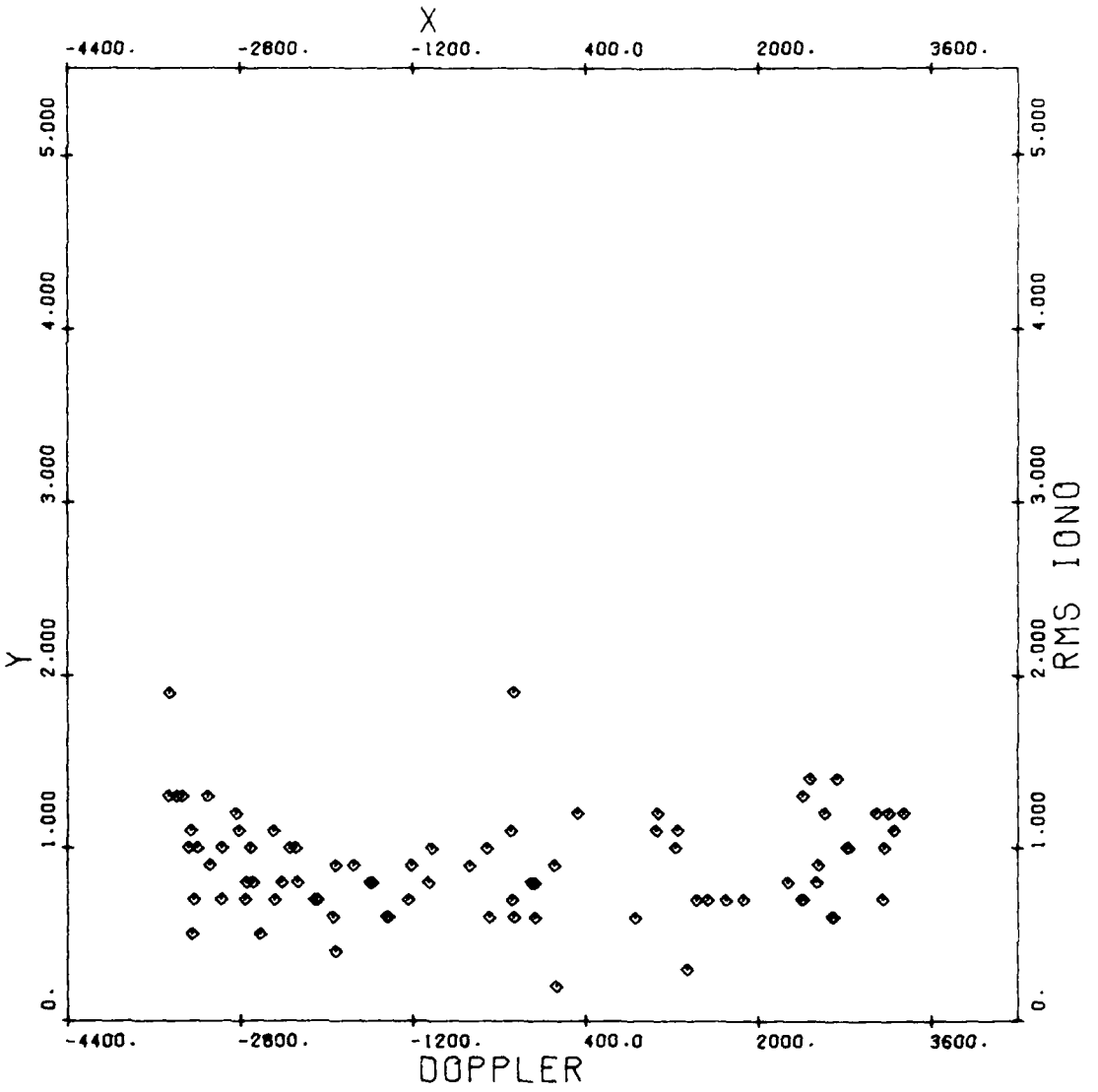

Figure A-32. 20-Min Ionospheric Correction to L_1 RMS (cm) vs Doppler (Hz), GPS SV-9, NSWC Dahlgren, Days 182-197 1980

9. 20-MIN IONOSPHERIC CORRECTION TO L_1 RMS (cm) VS DATE

The same residuals from plot 8 are plotted versus date in plot 9. There is no particular variation apparent with time and so the scatter cannot be due to a temporal change in the hardware.

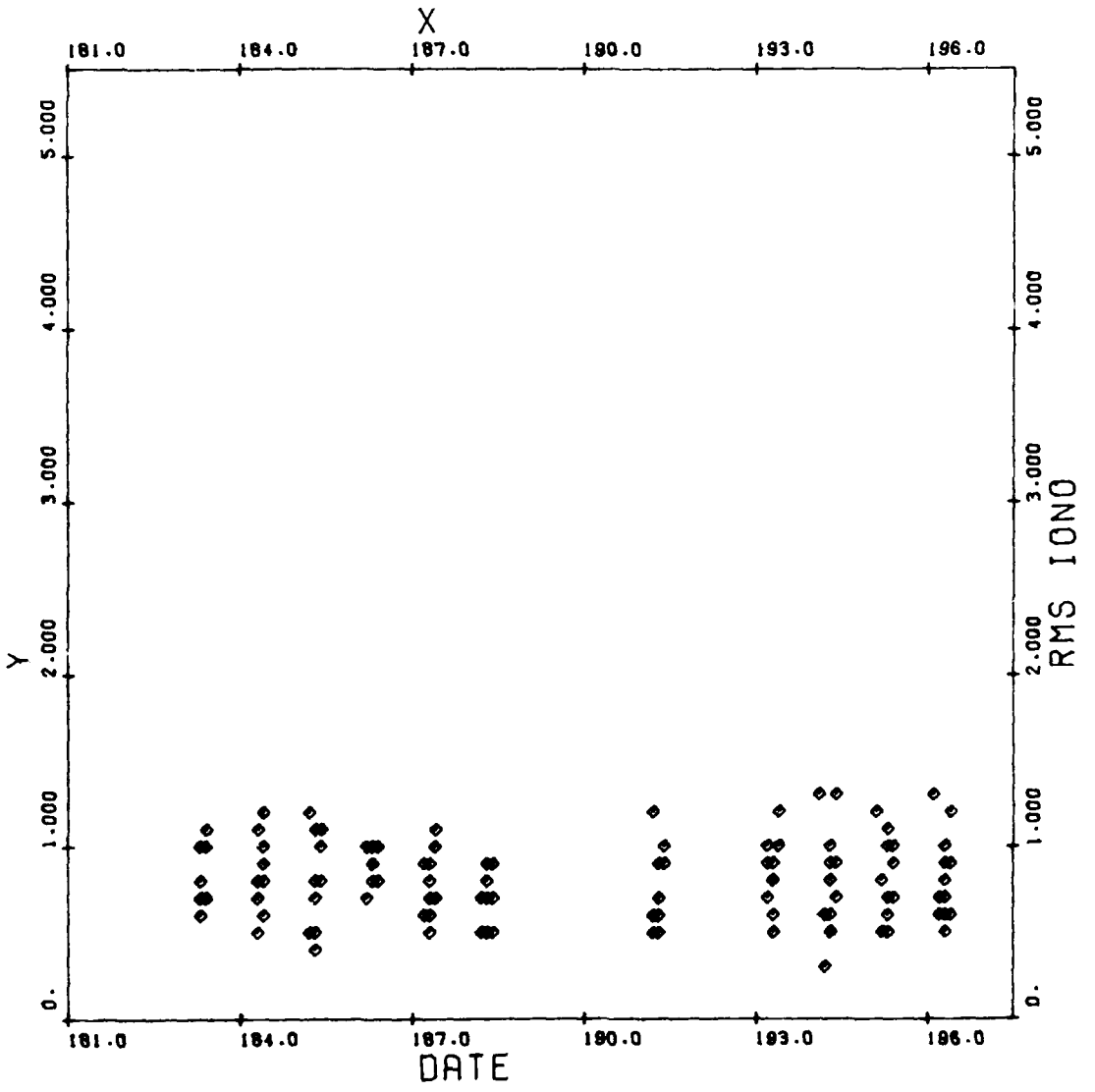

Figure A-33. 20-Min Ionospheric Correction to L_1 RMS (cm) vs Date, GPS SV-5, NSWC Dahlgren, Days 182-197 1980

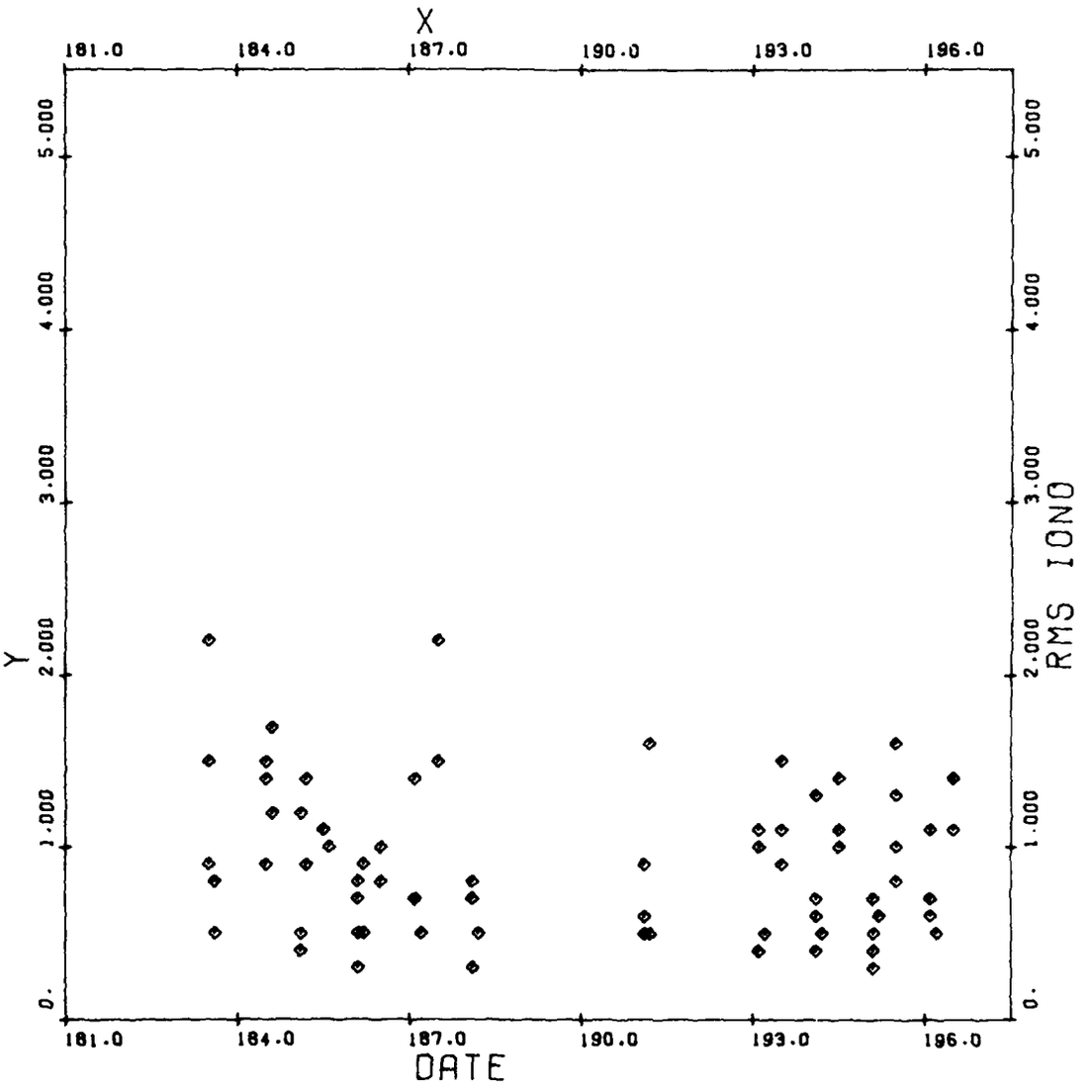

Figure A-34. 20-Min Ionospheric Correction to L_1 RMS (cm) vs Date, GPS SV-6, NSWC Dahlgren, Days 182-197 1980

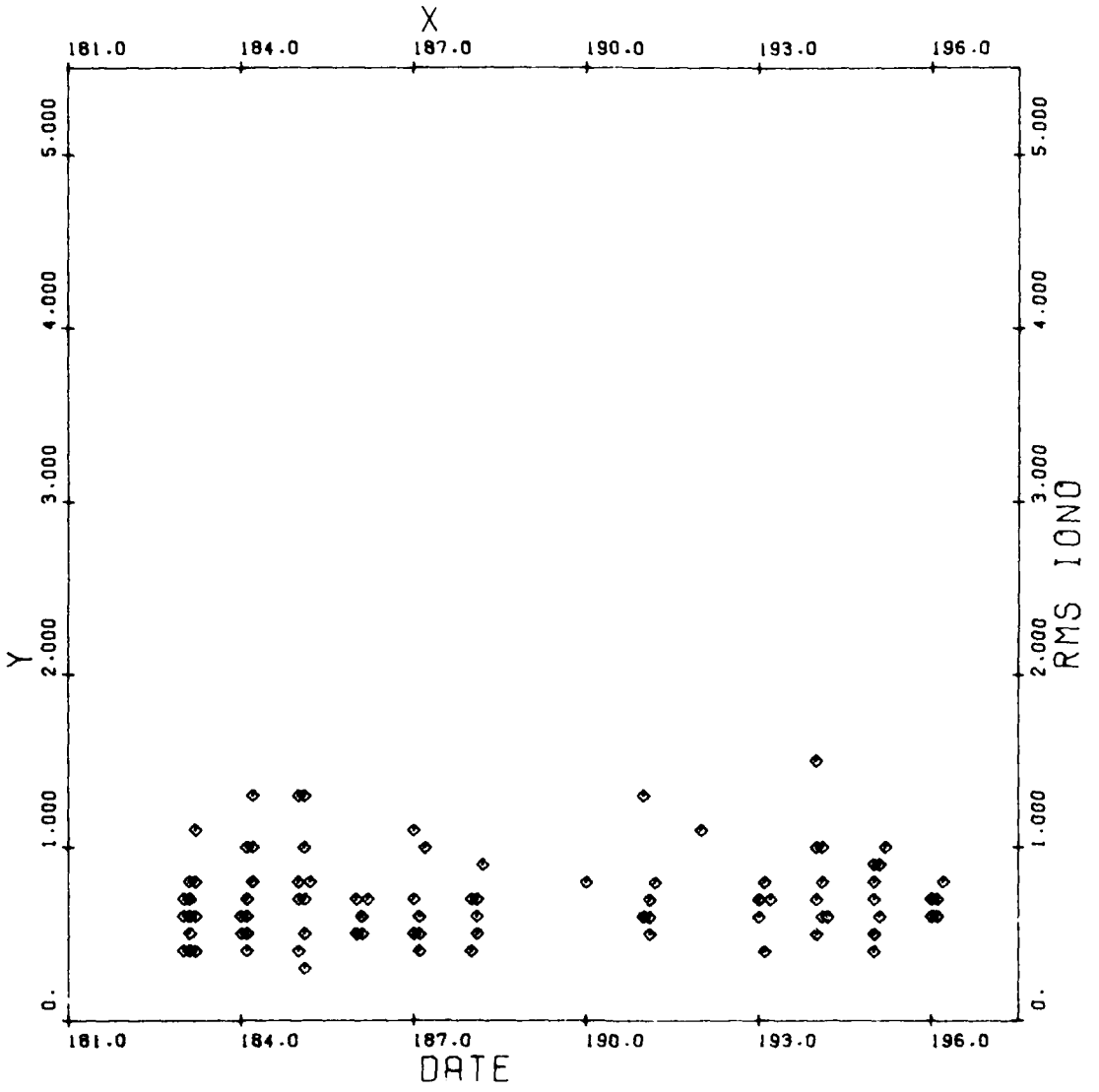

Figure A-35. 20-Min Ionospheric Correction to L_1 RMS (cm) vs Date, GPS SV-8, NSWC Dahlgren, Days 182-197 1980

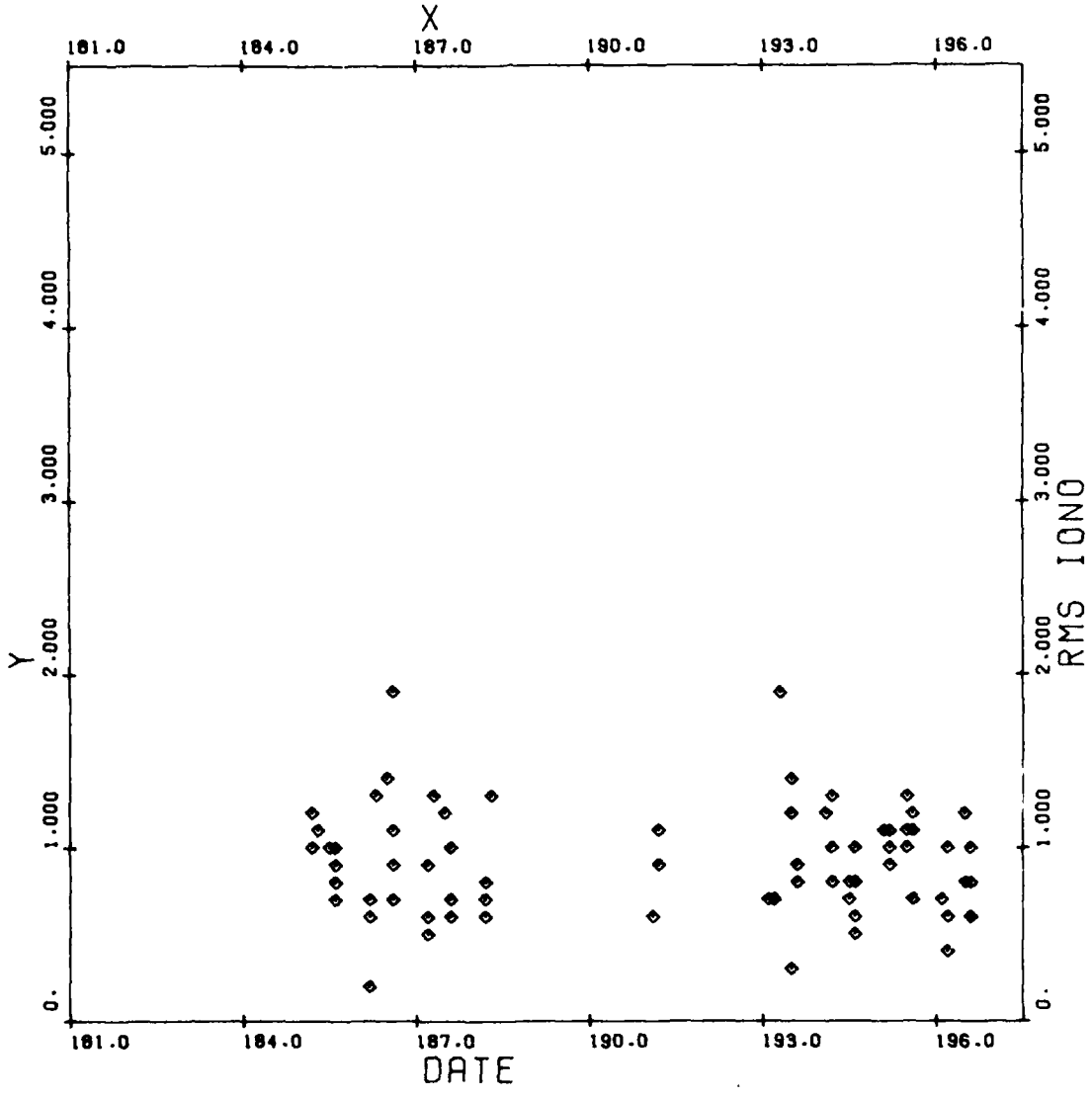

Figure A-36. 20-Min Ionospheric Correction to L_1 RMS (cm) vs Date, GPS SV-9, NSWC Dahlgren, Days 182-197 1980

10. 20-MIN IONOSPHERIC CORRECTION TO L_1 RMS (cm) VS ELEVATION (°)

The same residuals from plots 7 and 8 are plotted versus elevation angle in plot 10. Here, it becomes apparent that the scatter is due primarily to data from low-elevation angles. The SV-6 is particularly affected, perhaps because one of its two passes does not exceed 30°.

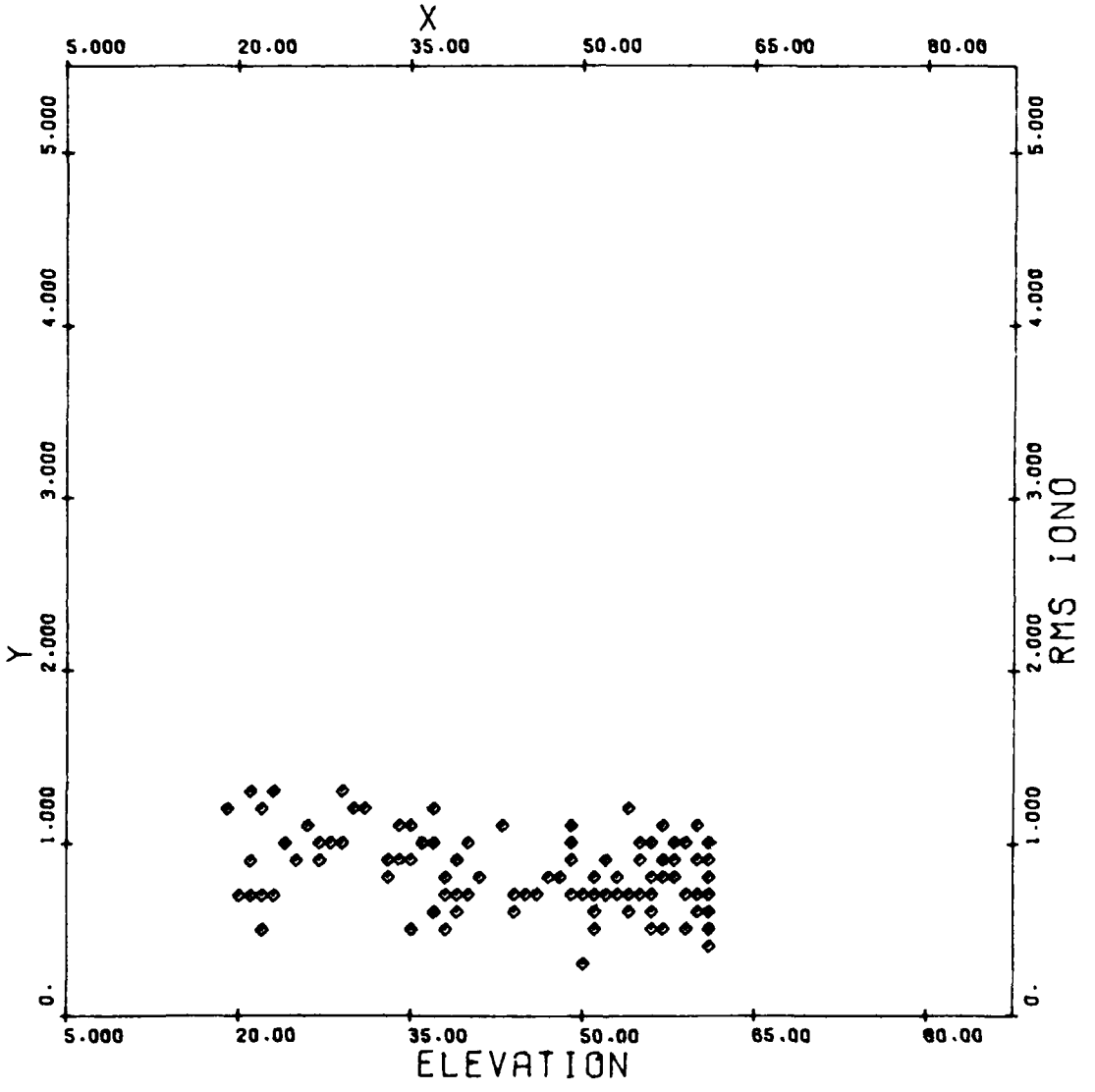

Figure A-37. 20-Min Ionospheric Correction to L_1 RMS (cm) vs Elevation (°), GPS SV-5, NSWC Dahlgren, Days 182-197 1980

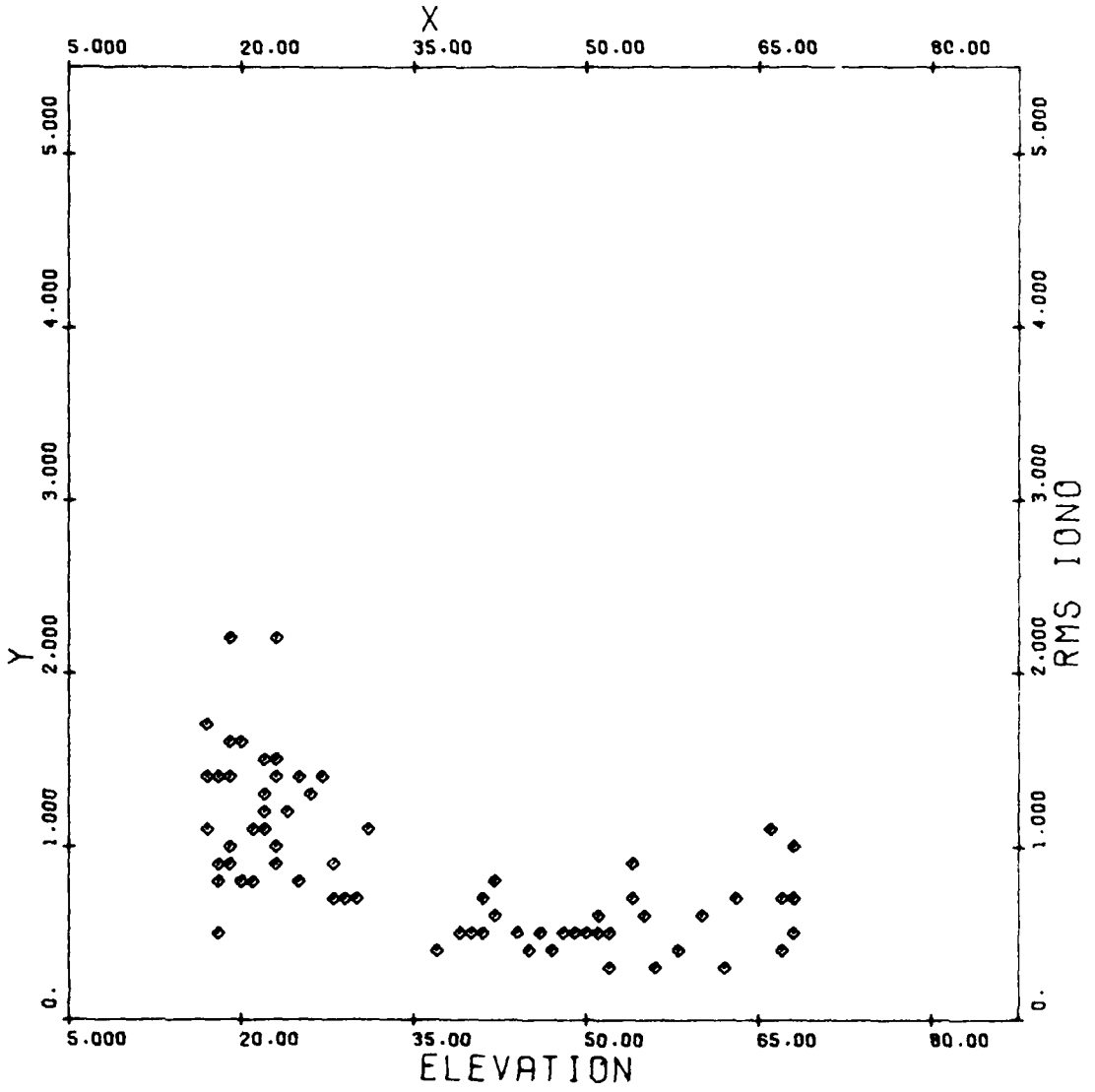

Figure A-38. 20-Min Ionospheric Correction to L_1 RMS (cm) vs Elevation (°), GPS SV-6, NSWC Dahlgren, Days 182-197 1980

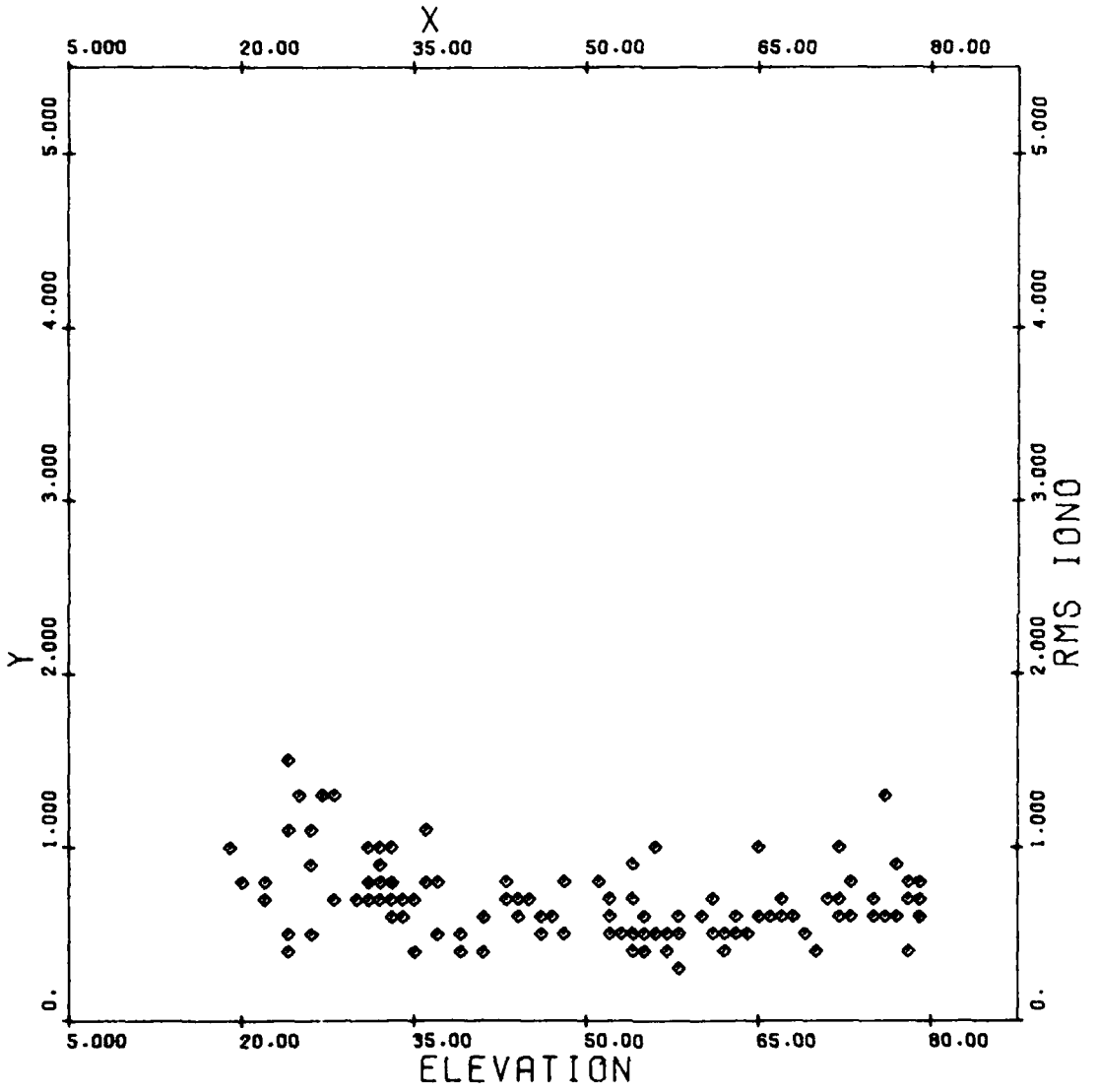

Figure A-39. 20-Min Ionospheric Correction to L_1 RMS (cm) vs Elevation (°), GPS SV-8, NSWC Dahlgren, Days 182-197 1980

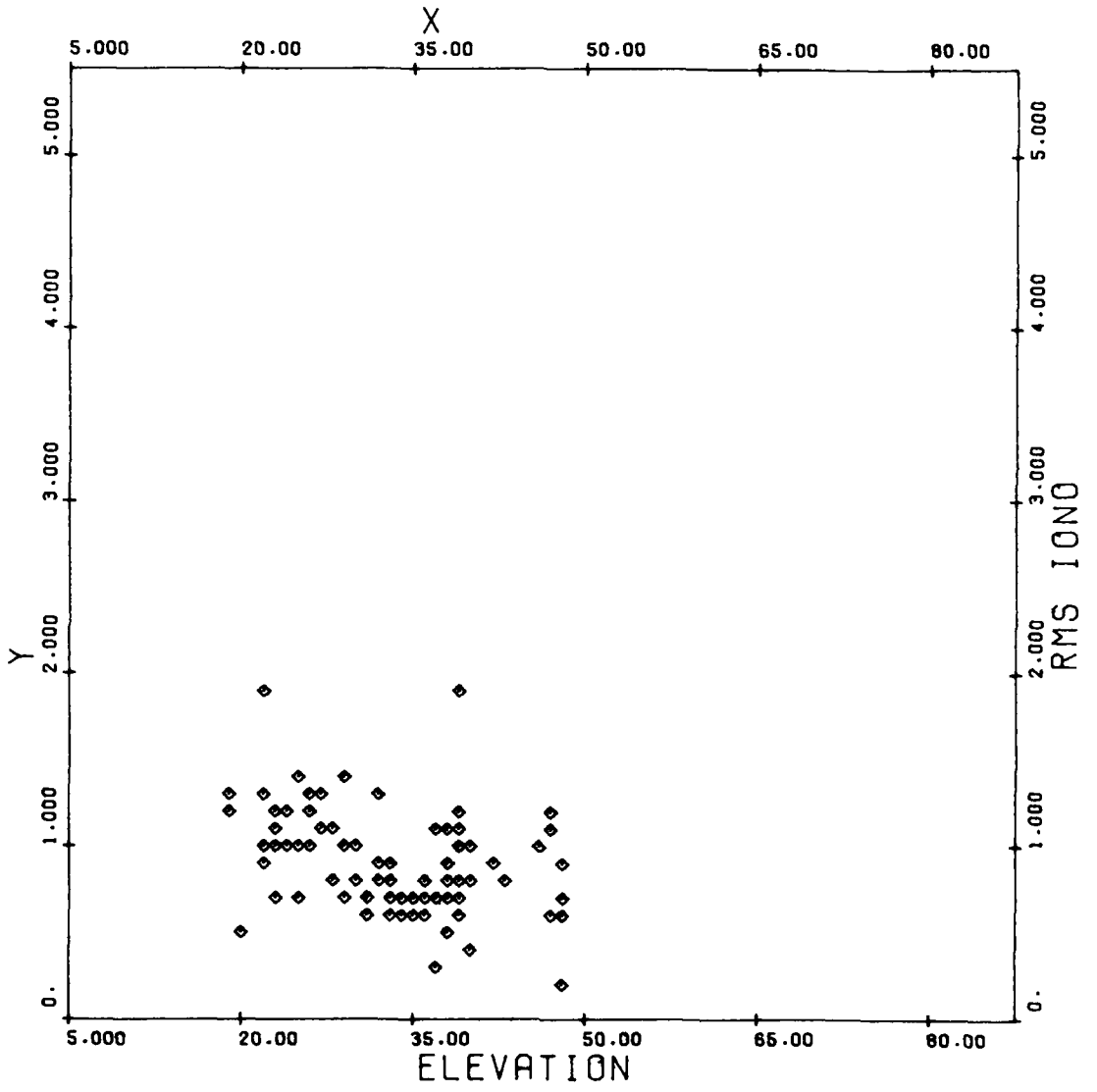

Figure A-40. 20-Min Ionospheric Correction to L_1 RMS (cm) vs Elevation (°), GPS SV-9, NSWC Dahlgren, Days 182-197 1980

11. IONOSPHERIC CORRECTION TO L_1 (cm) VS ELEVATION (°)

The ionospheric correction to L_1 computed from two-frequency Doppler is presented in plot 11. The corrections are negative during the portion of the pass that the range is decreasing and positive as the range increases. The convergence of the corrections at the peak elevation angle is quite apparent in the data; however, it does not appear to be symmetric about zero. Further investigations are warranted to explain this result.

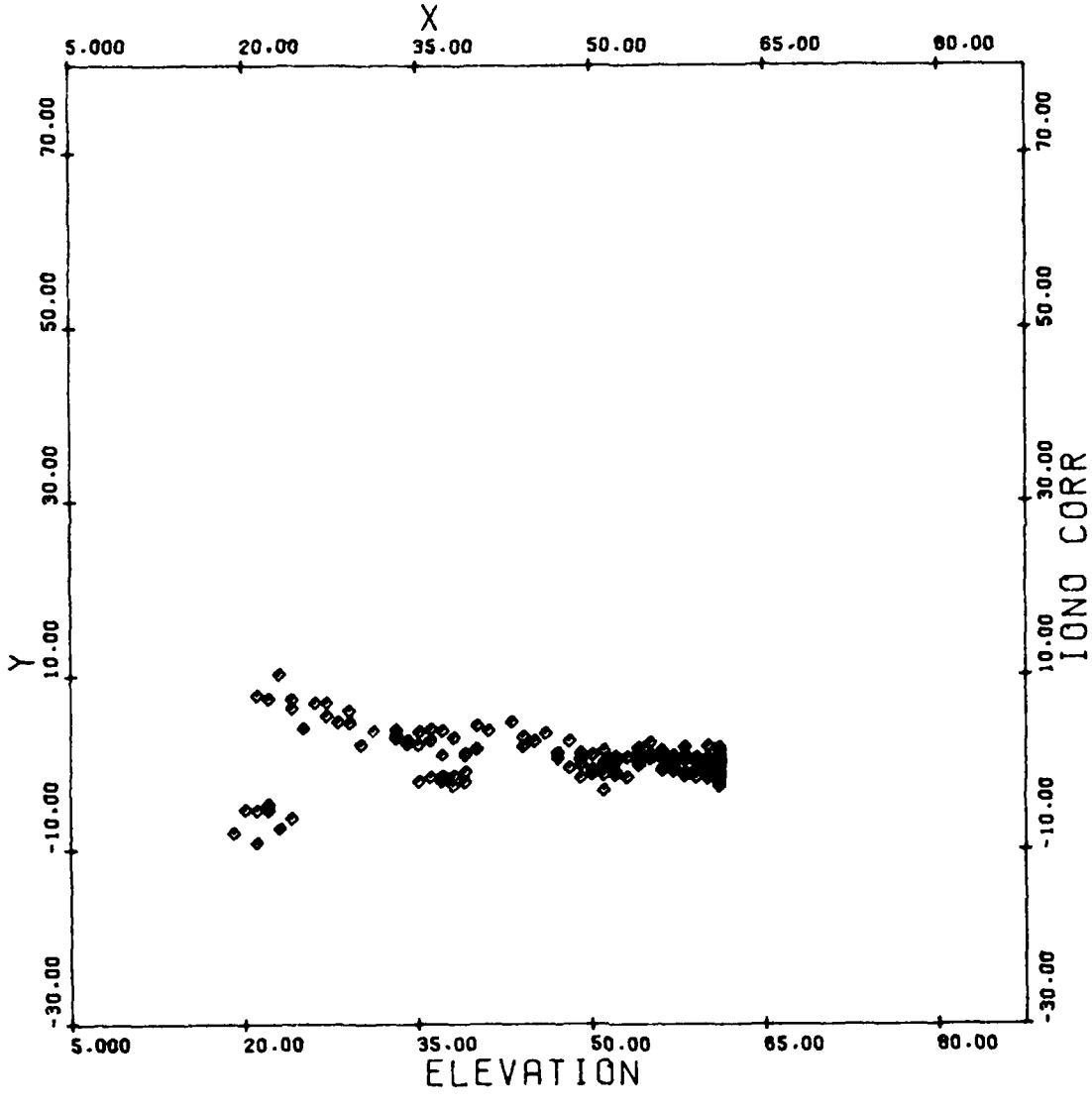

Figure A-41. Ionospheric Correction to L_1 RMS (cm) vs Elevation (°), GPS SV-5, NSWC Dahlgren, Days 182-197 1980

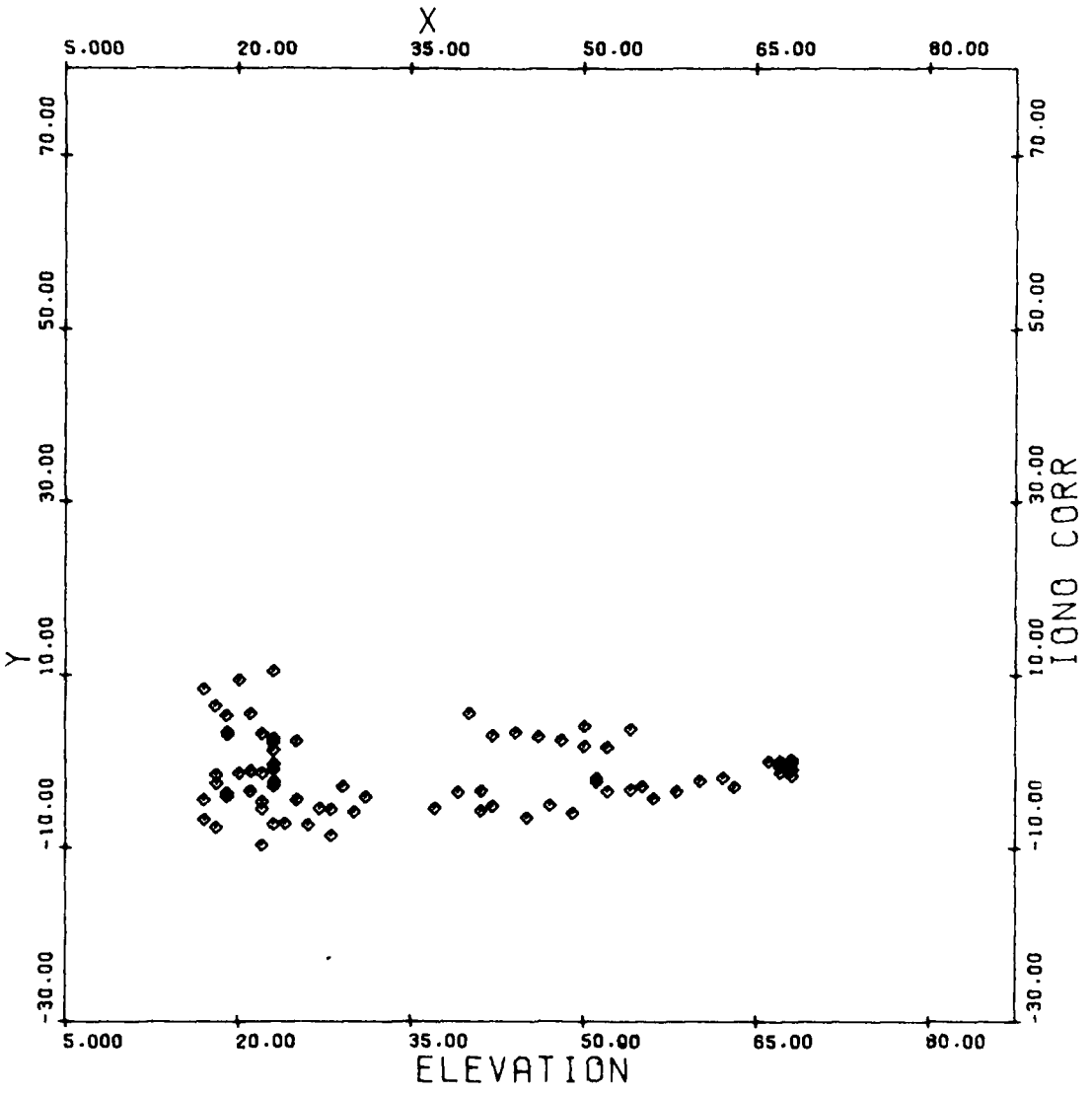

Figure A-42. Ionospheric Correction to L_1 (cm) vs Elevation (°), GPS SV-6, NSWC Dahlgren, Days 182-197 1980

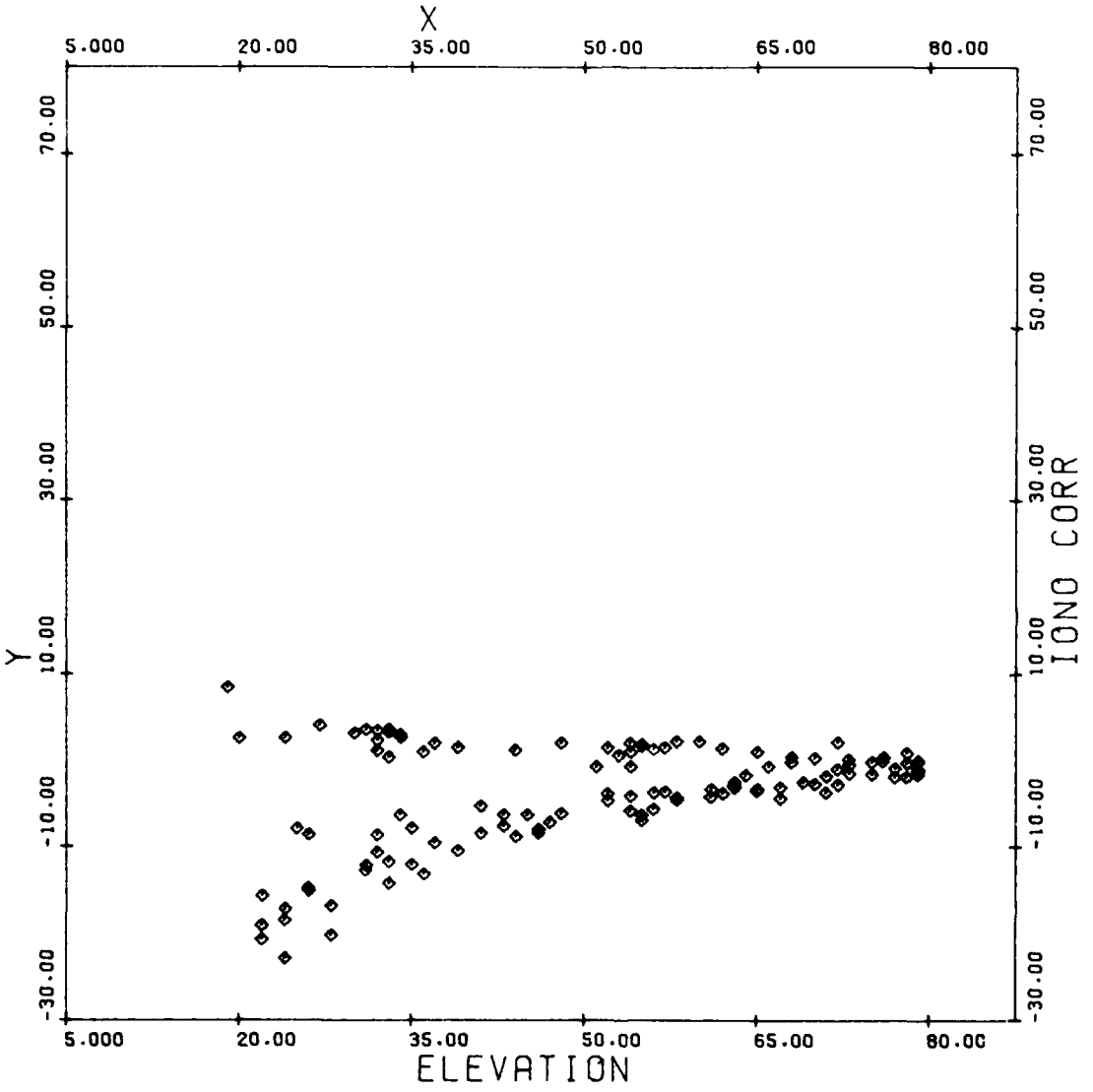

Figure A-43. Ionospheric Correction to L_1 (cm) vs Elevation (°), GPS SV-8, NSWC Dahlgren, Days 182-197 1980

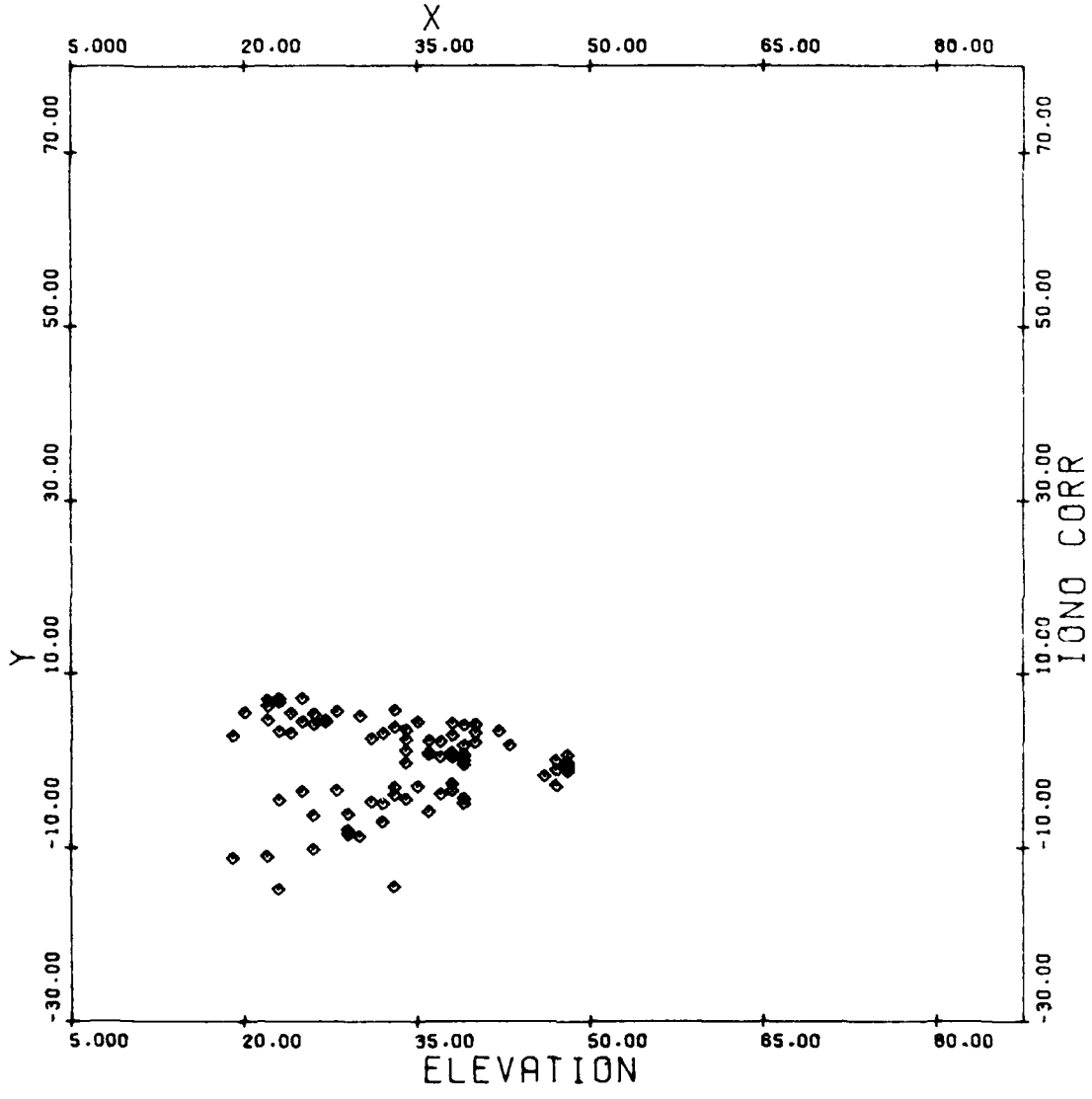

Figure A-44. Ionospheric Correction to L_1 (cm) vs Elevation (°), GPS SV-9, NSWC Dahlgren, Days 182-197 1980

CLOCK OFFSET, CPS-NGRS (nsec) VS DATE

The final plot demonstrates again the consistency of the derived offset, after the broadcast satellite clock corrections are applied to the L_1 pseudorange observations.

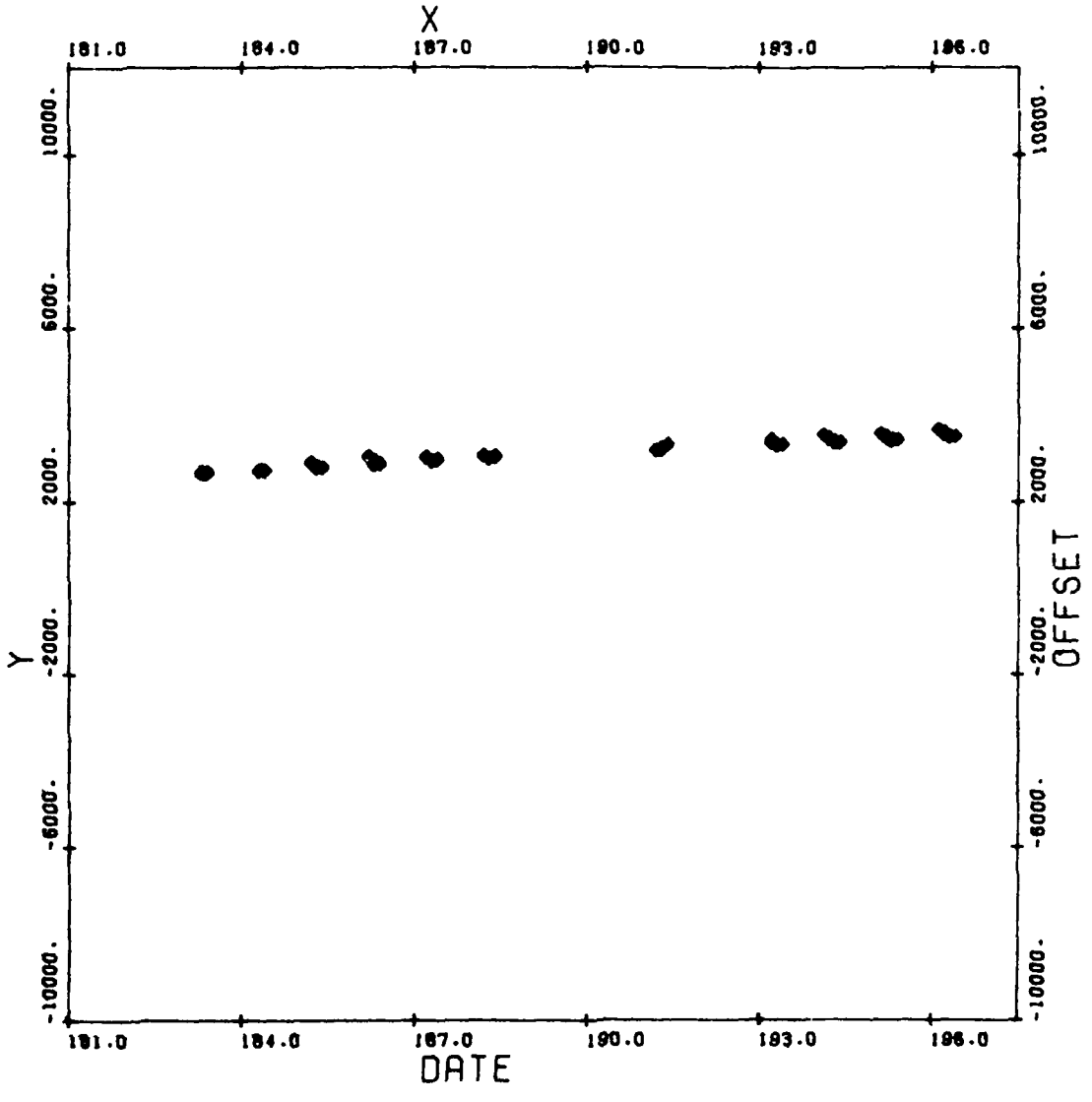

Figure A-45. Clock Offset, GPS-NGRS (nsec) vs Date, GPS SV-5, NSWC Dahlgren, Days 182-197 1980

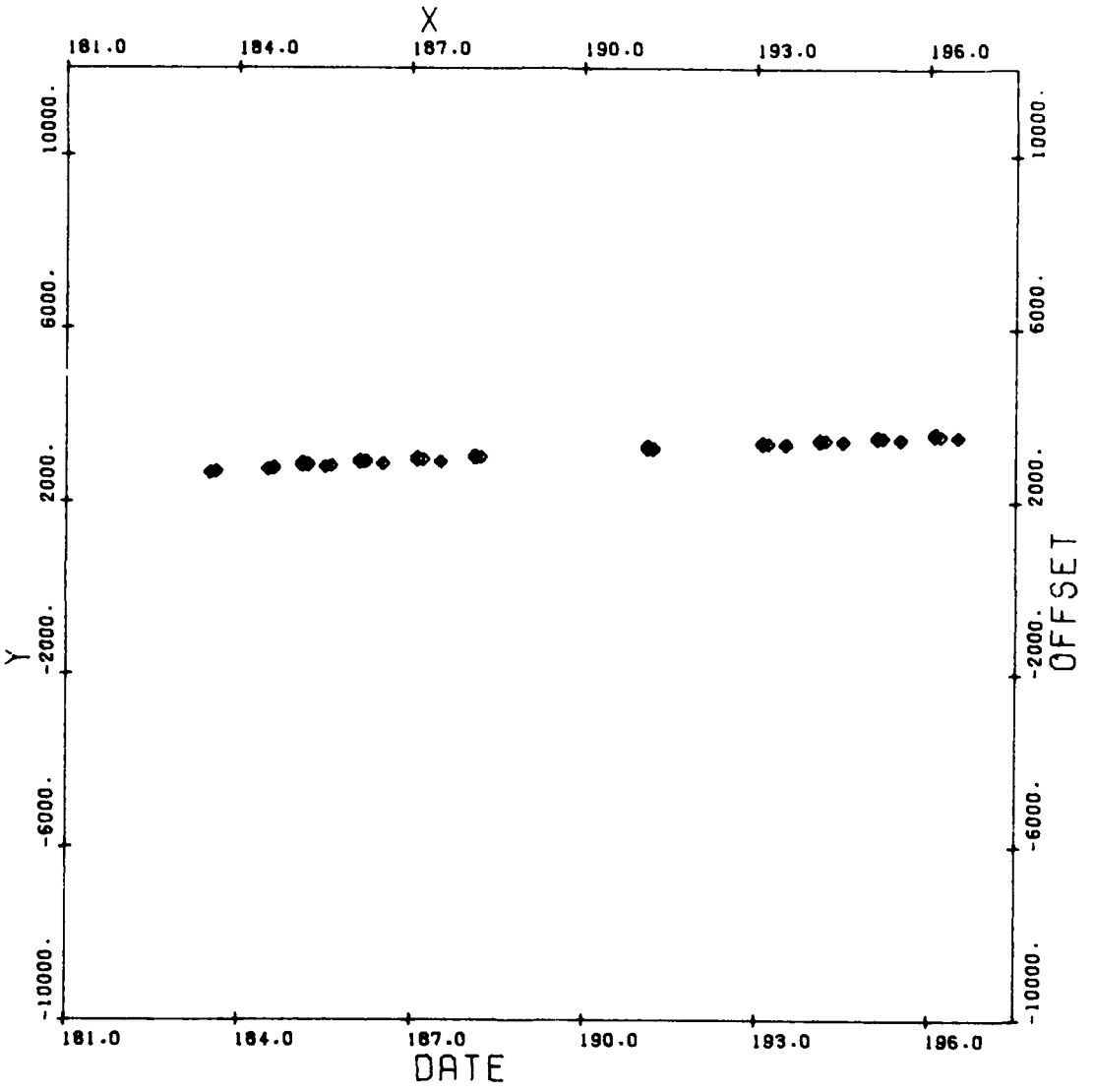

Figure A-46. Clock Offset, GPS-NGRS (nsec) vs Date,
GPS SV-6, NSWC Dahlgren, Days 182-197 1980

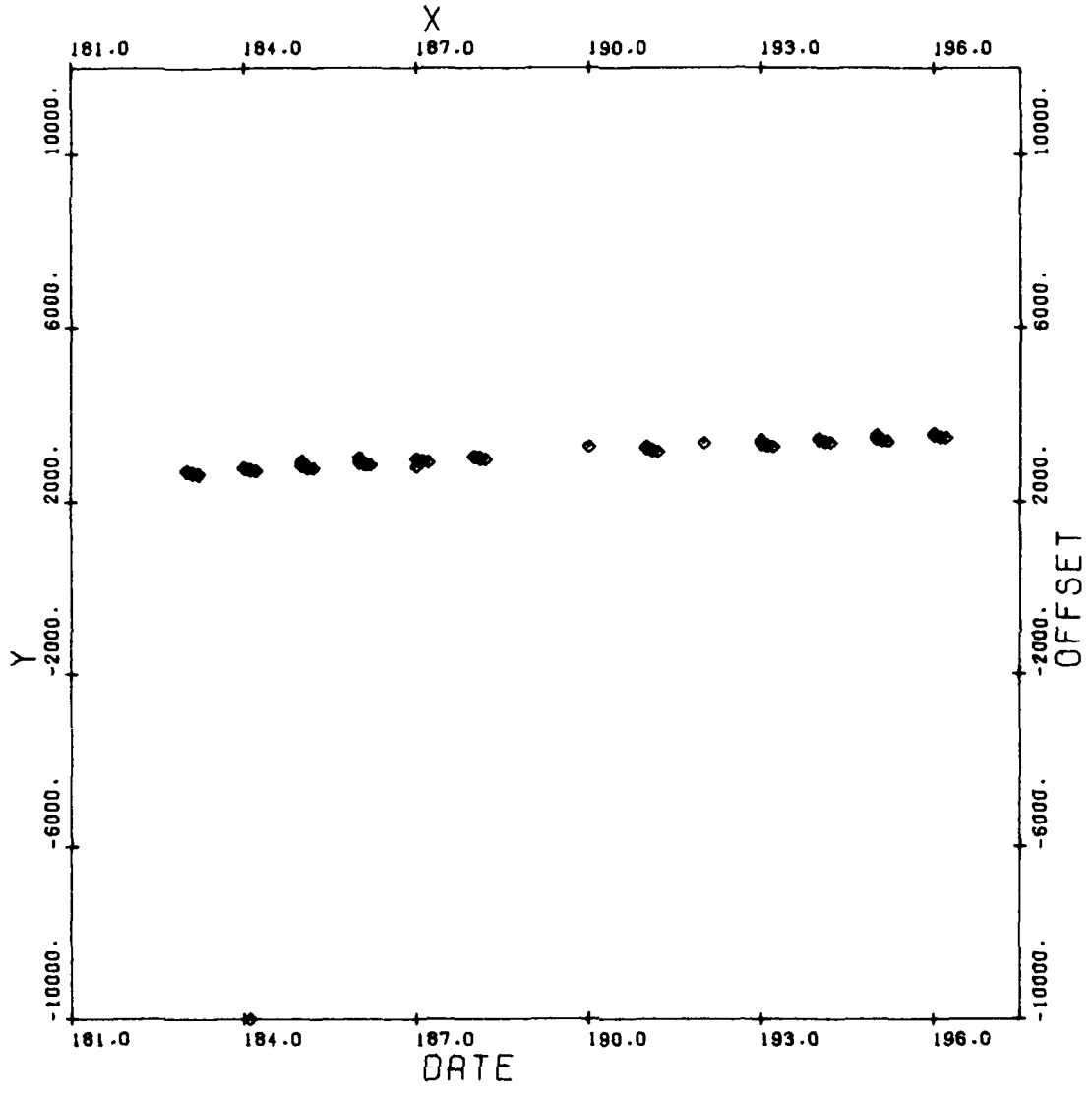

Figure A-47. Clock Offset, GPS-NGRS (nsec) vs Date,
GPS SV--8, NSWC Dahlgren, Days 182-197 1980

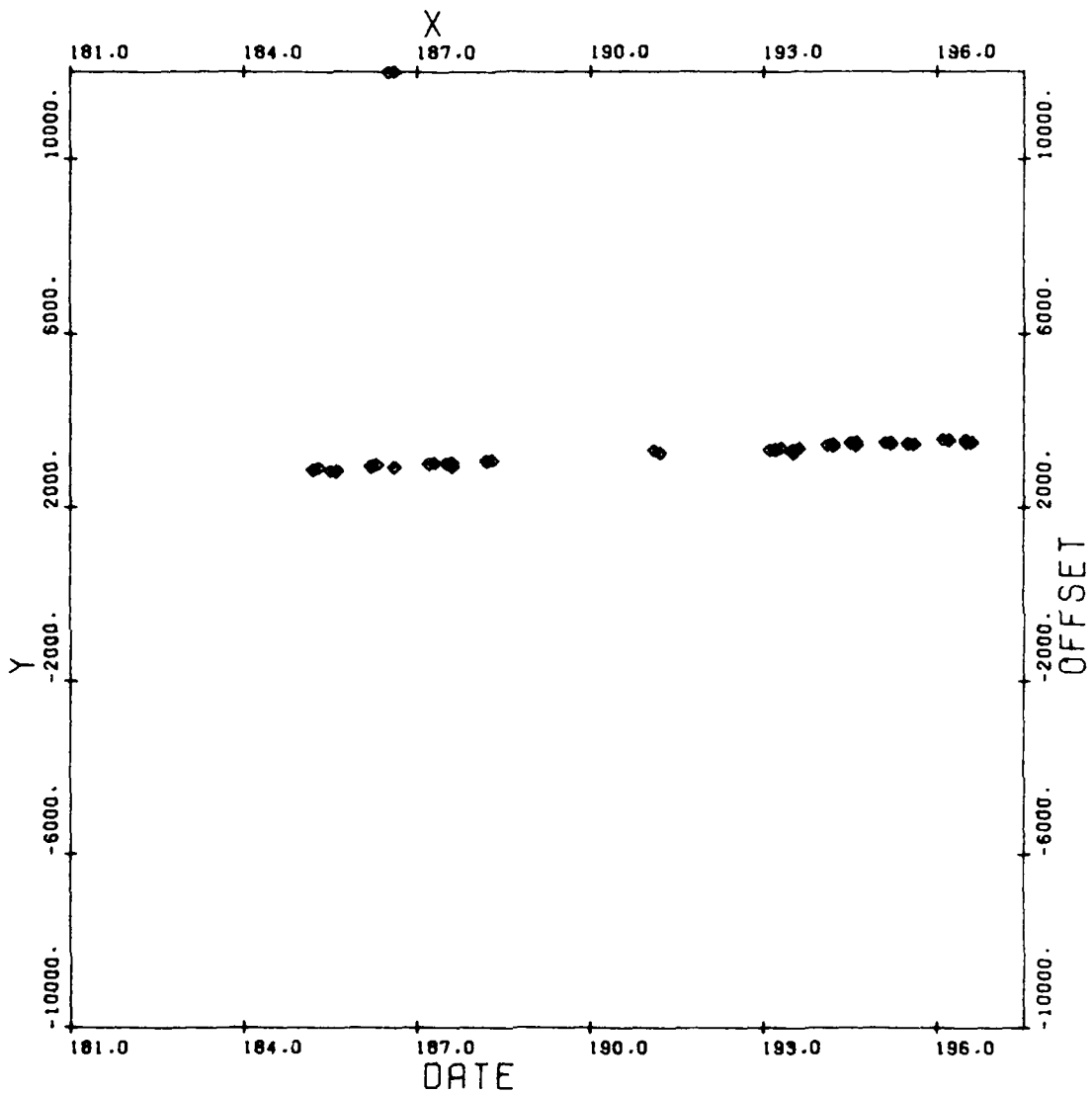

Figure A-48. Clock Offset, GPS-NGRS (nsec) vs Date,
GPS SV-9, NSWC Dahlgren, Days 182-197 1980

DISTRIBUTION

Shell Resources Canada Ltd.
400 4th Ave. S.W.
Calgary, Alberta
Canada T2P0J4
ATTN: Alex Hittel (4)

TASC
6 Jacob Way
Reading, MA 01867
ATTN: Gary Matchett

Charles R. Payne
6592/SPO, Code YED
P.O. Box 92960
World Way Postal Center
Los Angles, CA 90009

AFGL - PHP
Hanscom AFB
Bedford, MA 01731
ATTN: Jack Klobuchar

STI
1195 Bordeaux Drive
Sunnyvale, CA 94086
ATTN: J. J. Spiker, Jr. (5)

IBM
18100 Frederick Pike
Gaithersburg, MD 20760
ATTN: Fritz Byrne (3)

Applied Physics Laboratory
Johns Hopkins University
Johns Hopkins Road
Laurel, MD 20810
ATTN: Reginald Rhue
Joseph Wall
Edward Prozeller

Defense Mapping Agency Headquarters
U.S. Naval Observatory
Building 56
Washington, DC 20305
ATTN: Dr. Charles Martin (STT)

DISTRIBUTION (Continued)

Defense Mapping Agency
Aerospace Center
2nd & Arsenal St.
St. Louis, MO 63118
ATTN: George Stentz (2)

Professor Charles Counselman III
54-620 Massachusetts Institute of Technology
77 Massachusetts Ave.
Cambridge, MA 02139

Dr. Peter Bender
Joint Institute for Laboratory Astrophysics
University of Colorado
Boulder, CO 80302

Magnavox Research Laboratory
2829 Moricopa St.
Torrance, CA 90503
ATTN: Tom Stansel

CAPT John Bossler
6001 Executive Blvd.
Rockville, MD 20852
ATTN: OA/C1X8

Mr. Clyde Goad
6001 Executive Blvd.
Rockville, MD 20852
ATTN: OA/C1X8

Defense Mapping Agency
Hydrographic/Topographic Center
Code GST
6500 Brookes Lane
Washington, DC 20315
ATTN: Ben Roth
Hank Heuerman
Fran Varnum
Caroline Leroy (3)

U.S. Geological Survey
526 National Center
12201 Sunrise Valley Drive
Reston, VA 22092
ATTN: COL Paul E. Needham

DISTRIBUTION (Continued)

University of Texas
Applied Research Laboratory
Post Office Box 8029
Austin, TX 78712
ATTN: Dr. Arnold Tucker
Dr. James Clynch

Naval Research Laboratory
Code 7966
Building 53
Washington, DC 20315
ATTN: James Buisson (2)

Transportation System Center
DST 542
Kendall Square
Cambridge, MA 02142
ATTN: John Kraemer

Defense Technical Information Center
Cameron Station
Alexandria, VA 22314 (12)

Local:

E41
F14 (Saffos) (8)
K05
K10
K13 (Hermann) (20)
X210 (6)

DISTRIBUTION (Continued)

Defense Mapping Agency
Aerospace Center
2nd & Arsenal St.
St. Louis, MO 63118
ATTN: George Stentz (2)

Professor Charles Counselman III
54-620 Massachusetts Institute of Technology
77 Massachusetts Ave.
Cambridge, MA 02139

Dr. Peter Bender
Joint Institute for Laboratory Astrophysics
University of Colorado
Boulder, CO 80302

Magnavox Research Laboratory
2829 Moricopa St.
Torrance, CA 90503
ATTN: Tom Stansel

CAPT John Bossler
6001 Executive Blvd.
Rockville, MD 20852
ATTN: OA/C1X8

Mr. Clyde Goad
6001 Executive Blvd.
Rockville, MD 20852
ATTN: OA/C1X8

Defense Mapping Agency
Hydrographic/Topographic Center
Code GST
6500 Brookes Lane
Washington, DC 20315
ATTN: Ben Roth
Hank Heuerman
Fran Varnum
Caroline Leroy (3)

U.S. Geological Survey
526 National Center
12201 Sunrise Valley Drive
Reston, VA 22092
ATTN: COL Paul E. Needham